

**BIOCHEMICAL AND CELLULAR IMAGING STUDIES OF A NOVEL
CDC42-DEPENDENT FORMIN PATHWAY**

APPROVED BY SUPERVISORY COMMITTEE

Michael K. Rosen, Ph.D. (Supervisor)

Michael Roth, Ph.D. (Chair)

Rama Ranganathan, M.D., Ph.D.

Xiaodong Wang, Ph.D.

DEDICATION

To my parents, who gave me the confidence to try.

BIOCHEMICAL AND CELLULAR IMAGING STUDIES OF A NOVEL
CDC42-DEPENDENT FORMIN PATHWAY

by

ABHINAV SETH

DISSERTATION

Presented to the Faculty of the Graduate School of Biomedical Sciences

The University of Texas Southwestern Medical Center at Dallas

In Partial Fulfillment of the Requirements

For the Degree of

DOCTOR OF PHILOSOPHY

The University of Texas Southwestern Medical Center at Dallas

Dallas, Texas

December, 2005

Copyright

by

Abhinav Seth, 2005

All Rights Reserved

ACKNOWLEDGEMENTS

I am sincerely thankful to the many people who contributed their advice, wisdom and support towards the completion of this work. From excellent teachers to helpful collaborators to steadfast family and friends, I have been very fortunate, indeed.

During my graduate training, I have had the opportunity to learn from the best teachers. Dr. Michael Rosen is a great mentor and scientist whose enthusiasm to tackle new scientific challenges is contagious. Mike has taught me how to think about scientific problems rigorously and what it means to answer scientific questions properly. From new techniques to new discoveries, science is a continuous process of constant learning, and the most valuable lesson I have gained from Mike, is learning how to learn. I also appreciate the support and advice of my committee members Drs. Rama Ranganathan, Michael Roth and Xiaodong Wang. Their insights and suggestions have been of great value in overcoming particularly vexing experimental obstacles. I am especially grateful to Dr. Tim Clackson, a friend and teacher from my undergraduate days, for teaching me the most basic and essential of all scientific skills: how to read a paper.

I am extremely thankful to many collaborators whose assistance and instruction made the microscopy work possible. Dr. Christoph Wülfing trained me in the art of T-cell imaging and generously shared his insights and experiences in the complexities of live cell imaging. Dr. Simon Daefler kindly allowed access to his confocal microscope which facilitated the initial analysis of formin localization. Other collaborators have helped by generously sharing reagents and are mentioned in the texts of the following chapters.

The Rosen Lab is filled with talented and knowledgeable individuals who create an exciting environment in which to work. I have learned much from my

fellow labmates including Gaya, Daisy, Mara, Hui-Chun, Junko, Sanjay, Ilidio, Shae, David, Xiaocheng, Xiaolan and Ayman. I am particularly grateful to former lab member Eduardo Torres, now Dr. Torres, for his help with protein purification and biochemistry during my early days in the lab and for his excellent culinary skills. My current benchmate, Dr. Takanori Otomo, has been an excellent friend, teacher and collaborator. Initially, Takanori and I shared our pain as we struggled together to make different kinds of GTPase FRET sensors. By the time I got to the formin project, Takanori was already there, ready to guide me through the intricacies of formin and actin biochemistry. I would also like to thank Chinatsu Otomo for her tireless efforts to keep the lab running smoothly and, in particular, for helping clone the mDial constructs. I also thank Song Huang, a talented rotation student, who helped with the preliminary characterization of mDial localization. Throughout much of the sensor work, Neeta Mistry provided excellent technical assistance.

I am deeply indebted to Jason Mock for introducing me to phagocytosis, for persisting until I actually tried the assays, for sharing protocols and reagents and for many, many helpful discussions.

UT Southwestern is a special place because it couples scientific prowess with a friendly environment. I have directly benefited from this unique combination since my first day at UT Southwestern. Dr. Helen Yin was not only a great collaborator on the sensor project, but also kindly provided me lab “shelter” as I arrived in Dallas six months before the rest of the Rosen Lab. Dr. Masaya Yamamoto and Vivek K. Arora were helpful colleagues as well as welcoming friends, particularly during those early days. I thank Dr. Olaf Andersen of the Cornell MSTP and Dr. Rodney Ulane of the UT Southwestern MSTP for making the transition between programs painless and seamless. The UT Southwestern MSTP community is a wonderful source of support and wisdom and has taught me that, instead of being incompatible, an interest in basic science

and a clinical mindset can form a powerful combination when pursuing a career in academic medicine. The leaders and administrators of the MSTP, including Dr. Michael Brown, Dr. Dennis McKearin, Dr. Robert Munford, Robin Downing and Stephanie Robertson, all embody the ideals of scientific excellence and good citizenship which are the trademark qualities of UT Southwestern. Their example is a valuable source of inspiration for me and the rest of my MSTP colleagues.

While nature abhors a vacuum, it seems that scientific research is often conducted in one. In pursuit of my goals, I have not always given my friends and family the time they deserve, but their patience, understanding and encouragement have been invaluable to me. I am especially grateful to Eric and Hae-Won for their unwavering friendship. My brother-in-law Rishi and my cousins, Anchit and Varun, are my accomplished younger brothers who have been a source of rejuvenating comic relief and affection.

I can not fully express all that my parents, Usha & Suresh Seth, and my parents-in-law, Sarita & Vijay Mohan Bhargava, have done, but they have always given me their love and guidance. Research can be a frustrating experience at times, but whenever I felt discouraged, it was my parents who gave me the strength and confidence to keep trying.

Finally, I must recognize the one person who has contributed to every aspect of this work, my wife Rashu. She is my best friend, my source of inspiration, my advisor and my colleague. She shares my excitement when experiments work and bolsters my spirits when they do not. She motivates me to work hard and keeps my mind focused. She edits my manuscripts. She provides key reagents and protocols. She is my partner, in every sense of the word. She has done all of this while simultaneously completing her own graduate work in the lab of Dr. Zhijian “James” Chen, where she has uncovered deep truths about how the immune system works on a molecular level. She is Superwoman and I am very lucky that she is with me.

BIOCHEMICAL AND CELLULAR IMAGING STUDIES OF A NOVEL
CDC42-DEPENDENT FORMIN PATHWAY

Publication No. _____

Abhinav Seth, Ph.D.

The University of Texas Southwestern Medical Center at Dallas, 2005

Supervising Professor: Michael K. Rosen, Ph.D.

The Rho GTPases are important regulators of actin cytoskeletal dynamics during processes such as cell migration, cell polarization and cell division. Different Rho family members exert their effects on actin through specific downstream effectors including members of the WASP and Diaphanous-Related Formin (DRF) protein families. It is presently unclear if, and by what mechanisms, the level, timing and localization of Rho GTPase activity control

and coordinate effector activity to produce different types of cytoskeletal structures and rearrangements.

On a molecular level, autoinhibition is a common regulatory mechanism for many Rho GTPase effectors. Relief of autoinhibition of WASP by the Rho family member Cdc42 involves a significant GTPase-induced conformational change. Based on this conformational change, I have created a series of single-molecule, FRET-based sensors for active Cdc42 that can faithfully report on Cdc42 activity *in vitro* and in cells. These sensors may be valuable tools for studying the spatio-temporal dynamics of Cdc42 signaling *in vivo*.

The mechanisms of autoinhibition and activation are less well understood for the DRF family of GTPase effectors. DRFs are characterized by a C-terminal Diaphanous Autoregulatory Domain (DAD) that is postulated to regulate the actin assembly activity of the adjacent formin homology 2 (FH2) domain through autoinhibitory interactions with an N-terminal regulatory region, although this has only been shown directly for the DRF mDia1. Here, I show that the actin assembly activity of FRL α , a macrophage-specific DRF, is also autoinhibited by its N-terminal domain. In cells, autoinhibitory interactions also block a novel GTPase-independent membrane localization activity of the N-terminal domain in both FRL α and mDia1. Autoinhibitory control of FRL α activity and localization are specifically relieved by Cdc42. Timelapse microscopy was used to address

the potential physiological significance of the Cdc42-FRL α interaction during Fc- γ receptor mediated phagocytosis in macrophages, a Cdc42-dependent process. The data show that FRL α is required for efficient Fc- γ receptor mediated phagocytosis and that it is recruited to the phagocytic cup by Cdc42. These results suggest mutual autoinhibition of biochemical activity and cellular localization may be a general regulatory principle for DRFs and demonstrate an important role for a novel Cdc42-formin pathway in immune function.

TABLE OF CONTENTS

| | |
|---|--------|
| PRIOR PUBLICATIONS | xiii |
| LIST OF FIGURES AND TABLES | xiv |
| LIST OF ABBREVIATIONS | xvii |
| OVERVIEW | 20 |
| CHAPTER 1: Rational Design of Genetically Encoded FRET-Based Sensors of Cellular Cdc42 Signaling | |
| Abstract | 25 |
| Introduction | 26 |
| Experimental Procedures | 32 |
| Results | 37 |
| Discussion | 60 |
| CHAPTER 2: Sensor Optimization and Development of Imaging Assays for Cdc42-Mediated Biological Processes | |
| Abstract | 69 |

| | |
|-------------------------|-----|
| Introduction | 71 |
| Experimental Procedures | 73 |
| Results | 81 |
| Discussion | 121 |

CHAPTER 3: Autoinhibition Regulates the Actin Assembly Activity and Cellular Localization of the Diaphanous-Related Formins FRL α and mDia1

| | |
|-------------------------|-----|
| Abstract | 124 |
| Introduction | 126 |
| Experimental Procedures | 131 |
| Results | 142 |
| Discussion | 175 |

| | |
|-------------|-----|
| CONCLUSIONS | 189 |
|-------------|-----|

| | |
|----------|-----|
| APPENDIX | 197 |
|----------|-----|

| | |
|------------|-----|
| REFERENCES | 198 |
|------------|-----|

PRIOR PUBLICATIONS

- Seth, A., Otomo, T., Yin, H. L., and Rosen, M. K. (2003). Rational design of genetically encoded fluorescence resonance energy transfer-based sensors of cellular Cdc42 signaling. *Biochemistry* 42, 3997-4008.
- Labno, C. M., Lewis, C. M., You, D., Leung, D. W., Takesono, A., Kamberos, N., Seth, A., Finkelstein, L. D., Rosen, M. K., Schwartzberg, P. L., and Burkhardt, J. K. (2003). Itk functions to control actin polymerization at the immune synapse through localized activation of Cdc42 and WASP. *Current Biology* 13, 1619-1624.
- Clemons, P. A., Gladstone, B. G., Seth, A., Chao, E. D., Foley, M. A., and Schreiber, S. L. (2002). Synthesis of calcineurin-resistant derivatives of FK506 and selection of compensatory receptors. *Chemistry & Biology* 9, 49-61.
- Cannon, J. L., Labno, C. M., Bosco, G., Seth, A., McGavin, M. H., Siminovitch, K. A., Rosen, M. K., and Burkhardt, J. K. (2001). Wasp recruitment to the T cell:APC contact site occurs independently of Cdc42 activation. *Immunity* 15, 249-259.

LIST OF FIGURES AND TABLES

| | | |
|-------------|---|-----|
| Figure 1-1: | Conceptual Design of FRET-Based Sensors of Cdc42 Signaling. | 39 |
| Table 1 : | Properties of the Cdc42 Sensors. | 43 |
| Figure 1-2: | Biochemical Characterization of GBD-VCA Sensors. | 46 |
| Figure 1-3: | Affinity Measurements of Cdc42 Sensors for Rac1-GMPPNP. | 50 |
| Figure 1-4: | FRET Images of Transiently Transfected NIH 3T3 Cells. | 53 |
| Figure 1-5: | Quantitation of Cellular FRET Values. | 55 |
| Figure 2-1: | Characterization of CAAX-Tagged FRET-Based Cdc42 Sensors. | 82 |
| Figure 2-2: | Characterization of PM-Tagged FRET-Based Cdc42 Sensors. | 88 |
| Figure 2-3: | Comparison of CAAX-Tagged and PM-tagged FRET-Based Cdc42 Sensors. | 94 |
| Figure 2-4: | Cdc42 Activity Monitored with a FRET-based CAAX-tagged Sensor During Membrane Ruffling. | 99 |
| Figure 2-5: | Wide-field Fluorescence Images of NIH 3T3 cells Expressing CAAX-tagged Sensors. | 102 |

| | | |
|-------------|---|-----|
| Figure 2-6: | Wide-field Fluorescence Images of Phoenix-E Cells Expressing CAAX-tagged Sensors. | 107 |
| Figure 2-7: | Localization of Active Cdc42 During T cell Activation by APCs. | 111 |
| Figure 2-8: | FRET-based Imaging of Cdc42 Activity During Fc- γ Receptor Mediated Phagocytosis. | 115 |
| Figure 3-1: | The N-terminus of FRL α Negatively Regulates the Actin Assembly Activity of the C-terminal FH2 Domain. | 143 |
| Figure 3-2: | Autoinhibition Regulates FRL α Localization. | 147 |
| Figure 3-3: | Active Cdc42 Relieves Autoinhibition of FRL α Actin Assembly Activity. | 151 |
| Figure 3-4: | Active Cdc42 Relieves Autoinhibition of FRL α Localization. | 154 |
| Figure 3-5: | Autoinhibition Controls the Localization of the Rho-regulated DRF mDia1. | 159 |
| Figure 3-6: | Cdc42 recruits FRL α to the Phagocytic Cup During Fc- γ Receptor Mediated Phagocytosis. | 163 |
| Figure 3-7: | The Isolated C-terminus of FRL α is Recruited to the Phagocytic Cup During Fc- γ Receptor Mediated Phagocytosis Through its Interaction with Actin. | 166 |

- Figure 3-8: Recruitment of Active Cdc42 to the Phagocytic Cup During 170
Fc- γ Receptor Mediated Phagocytosis.
- Figure 3-9: Localization of DRFs During Complement Receptor 172
Mediated Phagocytosis.

LIST OF ABBREVIATIONS

APC – Antigen Presenting Cell

CC – Coiled-Coil

CCD – Charge-Coupled Device

CFP – Cyan Fluorescent Protein

CRIB – Cdc42/Rac Interactive Binding

DAD – Diaphanous Autoregulatory Domain

DD – Dimerization Domain

DID – Diaphanous Inhibitory Domain

DMEM – Dulbecco's Modified Eagle Medium

DNA- Deoxyribonucleic Acid

DRF – Diaphanous-Related Formin

EGF – Epidermal Growth Factor

EM – Electron Microscopy

FACS – Fluorescence Activated Cell Sorting

FBS – Fetal Bovine Serum

FITC – Fluorescein Isothiocyanate

FRET – Fluorescence Resonance Energy Transfer

G – GTPase Binding

GAP – GTPase Activating Protein

GBD – GTPase Binding Domain

GDI – Guanine Nucleotide Dissociation Inhibitor

GDP – Guanosine Diphosphate

GEF – Guanine Nucleotide Exchange Factor

GFP – Green Fluorescent Protein

GMPPNP - Guanosine 5'-[β,γ -imido]Triphosphate

GPCR - G-Protein Coupled Receptor

GST – Glutathione S-Transferase

GTP – Guanosine Triphosphate

MBP – Maltose Binding Protein

MCC – Moth Cytochrome C

MHC – Major Histocompatibility Complex

mRFP – monomeric Red Fluorescent Protein

ND – Neutral Density

PAGE – Polyacrylamide Gel Electrophoresis

PAK – p21 Activated Kinase

PBS – Phosphate Buffered Saline

PCR – Polymerase Chain Reaction

RBC – Red Blood Cell

RNA – Ribonucleic Acid

SDS – Sodium Dodecyl Sulphate

siRNA- short interfering RNA

VCA – Verprolin homology/Central hydrophobic/Acidic Domain

WASP – Wiskott-Aldrich Syndrome Protein

YFP – Yellow Fluorescent Protein

OVERVIEW

Actin is a ubiquitous 43 kDa eukaryotic protein that can polymerize to form filaments (Pollard and Cooper, 1986). These filaments form a cellular skeleton that is required for processes such as cell movement, division and polarization (Evangelista et al., 2003; Pollard and Borisy, 2003; Pollard and Cooper, 1986). The actin cytoskeleton is dynamic and can be remodeled locally in seconds depending on the needs of the cell. Actin filaments can be bundled and organized into specific architectures to produce networks with differing mechanical properties (Mitchison, 1992; Nicholson-Dykstra et al., 2005; Pollard and Borisy, 2003). The regulatory mechanisms controlling where, when and what kind of filaments and networks are produced is an active area of research. In this section, I will describe the general principles of actin regulation and focus on the important open questions in the field. Detailed descriptions of the molecules and signaling pathways will be presented in the following chapters where appropriate.

A number of signaling pathways cooperate to control the dynamics of the actin cytoskeleton. The Rho GTPases are members of the Ras superfamily of small GTPases and act as molecular switches to control many different effectors which have important effects on actin dynamics

(Bishop and Hall, 2000; Hall, 1998; Nobes and Hall, 1999). The Rho family is important for regulating a number of cytoskeletal processes including cell migration, cell division, cell polarization, neuronal growth cone motility, T cell activation and phagocytosis (Etienne-Manneville and Hall, 2002; Hall, 1998). The Rho family contains at least 22 members, but only three, Rho, Rac and Cdc42, have been characterized extensively (Sorokina and Chernoff, 2005). The studies on these three GTPases have established the general paradigms of cytoskeletal regulation by the Rho family.

Microinjection experiments with constitutively active mutants of Rho, Rac and Cdc42 were the first to reveal the importance of the Rho family in regulating the actin cytoskeleton (Nobes and Hall, 1995; Ridley and Hall, 1992; Ridley et al., 1992). The initial observations revealed that each of these three GTPases, when injected into fibroblasts, causes a unique effect on the actin cytoskeleton and leads to the formation of distinct filamentous actin structures; Rho causes bundling of actin into “stress fibers” which span the entire length of the cell (Ridley and Hall, 1992), Rac induces the formation of curtain-like or wave-like actin structures called “lamellipodia” all around the cell periphery (Ridley et al., 1992), and Cdc42 produces numerous “filopodia”, thin, finger-like actin-containing projections, which protrude from the cell surface (Nobes and Hall, 1995). Where studied, the less well-characterized Rho GTPases differ mainly in

their regulatory mechanisms, tissue expression profiles and non-cytoskeletal biological effects (Sorokina and Chernoff, 2005). Thus, Rho, Rac and Cdc42 are representative of the core actin cytoskeletal activities of the Rho family.

Rho family GTPases exert their effects on the actin cytoskeleton through specific sets of downstream effectors, ultimately activating different actin nucleation factors, Arp2/3 complex or formin family proteins, that can generate specific types of actin filaments (Bishop and Hall, 2000; Evangelista et al., 2003; Higgs and Pollard, 1999). Cdc42 and Rac activate Arp2/3 complex indirectly through WASP family proteins (Miki and Takenawa, 2003). Rho activates the formin protein mDia1 directly (Higgs, 2005). Cdc42 and Rac may also activate different formins, but the importance of these interactions for cytoskeletal regulation has not been extensively studied (Higgs, 2005). Rho GTPases also influence the activity of various actin regulatory factors including kinases, filament severing proteins, filament capping proteins, anti-capping proteins and phospholipids. Some effectors, like PAK, PI3-K and PLC- β , are common to different GTPases, while others, such as POSH, CIP-4, WASP and WAVE, are GTPase-specific (Bishop and Hall, 2000). The GTPase-specific effectors may modulate the actin structures produced by the common GTPase effectors and therefore, may be responsible for the distinct cytoskeletal phenotypes associated with each GTPase.

However, during a specific biological process such as cell migration, cell division or phagocytosis, Rho GTPases do not act in isolation. The actin structures observed during these processes can not simply be considered “linear combinations” of stress fibers, lamellipodia and filopodia. Rather the observed structures (e.g. “traveling waves” during migration, “rings” during cytokinesis or “cups and spheres” during phagocytosis) may arise from the concerted actions of the different Rho GTPases (Bretschneider et al., 2004; Castellano et al., 2001; Pelham and Chang, 2002; Scott et al., 2005). The molecular mechanisms by which the different downstream pathways are coupled and coordinated are not well understood. The concentration, or level, of activated GTPase may determine which of its downstream pathways are engaged during a given process. The spatial and temporal coordination of GTPase activation with effector availability may also be important. In addition, unidentified or incompletely characterized effectors may play specialized and significant roles in producing the distinct cytoskeletal structures observed during specific processes.

A powerful approach towards understanding the molecular functions of different Rho GTPases during specific cytoskeletal processes would be to develop quantitative methods to measure the temporal and spatial dynamics of activated GTPases in cells. This information could be coupled with similar profiles of the level, timing and localization of effector activity and then correlated with the timecourse of actin dynamics during a given process. Ultimately, one would

develop testable models of how different GTPase-effector pathways are coordinated and utilized by the cell to generate complex patterns of cytoskeletal dynamics. Clearly, this is a long-term goal that will require the sustained effort of many laboratories and individuals.

In this work, I describe my efforts towards developing a new series of GTPase imaging reagents and towards identifying the function of a novel GTPase-effector pathway. In Chapter 1, I present the development of FRET-based sensors for Cdc42 that were designed based on a detailed biochemical and structural understanding of how Cdc42 activates a specific effector called WASP. In Chapter 2, I discuss the use of those sensors towards developing live cell imaging assays to study the cytoskeletal dynamics during three biological processes: membrane ruffling during cell adhesion and spreading, T cell activation and Fc- γ receptor mediated phagocytosis. In Chapter 3, I demonstrate, using biochemistry and live cell imaging, that a previously incorrectly characterized cytoskeletal regulator called FRL α is actually a Cdc42 effector that plays an important role during Fc- γ receptor mediated phagocytosis. Finally, I will discuss the implications of these findings for future studies aimed at defining the roles of different Rho GTPases during specific cytoskeletal processes.

CHAPTER 1

Rational Design of Genetically Encoded FRET-Based Sensors of Cellular Cdc42 Signaling

Abstract

The temporal and spatial control of Rho GTPase signaling pathways is a central issue in understanding the molecular mechanisms that generate complex cellular movements. In its active state, the Rho family member Cdc42 induces a significant conformational change in its downstream effector, the Wiskott-Aldrich Syndrome Protein (WASP). Based on this conformational change, I have created a series of single-molecule sensors for active Cdc42 that utilize fluorescence resonance energy transfer (FRET) between cyan and yellow fluorescent proteins. *In vitro*, the Cdc42 sensors produce up to 3.2-fold FRET emission ratio changes upon binding active Cdc42. *In vivo*, the sensors faithfully report on Cdc42 activity. These results establish the successful creation of rationally-designed and genetically-encoded tools that can be used to image the activity of biologically and medically important molecules in living systems.

Introduction

Cellular signal transduction relies on dynamically regulated networks of molecular pathways. To properly integrate multiple signals and achieve efficient transfer of information along those pathways, cells must regulate the spatial and temporal activities of the component signaling molecules (Pawson and Scott, 1997; Teruel and Meyer, 2000). Therefore, in order to understand signal transduction, it is essential to study signaling processes within a cellular context.

Members of the Rho subfamily of small GTPases have effects on multiple cellular functions including cell migration, proliferation and gene expression. (Van Aelst and D'Souza-Schorey, 1997). To date most studies of this family have focused on three proteins, Rho, Rac and Cdc42 and their ability to regulate the actin cytoskeleton (Hall, 1998). Like other members of the Ras superfamily, the Rho proteins act as membrane localized molecular switches, which cycle between active GTP bound states and inactive GDP bound states. The intrinsic rates of nucleotide hydrolysis and exchange are slow and *in vivo* these processes are controlled by regulatory molecules that accelerate individual steps of the GTPase cycle (Scheffzek et al., 1998). The Dbl family of guanine nucleotide exchange factors (GEFs) activate the Rho GTPases by facilitating release of bound GDP, which results in GTP loading *in vivo* (Zheng, 2001). GTPase activating proteins

(GAPs) inactivate the Rho proteins by enhancing their intrinsic GTPase activity. Guanine nucleotide dissociation inhibitors (GDIs) inhibit Rho GTPases by sequestering them in the cytosol and by preventing dissociation of bound nucleotide. To date, many GAPs, GDIs and GEFs have been described with varying selectivity for the different Rho proteins (Van Aelst and D'Souza-Schorey, 1997).

Cdc42 has specific effects on cell motility, intracellular trafficking, establishment and maintenance of cell polarity, and RNA processing (Erickson and Cerione, 2001). Cdc42 mediates many of these effects through GTP-dependent interactions with effector proteins containing a Cdc42/Rac interactive binding (CRIB) motif (Aspenstrom, 1999; Bishop and Hall, 2000). The specific biological consequences of Cdc42 activation are dictated by the subset of effectors, and the degree to which each is activated, in response to a particular signal. Recent data suggest that effector choice depends greatly on the localization of activated GTPase (Cannon et al., 2001; Chiu et al., 2002; del Pozo et al., 2000). Thus, different cellular pools of Cdc42 may be selectively activated to regulate different cellular functions, but it has not been established which pools are associated with which functions. In addition, the mechanisms by which localized GTPase signals are generated are not well understood (Symons and Settleman, 2000). Attempts to study this aspect of Cdc42 biology have been

difficult because of the lack of tools for determining the precise sub-cellular localization of activated GTPases (as distinct from the total pool) in a living cell.

Despite the existing limitations, efforts have been made to understand the spatial and temporal aspects of Cdc42 signaling using anti-Cdc42 antibodies, mutant GTPases and chimeras of Cdc42 and green fluorescent protein (GFP). In the absence of stimulation, Cdc42 resides on nuclear, endoplasmic reticulum and Golgi membranes as well as in the cytoplasm, presumably bound to RhoGDI (Erickson et al., 1996; Kroschewski et al., 1999; Michaelson et al., 2001). Cdc42 also localizes to podosomes, actin-rich adhesion structures typically found in cells of the monocytic lineage (Linder et al., 1999). During Fc- γ receptor mediated phagocytosis, a Cdc42-dependent process, the GTPase accumulates at phagosome sites along the plasma membrane (Caron and Hall, 1998; Hoppe and Swanson, 2004). Cell polarization at the edge of a wounded monolayer also depends on Cdc42 activity and polarized cells demonstrate Cdc42 localization at their leading edges and on vesicles that appear to translocate from the tips of the cells toward the nucleus (Etienne-Manneville and Hall, 2001; Nobes and Hall, 1999). In addition, Cdc42 is active at the leading edges of motile cells and is required for the initiation of membrane protrusions induced by epidermal growth factor (EGF) (Itoh et al., 2002; Kurokawa et al., 2004; Nalbant et al., 2004).

The timing of Cdc42 activation can be detected using a biochemical assay that allows selective immunoprecipitation of GTP-bound Cdc42 using a fusion protein of glutathione S-transferase and the Cdc42 effector PAK (Benard et al., 1999; Etienne-Manneville and Hall, 2001). However, since this assay requires disruption of cells, it does not allow simultaneous observation of Cdc42 localization and activation. Further, sensitivity issues may prevent detection in cases where very little Cdc42 is activated. Some of these limitations are overcome by immunostaining fixed cells with the GTPase binding domain (GBD) of a specific Cdc42 effector, such as the Wiskott-Aldrich Syndrome Protein (WASP). Such reagents have been used to study the regulation of activated Cdc42 localization and effector activation at the immunological synapse in T cells (Cannon et al., 2001; Labno et al., 2003; Zeng et al., 2003). A GFP-GBD fusion protein has also been expressed in living cells to study the dynamic localization of active Cdc42 in response to cadherin signaling (Kim et al., 2000b). However, this methodology is limited in the amount of quantitative information it can yield. Thus, to accurately study the temporal and spatial dynamics of Cdc42 in living cells, better tools need to be developed.

Recent studies have begun to address the spatial and temporal dynamics of GTPases using fluorescence resonance energy transfer (FRET) experiments (Pertz and Hahn, 2004). Kraynov et. al. developed a bimolecular FRET-based method

for measuring the activity of ectopically expressed fluorophore-tagged Rac in cells microinjected with an appropriately matched fluorophore-tagged effector domain (Kraynov et al., 2000). This method has been used in fixed cells to study the spatial and temporal control of Rac activity in response to integrin signaling and changes in cell tension (Del Pozo et al., 2002; Katsumi et al., 2002). It has also been used in live cells to monitor Rac dynamics during neutrophil chemotaxis (Gardiner et al., 2002). A modified-version of this method, employing GFP-tagged Cdc42, was used to visualize localized Cdc42 activation in response to fluid shear stress in endothelial cells (Tzima et al., 2003). A novel ratiometric imaging method using a Cdc42-effector conjugated to a solvatochromic dye, whose fluorescence properties depend on the local chemical environment, has recently been developed to detect endogenous Cdc42 activation in microinjected fibroblasts (Nalbant et al., 2004; Touthkine et al., 2003). Bimolecular FRET strategies are inherently complicated by issues of fluorophore stoichiometry which are overcome by the solvatochromic dye system (Gordon et al., 1998). However, all of the strategies listed above require microinjection of at least one of the sensor components which complicates reagent preparation and delivery and limits the types of biological systems amenable to analysis.

Unimolecular FRET strategies based on the genetically encoded fluorophores cyan fluorescent protein (CFP) and yellow fluorescent protein (YFP)

eliminate issues of fluorophore stoichiometry and can be delivered to a variety of *in vivo* systems using standard gene delivery protocols. Therefore, several GTPase sensors have been developed which utilize changes in intramolecular CFP-YFP FRET to monitor GTPase activation. Mochizuki et. al. have reported the development of FRET-based sensors in which a Ras-Raf fusion protein is flanked by CFP and YFP (Mochizuki et al., 2001). When the Ras moiety of this construct is loaded with GTP, intramolecular association with the Raf element leads to detectable changes in CFP-YFP FRET. In addition to the CFP-YFP based Cdc42 sensors developed in the Rosen lab (described below) (Seth et al., 2003), other groups have developed similar constructs containing other GTPases fused to their effectors as sensors for Rho, Rac and Cdc42 (Itoh et al., 2002; Kurokawa et al., 2004; Yoshizaki et al., 2003).

Here, I describe the design and biochemical characterization of two novel classes of genetically encoded Cdc42 biosensors that utilize intramolecular FRET between CFP and YFP to monitor the activation state of the GTPase. The Cdc42 sensors are based on fluorophore-tagged fragments of WASP, which bind specifically to the active GTPase. Affinity measurements reveal that the two fluorescent proteins interfere only minimally with the affinity of WASP for Cdc42. The sensors yield up to 3.2-fold changes in CFP-YFP emission ratios upon binding the activated GTPase. *In vivo*, the sensors detect activity in cells

expressing either a constitutively active mutant of Cdc42 or wildtype Cdc42 and GEF proteins. Thus, the sensors reported here represent a novel and promising class of genetically encoded probes for elucidating Cdc42 signaling mechanisms *in vivo*.

Experimental Procedures

Plasmid Construction, Protein Expression and Purification

To facilitate cloning of the sensor constructs, I engineered a modified pet11a bacterial expression vector (Novagen) containing the enhanced CFP (ECFP) and enhanced YFP (EYFP) genes (Clontech) separated by a 5' Nco site and a 3' Xho site. To improve pH stability, the Q69K mutation was introduced into the EYFP gene using the QuikChange Site-Directed Mutagenesis Kit (Stratagene) (Miyawaki et al., 1999). The ECFP-EYFP vector can be used to insert any gene containing a 5' NcoI site and a 3' XhoI site.

For all of the Cdc42 sensors, different WASP sequences (Table 1) were cloned from human cDNA. The WASP GBD-VCA sensors, containing GGS-GGS linker sequences, were cloned from constructs reported previously (Buck et

al., 2001; Kim et al., 2000a). Each sensor protein was expressed in *Escherichia coli* and purified by anion exchange and hydrophobic exchange chromatography.

For mammalian expression, a modified pCMV-Script vector (Stratagene) was used. An internal NdeI site was removed and a new polylinker site with NdeI and BamHI cloning sites was inserted into this vector. The resulting vector was named pASTO. A version of pASTO encoding a C-terminal HA tag, named pASTO-HA, was also created. Each sensor protein was then transferred into the pASTO vector using NdeI and BamHI restriction sites.

Cdc42 was prepared and loaded with nucleotide as described previously (Abdul-Manan et al., 1999).

A mammalian expression plasmid encoding SopE, a Cdc42/Rac GEF from *Salmonella typhyrum*, was a gift from Dr. Jorge Galan (Yale University) (Hardt et al., 1998). Appropriate primers were used to transfer the SopE gene into pASTO-HA. Either the original plasmid or the pASTO-HA plasmid was used in the transfection assays.

The gene for FGD1, a mammalian Cdc42 GEF, (residues 330-710) encoded in the pFlag mammalian expression vector was a gift from Dr. Yi Zheng (Cincinnati Children's Hospital Medical Center) (Zheng et al., 1996).

Mammalian expression plasmids for Myc-tagged GTPase mutants were kindly provided by Dr. Melanie H. Cobb (UT Southwestern).

Fluorescence Spectroscopy

All *in vitro* fluorescence measurements were carried out on a Fluorolog-3 spectrofluorometer (JY Horiba, Edison, NJ). All biochemical assays were performed at 25 °C in buffer containing 20 mM HEPES pH 7.5, 150 mM KCl, 2 mM MgCl₂, and 2 mM DTT unless noted otherwise.

The ratio of 526 nm emission (maximum for YFP) to 476 nm emission (maximum for CFP) with 433 nm excitation (maximum for CFP) was recorded for each Cdc42 sensor in the presence or absence of saturating amounts of Cdc42 loaded with GMPPNP or GDP.

For affinity measurements, sensors were titrated with increasing amounts of Cdc42-GMPPNP. Data were fit to the following quadratic equation describing a single site binding isotherm using GraphPad Prism v. 3.0 software:

$$Y = (F_{\max} - F_{\text{init}}) * \left(\frac{K_d + [\text{Cdc42}] + [\text{Sensor}] - \sqrt{(K_d + [\text{Cdc42}] + [\text{Sensor}])^2 - 4 * [\text{Cdc42}] * [\text{Sensor}]}}{2 * [\text{Sensor}]} \right) + F_{\text{init}}$$

where Y = measured fluorescence intensity, F_{\max} = fluorescence intensity in the presence of saturating amounts of Cdc42, F_{init} = fluorescence intensity in the absence of Cdc42, [Sensor] = total sensor concentration, [Cdc42] = total Cdc42 concentration, and K_D = dissociation constant for Sensor-Cdc42 interaction.

Corrections for photobleaching and buffer volume were applied prior to fitting. Maximum changes in CFP-YFP emission ratio were determined with sensor concentration at K_D and Cdc42 concentration 10-fold above.

Cell Culture and Microscopy

NIH 3T3 fibroblast cells were maintained in Dulbecco's Modified Eagle Medium (DMEM) containing 10% fetal bovine serum (Invitrogen). Transfections were performed using Lipofectamine Plus (Invitrogen) in serum-free DMEM. Transfected cells were maintained in glass bottom 35 mm dishes (MatTek Corporation, Ashland, MA). Cells were imaged at 25 °C 30-36 hours after

transfection in Hank's Balanced Salt Solution (Invitrogen) using a Zeiss Axiovert 200M microscope equipped with a 75 W Xenon lamp.

FRET images were acquired using a 63X oil immersion objective, 2X2 or 4X4 binning, and the 86002v2 fluorescence filter and dichroic mirror set (Chroma Technology Corporation). For each cell, three images, CFP, YFP and FRET, were captured. CFP and YFP images were acquired using CFP excitation and emission filters and YFP excitation and emission filters, respectively. FRET images were acquired by using the CFP excitation filter and the YFP emission filter. Plates of transfected cells were scanned using a 1% Neutral Density (ND) filter to prevent photobleaching, while images were acquired with a 10% ND filter. Typically, exposure times of 100-500 ms were used to capture the fluorescence images. Background subtraction was based on cell-free regions of each plate. Quantitative measurements were typically based on cells exhibiting fluorescent intensities at least 25% above background. Images were collected using a Sensicam CCD camera (PCO Computer Optics GmbH, Germany) and analyzed with Slidebook software (Intelligent Imaging Innovations, Denver, CO). Each imaging experiment was repeated at least three times and a minimum of ten cells were analyzed per experiment.

Western Blot Analysis

To analyze sensor expression levels, NIH 3T3 cells were plated in 6-well dishes and transfected as described above. 36 hours after transfection, cells were washed with cold phosphate buffered saline (PBS) and resuspended in lysis buffer (20 mM Tris pH 7.5, 150 mM NaCl, 0.5% NP-40, 50 mM NaF, 1 mM NaVO₃, 0.5 mM PMSF, 5 µg/ml leupeptin, and 0.2 mM EGTA). After lysing the cells on ice for 10 minutes, the samples were centrifuged and the resulting supernatants were collected. Samples were normalized for protein content using the Coomassie Plus Protein Assay (Pierce) and run on an SDS PAGE gel. Western blotting to detect sensor expression was performed with primary mouse anti-GFP antibodies (Santa Cruz) and alkaline phosphatase conjugated secondary antibodies (Promega). Proteins were visualized using colorimetric methods (Promega).

Results

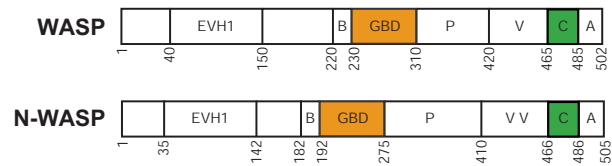
Design Strategy

WASP is a specific Cdc42 effector, unlike proteins such as PAK that can bind both Cdc42 and Rac (Bishop and Hall, 2000). The C-terminal region of WASP, termed the VCA, binds to the Arp2/3 complex and activates actin

polymerization (Figure 1-1A) (Higgs and Pollard, 1999; Zigmond, 2000). The N-terminal GBD is comprised of the CRIB motif, as well as other sequence elements that are necessary for high affinity interactions with Cdc42 (Figure 1-1A) (Rudolph et al., 1998; Thompson et al., 1998). Free WASP exists in an autoinhibited conformation in which the GBD interacts intramolecularly with the VCA (Kim et al., 2000a; Lei et al., 2000; Mott et al., 1999). Release of VCA, by disruption of the autoinhibited structure upon binding of active Cdc42 to the GBD, appears to be a key biochemical event in the activation of WASP (Abdul-Manan et al., 1999; Buck et al., 2001; Kim et al., 2000a).

The solution structure of the GBD bound to Cdc42, determined previously by others in the Rosen lab, reveals that the CRIB motif forms an intermolecular β -sheet with the $\beta 2$ strand of Cdc42 (Figure 1-1B). The structure of the GBD then terminates in a β -hairpin and α -helix unit, which packs against the switch I and II regions of the GTPase. The autoinhibited GBD-VCA structure shows that the GBD exists as an N-terminal β -hairpin and α -helix packed against four α -helices, one of which is contributed by VCA (Figure 1-1C) (Kim et al., 2000a). Thus, the N-terminal half of the GBD binds to Cdc42 while the C-terminal half binds to VCA. However, the GBD cannot simultaneously bind both Cdc42 and VCA because the central β -hairpin and α -helix unit is essential to the formation of either complex. Thus, the structural studies demonstrate that the autoinhibited

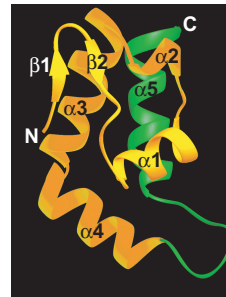
A



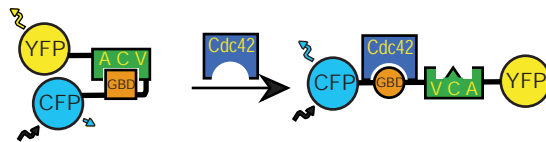
B



C



D



E

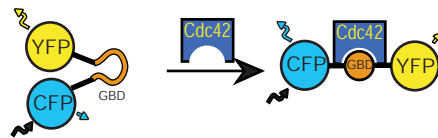


Figure 1-1

Figure 1-1. Conceptual Design of FRET-Based Sensors of Cdc42 Signaling.

- (A) Domain structure of WASP and N-WASP. The domains of WASP and N-WASP include an Enabled/VASP homology 1 domain (EVH1), Basic region (B), GTPase Binding Domain (GBD), Polyproline region (P), Verprolin homology region (V), Central hydrophobic region (C) and Acidic region (A). Note that N-WASP contains two tandem V regions.
- (B) Structure of Cdc42-GMPPNP bound to the GBD (residues 230-288) of WASP (Abdul-Manan et al., 1999; Carson, 1991). The GBD is orange, Cdc42 is blue and nucleotide is shown as a stick figure. The N and C termini are labeled. Secondary structure elements are labeled in white for the GBD and yellow for Cdc42. S1 = Switch I, S2 = Switch II.
- (C) Structure of the autoinhibited WASP domain (residues 242–310-GGSGGS-460-492) (Carson, 1991; Kim et al., 2000a). The GBD is orange and the C region of VCA is green. The N and C termini are labeled.
- (D) Schematic representation of the GBD-VCA FRET-based sensors.
- (E) Schematic representation of the GBD-only FRET-based sensors.

fold is incompatible with the Cdc42 bound structure of the GBD and that binding of Cdc42 must result in a marked conformational change of the autoinhibited complex.

Based on the structural data, it was hypothesized that appropriate fluorophores fused to the termini of the GBD-VCA construct should display measurable changes in intramolecular FRET upon Cdc42 binding (Figure 1-1D). In addition, since the isolated GBD is unstructured in solution, FRET changes in response to Cdc42 should occur in a fluorophore-tagged GBD-only construct as well (Figure 1-1E) (Kim et al., 2000a; Rudolph et al., 1998).

Since the aim was to develop sensors for Cdc42 signaling that could be used in living systems, the genetically encoded fluorophores CFP and YFP, whose fluorescence emission and absorption spectra are well-matched for FRET (Miyawaki and Tsien, 2000), were chosen for sensor development. Sensors were developed using sequences from both WASP and its homolog N-WASP. In order to optimize FRET changes upon activation, I created many constructs containing different GBD and VCA structural elements and surrounding residues (Table 1).

In Vitro Characterization of Cdc42 Sensors

Initially, four different GBD-only sensor constructs were created, each containing different portions of the GBD and surrounding residues. All of the purified sensors exhibit a high FRET value (yellow to cyan emission ratio) upon excitation of CFP when alone in solution (Table 1, Unbound FRET) with values ranging from 2.35 to 3.70. Upon addition of Cdc42 loaded with GMPPNP, a GTP analogue, all of the sensors show significantly decreased FRET values (Table 1, Bound FRET) ranging from 1.25 to 2.46. The ratio between the initial, unbound FRET and the final, bound FRET ranges from 1.47 for the B-GBD1 sensor to 1.87 for the GBD1 sensor (Table 1, *In Vitro* Ratio). These results are consistent with the hypothesis that binding of activated Cdc42 to an unstructured GBD-only construct can induce a significant conformational ordering, which is detectable by FRET. Moreover, the large magnitude of the FRET change for the GBD1 sensor suggests this construct may be useful for *in vivo* applications.

Next, I focused on development of the GBD-VCA sensors. Like the GBD-only sensors, each of the purified GBD-VCA sensors exhibits a high FRET value, ranging from 2.23 to 2.64, when alone in solution. In all cases, addition of Cdc42-GMPPNP causes a significant decrease in FRET, with final values ranging from 0.69 to 1.18 (Table 1). The B-GBD-C sensor, which contains the minimal

Table 1: Properties of the Cdc42 Sensors^a

| GBD-Only Sensors | Description | K _D for Cdc42 (nM) | In | | Transfected | |
|---------------------|---------------|-------------------------------------|---------|-------|---------------------------------|---------------------|
| | | | Unbound | Bound | Transfected with Cdc42V12 | In Vivo Ratio |
| B-CRIB | hWASP 225-251 | 133 ± 8 | 3.70 | 2.46 | 2.52 ± .16 | 2.09 ± .38 |
| B-GBD1 | hWASP 225-288 | 15 ± 3 | 2.45 | 1.66 | 1.81 ± .11 | 1.70 ± .13 |
| GBD1 | hWASP 230-288 | 19 ± 2 | 2.35 | 1.25 | 1.94 ± .11 | 1.37 ± .14 |
| GBD2 | hWASP 230-310 | 92 ± 6 | 2.50 | 1.50 | 1.93 ± .23 | 1.32 ± .08 |

| GBD-VCA Sensors | Description | K _D for Cdc42 (nM) | In | | Transfected | |
|--------------------|---|-------------------------------------|---------|-------|---------------------------------|---------------------|
| | | | Unbound | Bound | Transfected With Cdc42V12 | In Vivo Ratio |
| B-GBD-C | hWASP 225-310-GGSGGS-461-492 | 700 ± 38 | 2.28 | 1.18 | 1.52 ± .19 | 1.26 ± .08 |
| B-GBD-VCA | hWASP 225-310-GGSGGS-420-502 | 1300 ± 98 | 2.63 | 1.03 | 1.84 ± .32 | 1.03 ± .12 |
| N-GBD-VCA | hN-WASP 192-275-GGSGGS-393-505 | 178 ± 3 | 2.23 | 0.69 | 1.66 ± .06 | 0.96 ± .03 |
| N-GBD-DD- VCA | hN-WASP 192-275-GGSGGS-393-505 H211D,H214D | > 250000 | 2.14 | 2.04 | 1.76 ± .05 | 1.41 ± .07 |

^a The residues of human WASP (hWASP) or human N-WASP (hN-WASP) that comprise each sensor are listed. Each of the GBD-VCA sensors contains a (Gly-Gly-Ser)₂ linker between the GBD and VCA regions. K_D values are based on the results of three different titrations with Cdc42 loaded with GMPPNP. Errors were calculated during curve fitting. For the mutant N-GBD-DD-VCA sensor, *in vitro* FRET values have been determined with the same concentration of Cdc42 as for the wildtype sensor (10 μM, see text).

portion of the VCA involved in GBD binding, yields a FRET ratio change of 1.9-fold which is similar to the result for the GBD1 sensor. However, B-GBD-VCA, which contains the full VCA sequence, gives a much higher FRET change of 2.6-fold. A GBD-VCA sensor derived from N-WASP, called N-GBD-VCA, yields the highest FRET change, 3.2-fold, of any sensor tested (Figure 1-2A).

The observation that the unbound FRET is always greater than the bound FRET supports the idea that addition of Cdc42 causes separation of the two fluorophores. For each of the GBD-VCA sensors, the bound FRET value decreases as the length of the linker between GBD and C increases. Thus, B-GBD-VCA has a lower bound FRET than B-GBD-C (1.03 vs. 1.18, respectively), while N-GBD-VCA, which has an additional 27 amino acids in the linker as compared to B-GBD-VCA, has the lowest bound FRET value of 0.69 (Figure 1-2, Table 1). The correlation between bound FRET and linker length for the GBD-VCA sensors supports the hypothesis that binding of Cdc42 substantially disrupts the structure of the autoinhibited WASP domain.

Control experiments were performed to ensure that binding of Cdc42-GMPPNP to the sensor is responsible for the observed FRET changes. Cdc42-GDP did not induce FRET changes in either the GBD2 sensor (data not shown) or the N-GBD-VCA sensor (Figure 1-2A). Mutation of two conserved histidine

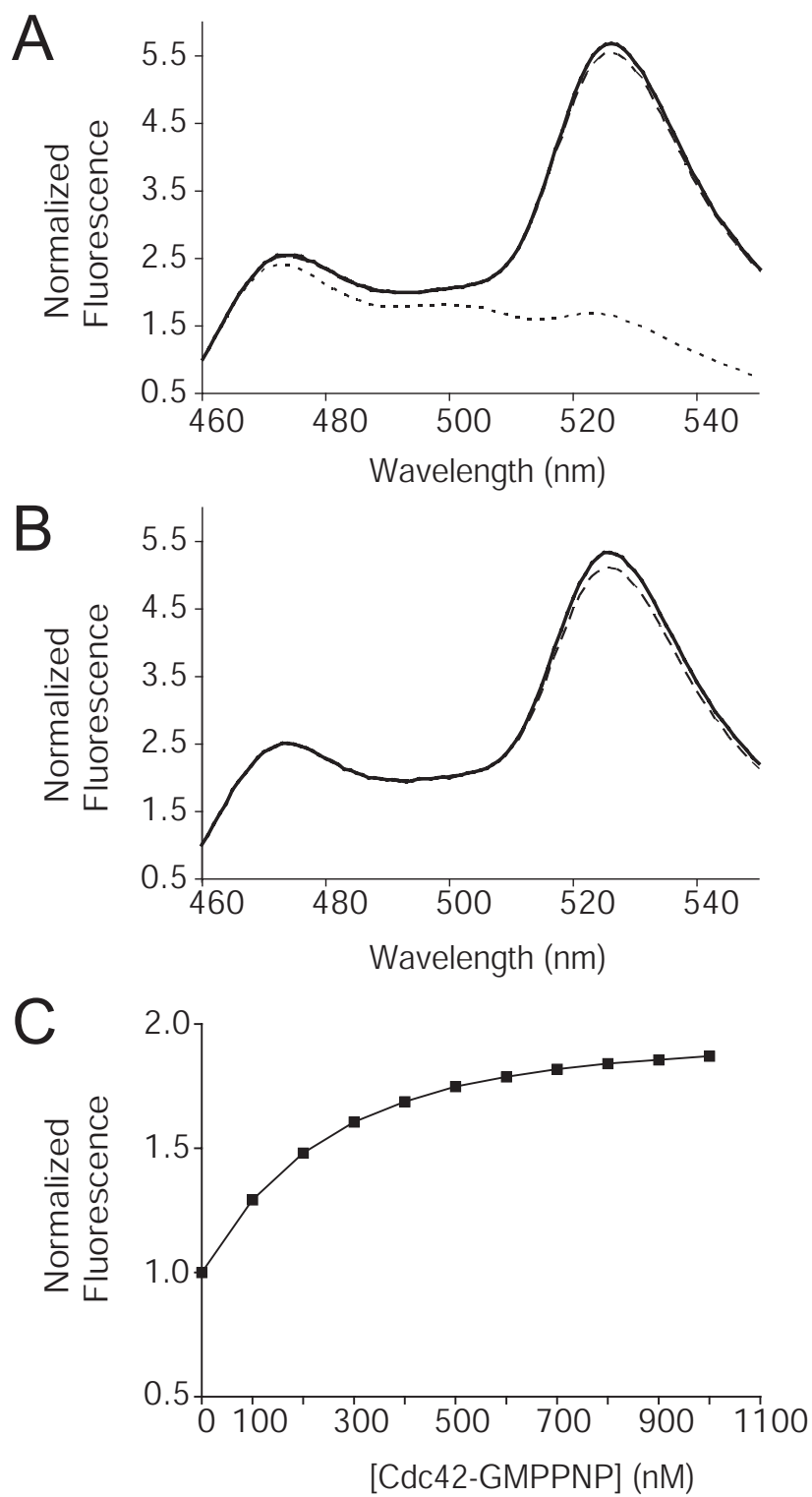


Figure 1-2

Figure 1-2. Biochemical Characterization of GBD-VCA Sensors.

- (A) Fluorescence emission spectra (excitation wavelength, $\lambda_{\text{ex}} = 433 \text{ nm}$) of $0.2 \text{ }\mu\text{M}$ N-GBD-VCA sensor free (—) and in the presence of $10 \text{ }\mu\text{M}$ Cdc42-GMPPNP (- - -) or $10 \text{ }\mu\text{M}$ Cdc42-GDP (— —).
- (B) Fluorescence emission spectra (excitation wavelength, $\lambda_{\text{ex}} = 433 \text{ nm}$) of $0.2 \text{ }\mu\text{M}$ N-GBD-DD-VCA sensor free (—) and in the presence of $10 \text{ }\mu\text{M}$ Cdc42-GMPPNP (- - -). Spectra are normalized to the emission at 460 nm .
- (C) Titration of $0.1 \text{ }\mu\text{M}$ N-GBD-VCA sensor with Cdc42-GMPPNP. Changes in CFP emission ($\lambda_{\text{em}} = 476 \text{ nm}$) are shown. The spectrum is normalized to the fluorescence emission in the absence of Cdc42. The line calculated by fitting the data to a single site binding model is shown. Standard deviations of each value, determined from three different titrations, are smaller than the data symbols.

residues in the CRIB motif (residues 211 and 214 in N-WASP) to aspartate has been shown to significantly decrease affinity for Cdc42 (Miki et al., 1998). When these mutations are introduced into the N-GBD-VCA sensor, the mutant protein, N-GBD-DD-VCA, has an initial FRET value of 2.14. Addition of Cdc42-GMPPNP at levels sufficient to saturate wildtype sensor decreases the FRET slightly, to a value of 2.04 (Figure 1-2B). The GBD2 sensor with analogous mutations also has a much weaker response to Cdc42-GMPPNP (data not shown). The slight decreases in FRET for these two mutant sensors are attributed to the residual affinity of the mutants for Cdc42, as discussed below. These results show that both the GBD-only and GBD-VCA sensor proteins are specific for the activated state of Cdc42 and that binding of the GTPase to the sensor protein is necessary for changes in FRET.

The GTPase-induced fluorescence changes were used to measure the binding affinity of each of the sensors for Cdc42-GMPPNP. Either changes in CFP fluorescence or YFP fluorescence could be modeled to an equation describing a 1:1 stoichiometric binding event to determine a dissociation constant (K_D) for the Cdc42-sensor interaction. The CFP-based binding curve for the N-GBD-VCA sensor yields a K_D of 178 nM (Figure 1-2C). As a control, sedimentation equilibrium analytical ultracentrifugation was used to demonstrate that the N-GBD-VCA sensor is indeed monomeric under the conditions of the *in*

vitro assay (data not shown, experiment performed by Dr. Derk D. Binns). The affinity measurements for all the other GBD and GBD-VCA sensors are listed in Table 1. In all instances, the GBD-only sensors have appreciably higher affinity for Cdc42-GMPPNP than the GBD-VCA sensors. These results are consistent with a model in which Cdc42 binding causes significant conformational rearrangement of the autoinhibited GBD-VCA structure and where the energy used to drive this change is drawn from energy inherent in the GBD-GTPase contacts (Buck et al., 2001; Kim et al., 2000a).

In parallel experiments, the affinities of the N-GBD-VCA and GBD1 sensors for Rac1-GMPPNP were determined to be $19.8 \pm 0.8 \mu\text{M}$ and $22.2 \pm 0.6 \mu\text{M}$, respectively (Figure 1-3). These results establish that the WASP-based biosensors have 100-1000-fold specificity for activated Cdc42 over activated Rac.

Titration of the N-GBD-DD-VCA mutant sensor yielded measurable FRET changes at relatively high concentrations of Cdc42-GMPPNP. The results indicate that the H211D/H214D mutations reduce the affinity of Cdc42 for the GBD from 178 nM to at least 250 μM , a difference of more than 1000-fold (Table 1). Thus, although these mutations have been reported to qualitatively abrogate GTPase binding, some residual affinity remains and binding will occur at high protein concentrations (Miki et al., 1998).

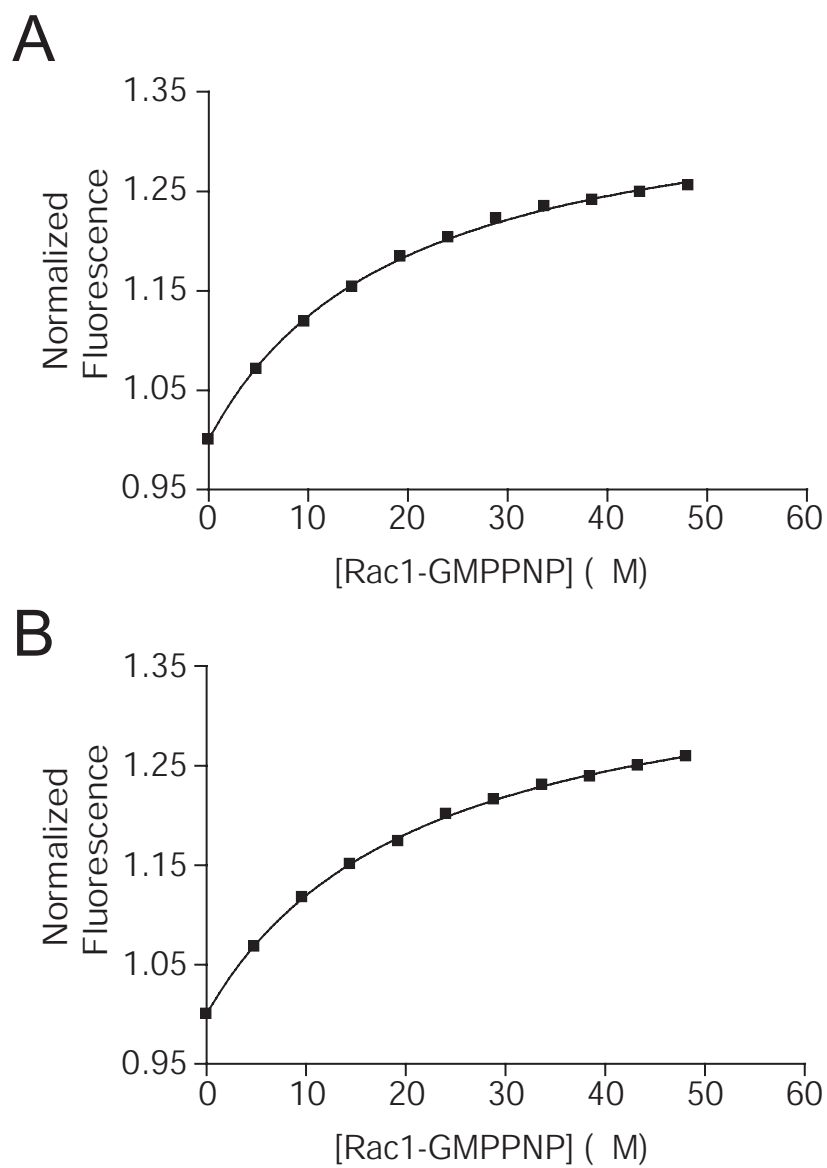


Figure 1-3

Figure 1-3. Affinity Measurements of Cdc42 Sensors for Rac1-GMPPNP.

- (A) Titration of 0.1 μ M N-GBD-VCA sensor with Rac1-GMPPNP. Changes in CFP emission ($\lambda_{\text{em}} = 476$ nm) are shown. The spectrum is normalized to the fluorescence emission in the absence of Rac1. The line calculated by fitting the data to a single site binding model is shown.
- (B) Titration of 0.1 μ M GBD1 sensor with Rac1-GMPPNP. Changes in CFP emission ($\lambda_{\text{em}} = 476$ nm) are shown. The spectrum is normalized to the fluorescence emission in the absence of Rac1. The line calculated by fitting the data to a single site binding model is shown.

The FRET-based affinity measurements for WASP-Cdc42 interactions are consistent with the values measured by isothermal titration calorimetry, and both methods yield affinities that are approximately 7-fold higher than the widely used strategies employing fluorescently-labeled GMPPNP (Rudolph et al., 1998; Rudolph et al., 2001).

Measurement of FRET in Living Cells Using Cdc42 Sensors

The ability of the Cdc42 sensors to measure GTPase activity *in vivo* was assessed using transiently transfected NIH 3T3 cells. Cells were transfected either with sensor alone or with sensor and Cdc42V12, a constitutively active mutant. FRET values were calculated by measuring the intensity of light emitted through CFP and YFP filters in response to sample excitation through a CFP filter. FRET values for an entire cell were measured by averaging the FRET at every point in the cell. The amount of sensor at each point was assumed to correlate with the intensity of YFP emission upon YFP excitation (Gordon et al., 1998). Representative cell images color-coded for FRET and intensity-normalized for sensor amount are shown in Figure 1-4, and whole cell FRET values are shown in Figure 1-5. Cells transfected with N-GBD-VCA sensor alone have an average FRET value of 1.66, compared to an initial FRET value of 2.23

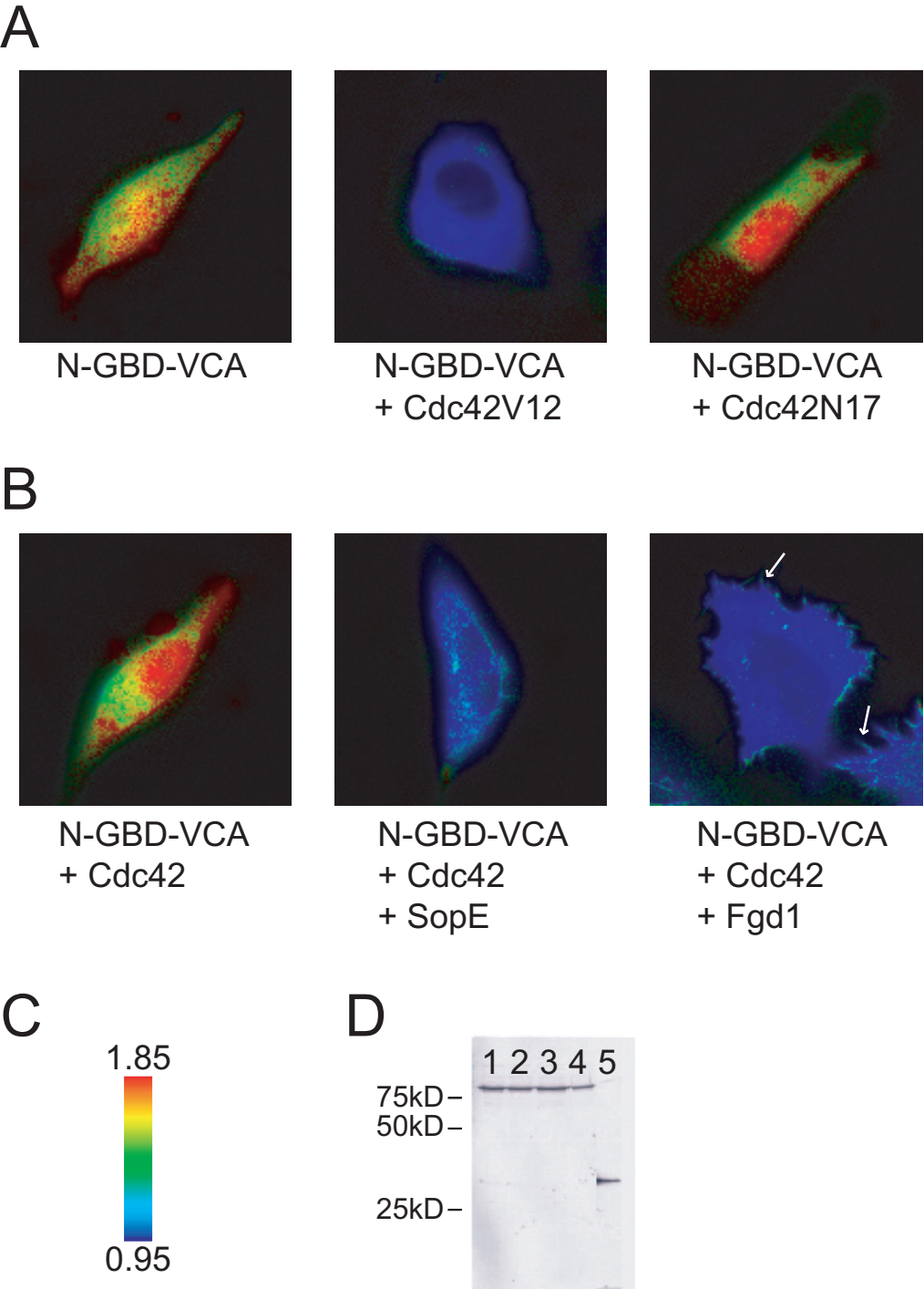


Figure 1-4

Figure 1-4. FRET Images of Transiently Transfected NIH 3T3 Cells.

- (A-B) Images of cells transfected with plasmids encoding the N-GBD-VCA sensor alone or together with the constructs indicated below each panel. Images have been color-coded to represent the sensor concentration and FRET value ($[\text{YFP channel emission intensity}]/[\text{CFP channel emission intensity}]$ upon CFP excitation) distribution throughout the cell. Color hues correspond to the FRET value. The numerical FRET range described by the color hues is depicted in the spectral bar shown in panel C. Intensity of each pixel is determined by the YFP channel intensity, which correlates with total sensor amount, at that position. Arrows indicate the position of filopodia. Images are representative of the results obtained after analyzing at least ten cells from a minimum of three different experiments for each condition.
- (C) Spectral bar depicting the numerical FRET range represented by the color scale in panels A and B.
- (D) Western blot, stained with an anti-GFP antibody, demonstrating sensor expression in cells transfected with plasmids encoding: Lane 1, N-GBD-VCA sensor; Lane 2, N-GBD-VCA sensor + Cdc42V12; Lane 3, N-GBD-DD-VCA sensor; Lane 4, N-GBD-DD-VCA sensor + Cdc42V12; Lane 5, GFP.

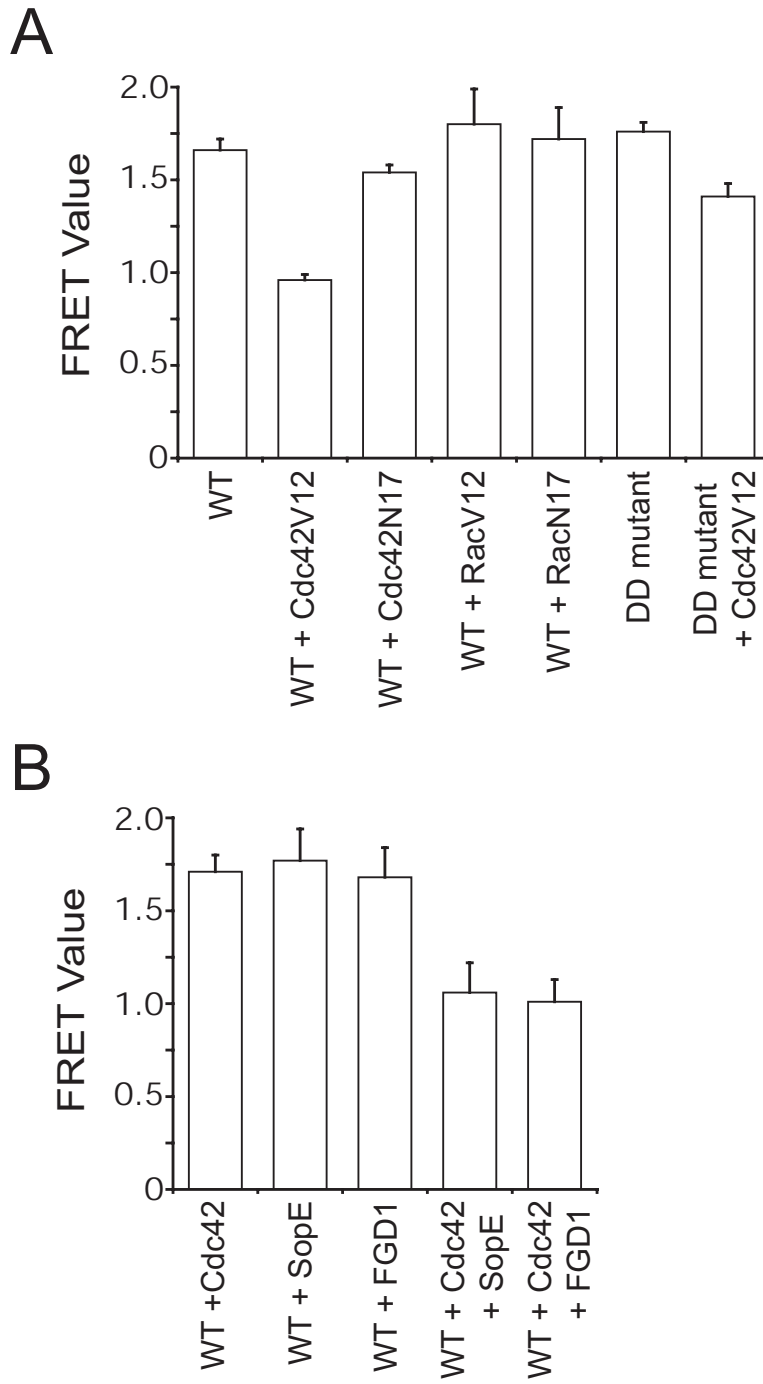


Figure 1-5

Figure 1-5. Quantitation of Cellular FRET Values.

Each bar represents the average cellular FRET value ($[\text{YFP channel emission intensity}]/[\text{CFP channel emission intensity}]$ upon CFP excitation) of ten cells transfected with the indicated plasmids. Error bars represent the standard deviations for a minimum of three different transfections for each condition.

- (A) Experiments with the N-GBD-VCA sensor, labeled as WT, and N-GBD-DD-VCA sensor, labeled as DD mutant, and various Rho GTPase mutants.
- (B) Experiments with the N-GBD-VCA sensor, labeled as WT, and different Cdc42 GEFs.

in vitro (Figures 1-4A, 1-5A, Table 1). The sensor appears to be uniformly distributed and most of the transfected cells maintain the spindled morphology typical of NIH 3T3 cells. The average FRET value decreases to 0.96 in cells cotransfected with sensor and Cdc42V12 (Figures 1-4A, 1-5A). The cells also become less elongated and sensor staining in the nucleus is observed to decrease. The overall FRET change for N-GBD-VCA is 1.7-fold *in vivo*, which compares favorably to analogous CFP/YFP-based sensors reported in the literature, but is 47% less than the 3.2-fold FRET change obtained *in vitro* (Table 1). Each of the Cdc42 sensors was tested in the *in vivo* assay and, in each case, cells transfected with sensor alone have a significantly higher FRET value than those cotransfected with sensor and Cdc42V12 (Table 1). The reduction in FRET change between the *in vivo* and *in vitro* experiments is greatest for N-GBD-VCA as the rest of the sensors show only 20-30% reductions. Despite the reduction of FRET change, each of the sensors does accurately report Cdc42 activity *in vivo*, and, in general, the sensors with the largest FRET changes *in vitro* also show the largest changes *in vivo*. The best *in vivo* sensor is B-GBD-VCA, which shows a 1.8-fold change in FRET in cells expressing activated Cdc42.

Several control experiments were performed with N-GBD-VCA to ensure that the FRET changes observed in cells are due to specific interactions between the sensor and activated Cdc42. When cells were cotransfected with sensor and

wildtype Cdc42 or Cdc42N17, a dominant inhibitory mutant which is believed to act by sequestering GEFs from wildtype GTPase, no significant reduction in FRET was observed (Figures 1-4, 1-5A) (Feig, 1999). Further, no FRET changes were measured in cells cotransfected with sensor and RacV12 or RacN17 (Figure 1-5A), consistent with the *in vitro* results, indicating the sensor is a specific monitor of Cdc42 activity *in vivo*. Finally, western blot analysis reveals that the observed changes in FRET are not due to sensor degradation, which could produce an artifactual decrease in FRET (Figure 1-4D).

In the presence of Cdc42V12, the N-GBD-DD-VCA mutant sensor did show a slight decrease in FRET value from 1.76 to 1.41, although the overall change is much less than for the wildtype sensor (Figure 1-5A). In the context of the transient transfection assay, this result is most likely attributable to the residual affinity of the mutant sensor for active GTPase. This is reasonable given the measured K_D value of 250 μ M for the interaction between mutant sensor and Cdc42, and previous reports that transiently expressed fluorescent proteins can reach cellular concentrations as high as 800 μ M using standard transfection protocols (Miyawaki et al., 1999).

Next, I examined whether the sensors could detect activation of wildtype Cdc42 upon stimulation with GEF by cotransfecting cells with sensor, Cdc42 and exchange factor. The FRET value decreases dramatically in these multiply

transfected cells containing either SopE, a potent Cdc42 exchange factor from *S. typhirium*, or the DH-PH module of Fgd1, a mammalian Cdc42 exchange factor (Figure 1-4B, 1-5B) (Hardt et al., 1998; Zheng et al., 1996). To test whether the sensors could detect activation of endogenous Cdc42, I cotransfected cells with only sensor and exchange factor. However, these conditions do not elicit detectable FRET changes in NIH 3T3 cells (Figure 1-5B). Therefore, with the technical conditions used for the present set of experiments, the sensors can detect activation of overexpressed wildtype Cdc42, but not endogenous protein.

Compared to cells cotransfected only with sensor and GEF, which have average FRET values of 1.76 and 1.69, for SopE and Fgd1, respectively, cells cotransfected with sensor, GEF and wildtype Cdc42 yield FRET values of 1.06 and 1.01. Thus, similar to the results with overexpression of Cdc42V12, transfection of either SopE or Fgd1 into Cdc42-supplemented cells causes a 1.7-fold reduction in FRET. Both SopE and Fgd1 induce filopodia and membrane ruffling, presumably due to GTPase activity, in the Cdc42-supplemented cells. However, the effect of Fgd1 is significantly greater in terms of number of filopodia per cell (Figure 1-4B). As a control, cells cotransfected with only sensor and Cdc42 do not display any significant morphological changes and have a high FRET value of 1.71, indicating that Cdc42 is not active on its own (Figure

1-4B, 1-5B). Taken together, these results demonstrate the ability of the Cdc42 sensors to specifically detect activated Cdc42 *in vivo*.

Discussion

Design and Validation

In this study, I sought to develop genetically encoded sensors that would specifically detect Cdc42 activity *in vivo* using intramolecular FRET. The sensors described here will report directly on the Cdc42 pathway, without interference from Rac, because they are based on the GBD regions of WASP and N-WASP, specific effectors of Cdc42. The successful creation of these sensors stems directly from the detailed understanding of the biophysical and biochemical characteristics of the Cdc42-WASP interaction. These structural insights allowed the development not only of sensors based on the GBD of WASP, but also the construction of molecules encompassing a larger region of WASP, the GBD-VCA, which was hypothesized, correctly, to undergo even larger FRET changes than the GBD alone.

There are a number of potential pitfalls associated with FRET-based imaging technologies that I have attempted to overcome in my design strategy

(Gordon et al., 1998). Whenever analyzing a FRET signal, one must ascertain that confounding factors, such as donor bleedthrough and direct acceptor emission, are not producing artificial results. Some GTPase sensors have been developed that utilize FRET-paired fluorophore-tagged GTPases together with fluorophore-tagged GBDs (Del Pozo et al., 2002; Hoppe and Swanson, 2004; Katsumi et al., 2002; Kraynov et al., 2000; Plafker and Macara, 2002; Tzima et al., 2003). These bimolecular strategies require proper accounting of relative donor and acceptor concentrations, since artifactual FRET changes can be observed if these are not uniform throughout the cell over the course of the experiment. Incorporating FRET-paired fluorophores into a single molecule simplifies the collection and analysis of FRET data (Gordon et al., 1998). Some bimolecular FRET studies have employed microinjection of one or both fluorescent partners, which limits their possible range of applications. However, in these cases, the scope of accessible small molecule fluorophores is much greater compared to studies limited to the genetically encoded fluorescent proteins. The primary advantage of this is that the fluorophores can be much brighter and smaller than their fluorescent protein counterparts, thereby endowing their probes with much greater sensitivity (Pertz and Hahn, 2004). The broad range of small molecule fluorophores with differing emission and excitation wavelengths also facilitates multi-color imaging applications. However, the palette of available fluorescent proteins is steadily increasing (Shaner et al.,

2005). While they do have some advantages, the principle drawback of current bimolecular strategies is that they do not have the potential to monitor endogenous GTPase activity because the protein being studied must be fluorescently labeled.

The sensors reported here are genetically encoded and can be easily delivered into many different cellular systems. With improved sensitivity they have the potential to monitor endogenous Cdc42. In addition, sensor-expressing stable cell lines can be generated. These benefits will afford a wide range of biological applications. These design considerations could also facilitate high-throughput screens for molecules able to modulate Cdc42 signaling *in vivo*, to control processes such as tumor metastasis (Boettner and Van Aelst, 2002).

Comparison with Other Unimolecular Ratiometric GTPase Sensors

Two general design strategies have been widely used to develop unimolecular CFP-YFP FRET-based sensors for small GTPases (Pertz and Hahn, 2004). One strategy, as described here, employs flanking a GTPase effector domain with CFP and YFP. These are true GTPase sensors as they respond directly to the concentration of activated GTPase. Such GTPase sensors have been developed for Cdc42, by the Rosen lab (described here), and for Cdc42, Rac

and Rho by others (Itoh et al., 2002; Seth et al., 2003; Yoshizaki et al., 2003). The other strategy employs fusing a GTPase with an effector domain and flanking the resulting GTPase-effector chimera with CFP and YFP. These sensors are substrates for the GEFs and GAPs that modulate GTPase activity and so they monitor the balance of upstream regulatory signals for a given GTPase. These types of probes, termed GEF-sensors, have been developed for Ras, Rap1, Cdc42, Rac and Rho (Itoh et al., 2002; Mochizuki et al., 2001; Seth et al., 2003; Yoshizaki et al., 2003).

Biochemical experiments in the Rosen lab have revealed that the Cdc42-GEF sensors respond to GAP proteins with slower kinetics than wildtype GTPases (Seth et al., 2003). These delayed kinetics are most likely due to protection of the GTPase moiety of the sensor from GAPs by the covalently tethered effector domain. Since all the existing GEF-sensors have similar molecular construction patterns, it is probable that they all exhibit slower responses to GAP proteins. Thus, sensors of this class may primarily be useful for monitoring the kinetics of GTPase activation, and may be more limited for studying processes requiring rapid GTP turnover. These limitations highlight the importance of development and utilization of complementary probes (e.g. sensors for both GTPases and GEFs) to allow timing issues to be more accurately studied.

The direct Cdc42 sensor developed by Itoh et. al. is based on the CRIB domain of PAK and so is not directly analogous to any of the WASP-based Cdc42 sensors I developed. Qualitatively, the PAK-based sensor yields FRET ratio changes similar to my GBD-only sensors, but the PAK-based sensor, by design, responds to both Cdc42 and Rac (Itoh et al., 2002). Quantitative comparisons are not possible due to the lack of published biochemical data on the PAK-based sensor.

Recently, a novel ratiometric imaging method has been developed for Cdc42 (Nalbant et al., 2004; Touthkine et al., 2003). This method employs conjugation of the WASP GBD to a bright, solvatochromic dye, whose fluorescence properties are very sensitive to its local chemical environment (Touthkine et al., 2003). Similar to the N-GBD-VCA sensor described here, the fluorescence of the dye-conjugated GBD increases approximately 3-fold upon binding Cdc42 *in vitro* (Nalbant et al., 2004; Touthkine et al., 2003). Presumably, Cdc42-induced conformational changes in the GBD affect the fluorescence of the dye by significantly reducing its degree of solvent-exposure (Nalbant et al., 2004). Conjugating the dye to a GBD-GFP fusion protein, resulted in a ratiometric sensor for Cdc42, called MeroCBD (for merocyanine dye conjugated to Cdc42 Binding Domain), where the GFP fluorescence is Cdc42-independent and the dye fluorescence is Cdc42-dependent (Nalbant et al., 2004).

Like the FRET-based ratiometric sensors, the MeroCBD sensor can be used to quantitatively measure Cdc42 activity *in vivo*. Using assays similar to the ones described here, MeroCBD exhibits a 3-fold change in ratio in fibroblast cells expressing constitutively active Cdc42 compared to wildtype cells (Nalbant et al., 2004). This result is better than for any of the FRET-based sensors reported thus far. MeroCBD has already been used to understand the role of Cdc42 in regulating membrane protrusions in motile cells and should have important applications in the future (Nalbant et al., 2004). Even though MeroCBD must be microinjected into cells, it will be useful particularly because of its high sensitivity and large dynamic range.

Future Directions

Using the FRET-based biosensors reported here, it should be possible to obtain detailed spatial and temporal information on Cdc42 responses evoked by various stimuli. The current experimental conditions did not allow direct observation of endogenous Cdc42 activation and activity could only be detected in cells supplemented with Cdc42. In the model *in vivo* system presented here, exchange factors induce a relatively uniform activation of Cdc42 throughout the cell. This uniform activation is likely due to the high levels of Cdc42 found in

these cells and an important future goal is to determine how the pattern of Cdc42 activation differs in cells expressing endogenous levels of GTPase. It is possible that endogenous Cdc42 activity is not observed in my model system because the relative concentration of sensor to Cdc42 is too high, which results in a high background level of unbound sensor even under maximal activation.

To suppress this background noise, either Cdc42 will have to be expressed ectopically, thereby artificially increasing its cellular concentration, or the sensors will have to be produced at much lower concentrations in the cell. Since the goal of these studies is to study endogenous signaling pathways, efforts should be focused on achieving the latter by creating low-expression level cell lines. But low-expression will have to be balanced with detection sensitivity and brighter fluorophores may have to be considered for applications where high background autofluorescence interferes with CFP or YFP detection.

Another issue is that active Cdc42 is membrane localized, while inactive Cdc42 is sequestered in the cytosol by RhoGDI (Symons and Settleman, 2000). It is not clear how interaction with RhoGDI affects the ability of the sensors to detect GTPase activity, but membrane targeting of the sensors could likely eliminate the confounding observation of GDI complexes. Membrane localization will also increase the sensitivity of the probes by restricting them to the sites of Cdc42 action, thereby eliminating the high background signal from

physiologically irrelevant sensor in the cytosol. Indeed, plasma membrane targeting is necessary for detecting endogenous Cdc42 activity in motile cells using the direct Cdc42 sensor developed by Itoh et. al. (Itoh et al., 2002). However, Cdc42 must transit several distinct types of membrane systems, such as Golgi, plasma and vesicular membranes, to carry out its many varied functions (Ridley, 2001). The specific membrane-targeting signal used to control sensor localization may bias the membrane distribution of the sensor and may only allow a subset of Cdc42-dependent processes to be observed. This could be overcome by using different targeting sequences for different applications. Evanescent wave microscopy, a particularly sensitive technique for observing events proximal to the microscope objective, may also prove useful for studying certain aspects of Cdc42 biology. Confocal imaging may be useful for other applications. It is unlikely that any single sensor system will address all the complexities associated with Cdc42. Therefore, the optimal study of GTPase signaling *in vivo*, will likely require the use of several complementary reagents, methods and technologies. Several possible strategies have been described above and implementing these devices is an important goal for the future.

Thus far, I have created a series of Cdc42 sensors varying 100-fold in terms of their affinity for active Cdc42. Consistent with a sequestration model of VCA activation, the GBD-only sensors have higher affinities for active Cdc42,

while the GBD-VCA sensors possess the highest FRET ratio changes. Theoretically, both the high affinity and the high ratio sensors should be of value in further *in vivo* studies. In applications where sensitivity is an issue, the high affinity sensors should enable detection of relatively low amounts of Cdc42 activation. In other instances, the high ratio-changing sensors should serve to more finely describe the range of Cdc42 activation levels that can be achieved in the cell. Thus, not only will the sensors be used to determine the spatial and temporal characteristics of Cdc42 activation in response to various stimuli, they could also be used for quantitatively analyzing the amount of Cdc42 that becomes activated by each stimulus. By comparing and contrasting the activation profile of Cdc42 in response to various stimuli, it might be possible to understand the molecular basis for the pleiotropic cellular actions of Cdc42.

These results show that the Cdc42 sensors are faithful reporters of Cdc42 signaling pathways *in vivo*. I have established the feasibility of using these sensors for studying the real-time dynamics of endogenous Cdc42 in living cells. In future applications, these sensors have the potential to address unanswered questions about Cdc42 biology and elucidate general principles regarding the proper regulation of cellular signal transduction.

CHAPTER 2

Sensor Optimization and Development of Imaging Assays for Cdc42-Mediated Biological Processes

Abstract

To better understand the molecular mechanisms by which Cdc42 regulates the actin cytoskeleton, it will be necessary to determine if and how the level, localization and timing of Cdc42 activity correlate with particular cytoskeletal structures and rearrangements. The proof-of-principle experiments described in the previous chapter demonstrated the feasibility of using genetically-encoded, FRET-based Cdc42 sensors to monitor Cdc42 activity in living cells. This chapter describes efforts to improve the sensitivity of the original, soluble FRET-based probes by targeting them to cellular membranes, the sites of Cdc42 action. The optimized sensors were then used to establish imaging assays for three biological processes that depend on Cdc42-mediated cytoskeletal rearrangements: membrane ruffling during cell spreading, T cell activation and Fc- γ receptor

mediated phagocytosis. The experimental complexities and future prospects of FRET-based imaging for each of these systems will be discussed. In addition, parallel experiments using non-FRET-based imaging reagents have started to yield interesting insights into the dynamics of Cdc42 activation during T cell activation and Fc- γ receptor mediated phagocytosis.

Introduction

After the initial construction and validation of the FRET-based Cdc42 sensors described in the previous chapter, I focused my efforts on achieving two objectives. The first was to engineer improved sensors that could monitor endogenous Cdc42 activity, as compared to the original sensors which could only be used in cells supplemented with additional Cdc42 (described in previous chapter). The second was to establish a cellular model system in which the sensors could be used to answer questions about Cdc42 signaling in a physiologically meaningful setting. Here, I will describe the progress made in achieving both of these objectives.

As discussed in the previous chapter, addition of membrane targeting sequences to the sensors may increase their sensitivity, and thereby facilitate detection of endogenous Cdc42. Many of the previously described unimolecular FRET-based GTPase sensors incorporate membrane localization sequences which may indicate that this is a necessary design feature (Itoh et al., 2002; Mochizuki et al., 2001; Yoshizaki et al., 2003). Here, I will describe the different membrane targeting strategies that were employed and analyze their effects on sensor function.

FRET-based GTPase sensors have been used to study Rho GTPase signaling in a variety of processes including cell motility, EGF-induced membrane ruffling, neutrophil chemotaxis, Fc- γ receptor mediated phagocytosis and cell division (Gardiner et al., 2002; Hoppe and Swanson, 2004; Itoh et al., 2002; Kraynov et al., 2000; Kurokawa et al., 2004; Yoshizaki et al., 2003). Even though these studies have described the spatial and temporal patterns of Cdc42 activation during these processes, key questions still remain as to how much GTPase gets activated during a given process and if, and by what mechanisms, the degree of Cdc42 activation is correlated with specific cytoskeletal rearrangements. With these questions in mind, the Cdc42 sensors described in the previous chapter were applied towards understanding various actin-cytoskeleton-dependent biological processes including membrane ruffling during cell spreading, T cell activation by B cells and Fc- γ receptor mediated phagocytosis.

Although the model systems studied are quite biologically disparate, much of the work described here involved the development of general protocols for adapting biological assays to the microscope stage. Ultimately, sensitivity issues prevented the development of reproducible and robust FRET-based assays for membrane ruffling, T cell activation or phagocytosis. However, these systems are amenable to study by non-FRET imaging reagents and I have been able to develop GFP-based reagents which can shed meaningful insights into Cdc42

biology, particularly during T cell activation and Fc- γ receptor mediated phagocytosis. The former results are presented here and the latter in the following chapter.

Experimental Procedures

Constructs

All membrane tethered sensor constructs were created using standard PCR and cloning techniques. Mutant constructs were generated using PCR or using the QuikChange Site-Directed Mutagenesis Protocol (Stratagene). GTPase constructs for mammalian expression were provided by Dr. Melanie H. Cobb (UT Southwestern). SopE cDNA was provided by Dr. Jorge Galan (Yale University). FGD1 cDNA was provided by Dr. Yi Zheng (Cincinnati Children's Hospital Medical Center).

Cell Culture and Microscopy

Imaging Systems

For NIH 3T3 fibroblasts and RAW macrophages, microscopy was performed on a Zeiss Axiovert 200M inverted microscope equipped with a 75 W

xenon lamp. Fluorescence images were acquired using a 10% ND filter. Images were collected using fluorescence filter sets from Chroma and a Sensicam CCD camera (PCO Computer Optics). Slidebook software (Intelligent Imaging Innovations) was used to acquire and analyze the images.

T cell imaging was performed using a Nikon TE2000-S inverted microscope equipped with a Lambda DG-4 xenon arc lamp/wavelength switcher (Sutter Instruments). Images were collected using fluorescence filter sets from Chroma and a Princeton Instruments CCD camera (Roper Scientific, model RTE/CCD-1300-Y/HS). Metamorph software (Molecular Devices) was used to acquire and analyze the images.

Other imaging parameters varied between experiments and are detailed below.

Characterization of Membrane Tethered Sensors

The cell culture, FRET imaging and data analysis methods for these assays were identical to those described in the previous chapter.

Cell Adhesion and Spreading Assays

NIH3T3 cells were maintained, transfected and imaged as before except for the following differences. Transfections of NIH 3T3 cells were performed in 6-well dishes. 24 hours after transfection, cells were trypsinized and resuspended in Leibovitz's L-15 CO₂-independent medium containing 10% FBS (Invitrogen). Cells were then replated on 35 mm glass bottom dishes and incubated in a CO₂-free incubator at 37 °C. 4 hours after replating, cells were transferred to the microscope stage. During imaging, the heated stage was maintained at 37 °C while connected to a humidifier module (Zeiss). To further prevent media evaporation, the cells were covered with an optically clear FoilCover (Zeiss). The 100X oil-immersion objective was also maintained at 37 °C using an objective heater.

Timelapse microscopy was performed for various lengths of time depending on the experiment. For each timepoint, 4 images, CFP, YFP, FRET and DIC were acquired using 2X2 binning. Typically, 400 ms exposures were used to capture the CFP and FRET images, 80 ms exposures were used for YFP images and 50-100 ms exposures were used for DIC images. Background subtraction was based on cell-free regions of each image. For each timepoint, the FRET/CFP channel intensity ratio (defined as the FRET value) was calculated for every pixel in the image.

T cell Activation Assays

Retrovirally-transduced, *in vitro*-primed primary T cells were obtained as described previously (Tskvitaria-Fuller et al., 2003). Briefly, a Moloney murine leukemia virus-derived retroviral expression system was used for these studies (Costa et al., 2000). Standard cloning techniques were used to insert various sensor constructs into the previously described pGC or pGCGK retroviral expression plasmids (Costa et al., 2000; Tskvitaria-Fuller et al., 2003). The sensor-encoding plasmids were then transfected into Phoenix-E cells, a retrovirus-producing cell line derived from 293T cells, using a calcium phosphate precipitation method (Costa et al., 2000; Pear et al., 1993). After 60 hours, the Phoenix-E cells were imaged on a fluorescence microscope to verify sensor expression and judge transfection efficiency. Virus-containing supernatants from the Phoenix-E plates were then used to transduce primary T cells isolated from 5C.C7 TCR transgenic mice. The 5C.C7 TCR binds to moth cytochrome C (MCC) peptide (residues 92-103) presented on I-E^k (Seder et al., 1992). After 4 days, fluorescent T cells were isolated by FACS. The sorted T cells were allowed to expand for 3-4 days before being used for imaging assays. CH27 cells, a B cell lymphoma cell line, were loaded with 10 μ M MCC and used as APCs to activate the T cells during imaging.

For imaging, T cells and APCs were resuspended in imaging media (PBS, 1 mM MgCl₂, 1 mM CaCl₂ and 10% FBS) immediately prior to being moved to the microscope stage. The microscope and 40X objective were maintained at 37 °C during imaging. APCs were added to one well of an 8-chambered cover glass slide (Lab-Tek, Nunc) and allowed to settle to the bottom of the chamber. T cells were then added slowly to the chamber with minimal disturbance of the settled APCs. Once a suitable field was identified, a 15 minute timelapse acquisition was started. One DIC image and a z-stack of GFP images were acquired every 20 seconds using 2X2 binning. The GFP z-stack covered the entire height of the T cell and consisted of 21 images spaced 1 µm apart. Exposure time was 200 ms for the DIC image as well as for each GFP image in the z-stack.

For each acquisition, the number of T cell-APC couples and the times at which they formed were determined. The GFP signal at the T cell/APC interface was analyzed at different time points before and after couple formation. Three-dimensional reconstructions of each couple were generated as previously described (Wulfiging et al., 2002) and used to determine the sensor accumulation pattern at different times as discussed in the text. For FRET-based imaging, this basic protocol would have been modified to accommodate the increased number of fluorescent images that would have been acquired. However, the low CFP

detection sensitivity prevented FRET-based experiments in this system and so a standardized FRET protocol was not established.

Fc- γ Receptor Mediated Phagocytosis Assays

RAW 264.7 cells were purchased from the ATCC and maintained in DMEM containing 10% FBS and 1 mM sodium pyruvate (Invitrogen). Cells were transfected with 5 μ g total DNA using Lipofectamine 2000 according to the manufacturer's protocol (Invitrogen). Cells were seeded into 6-well plates at a density of 1×10^6 cells/well one day prior to transfection. IgG-opsonized sheep red blood cells (RBCs) (Colorado Serum Company) were prepared for Fc- γ receptor mediated phagocytosis essentially as described previously (Greenberg et al., 1990). RBCs (80-100 μ L packed cell volume) were washed with 1 mL BWD buffer (20 mM HEPES [pH7.4], 125 mM NaCl, 5 mM KCl, 5 mM glucose, 10 mM NaHCO₃, 1 mM KH₂PO₄, 1 mM MgCl₂, 1 mM CaCl₂) 2 times and opsonized with subagglutinating concentrations of rabbit anti-sheep RBC IgG (ICN Pharmaceuticals) for 20 minutes at 37 °C, followed by a 20 minute incubation at 4 °C. Opsonized RBCs were pelleted by centrifugation at 2500 rpm for 5 minutes. The RBCs were washed 3 times with 1 mL BWD buffer and then resuspended in 1 mL BWD and stored at 4 °C.

24 hours after transfection, RAW cells were washed and scraped into 1 mL of fresh medium. The resuspended cells were plated onto 35 mm glass-bottom dishes (MatTek) and allowed to adhere for 6-8 hours. 1 hour prior to imaging, cells were washed with BWD 3 times and returned to the 37 °C incubator in 1 mL of BWD. For imaging, cells were incubated at 37 °C on a heated stage connected to a humidifier module (Zeiss). To further prevent media evaporation, the cells were covered with an optically clear FoilCover (Zeiss). To start phagocytosis, 1 mL of 50-fold diluted opsonized RBCs was added dropwise to the macrophages on the microscope stage. In the next 5-10 minutes, a fluorescent macrophage was selected for observation and then image acquisition was started.

For each imaging run, 61 timepoints were collected and each image was acquired using 2X2 binning and a heated 63X objective. In early experiments with the CFP-based sensor, a single plane was imaged throughout the entire acquisition. At each timepoint, a CFP, YFP, FRET and DIC image was collected. Exposure times were 1000 ms for the CFP and FRET channels, 200 ms for the YFP channel and 50-100 ms for the DIC channel. The images were collected at maximum speed, which resulted in 1 timepoint acquired every 9 seconds. For later experiments with the cerulean-based sensor, a 3 plane z-stack of fluorescent images, spaced 2.0 μm apart, was acquired at each timepoint. In each plane, a CFP, YFP and FRET channel was collected. In addition, one DIC image was

acquired at each timepoint. Using cerulean, the CFP and FRET exposure times were reduced to 400 ms. The images were collected at maximum speed, which resulted in 1 timepoint acquired every 14 seconds.

Each fluorescent image was background corrected based on cell-free regions of the image. For each phagocytic event, the optimal plane (where the phagocytic cup was in best focus as judged by eye) was determined at each timepoint (only necessary for the imaging experiments in which multiple planes were acquired). The best planes were then stitched together to create a 2D timelapse imaging series for each phagocytic event. For each event, the timepoint at which pseudopod fusion occurred, visualized most easily in the fluorescent images, was set as the zero time reference (Marshall et al., 2001). Only events in which the macrophage and RBC could be observed 8 timepoints before fusion and 23 timepoints after fusion were further analyzed.

To analyze FRET changes during phagocytosis the average CFP/FRET ratio was calculated for the portion of the cell in contact with the RBC. For every timepoint, a mask was created around the region of contact between the macrophage and the RBC. For early timepoints, the mask is flat and represents the binding site of the RBC on the macrophage. As the pseudopods advance along the perimeter of the RBC, the mask becomes U-shaped and encompasses the two pseudopods as well as the base of the phagocytic cup. At fusion and subsequent timepoints, the mask forms a circle around the RBC. For each pixel in

each mask at each timepoint, the ratio of CFP intensity to FRET intensity was calculated. The ratio values for each mask were then averaged together to generate an average CFP/FRET ratio at the site of phagocytosis at every timepoint. These ratios were used to generate the pseudocolored images and graphical data shown in Figure 2-8.

Results

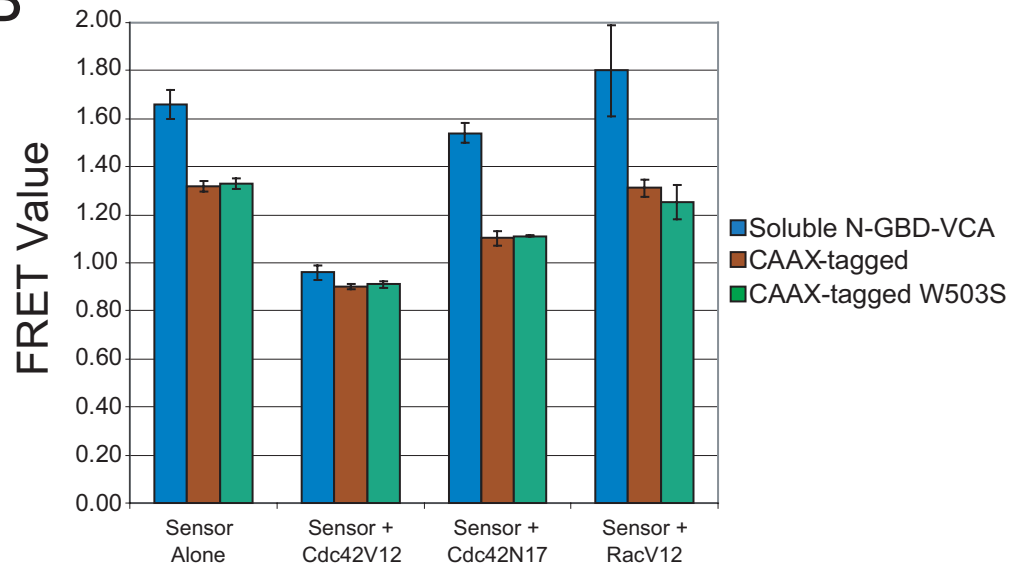
Membrane Targeting of Cdc42 Sensors

To help improve sensitivity, membrane targeting sequences were fused to the Cdc42 FRET sensors described in the previous chapter. Two different membrane tethers were chosen: the C-terminal CaaX box of Cdc42 and the plasma membrane targeting motif of neuromodulin. Many small GTPases are localized to membranes via prenylation of their unique CaaX boxes (Clarke, 1992). The specific membranes to which the GTPase is localized varies depending on the sequence composition of the ~20 residues adjacent to and including the CaaX box (Choy et al., 1999; Michaelson et al., 2001). To create a sensor whose localization would closely match that of endogenous Cdc42, the C-terminal 14 residues (including CaaX box) of Cdc42 itself were used as the membrane targeting signal (Figure 2-1A). In addition, since many important

A

CAAX-tag Sequence: }EPPEPKKSRRCVLL

PM-tag Sequence: MLCCMRRTKQVEKNDEDQKI{

B**C**

CAAX-tagged Sensor

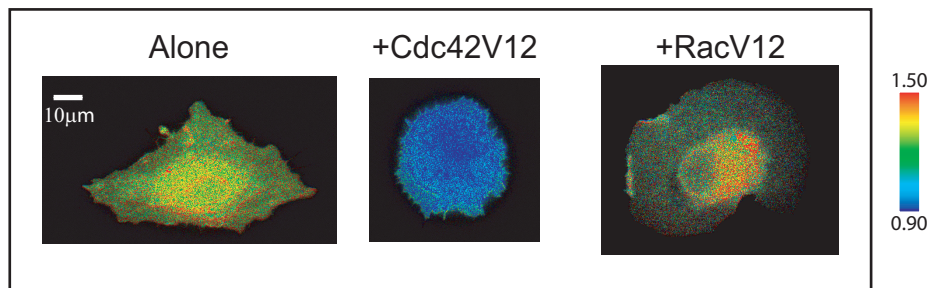


Figure 2-1

Figure 2-1. Characterization of CAAX-Tagged FRET-Based Cdc42 Sensors.

- (A) Amino acid sequences of the C-terminal CAAX-tag and the N-terminal PM-tag used in this work to target the FRET-based sensors to membranes.
- (B) Each bar represents the average cellular FRET value ($[\text{YFP channel emission intensity}]/[\text{CFP channel emission intensity}]$ upon CFP excitation) of at least ten cells transfected with the indicated sensor and GTPase mutants. Error bars represent the standard deviations for a minimum of three different transfections for each condition.
- (C) Images of cells transfected with plasmids encoding the N-GBD-VCA-W503S-CAAX sensor alone or together with the indicated GTPase mutant. Images have been color-coded to represent the sensor concentration and FRET value ($[\text{YFP channel emission intensity}]/[\text{CFP channel emission intensity}]$ upon CFP excitation) distribution throughout the cell. Color hues correspond to the FRET value. The numerical FRET range described by the color hues is depicted in the spectral bar adjacent to the panel of images. Intensity of each pixel is determined by the YFP channel intensity, which correlates with total sensor amount, at that position. Images are representative of the results obtained after analyzing at least ten cells from a minimum of three different experiments for each condition.

Cdc42 functions occur at the plasma membrane, the N-terminal 20 residues of neuromodulin, a plasma membrane-specific targeting sequence that is doubly palmitoylated, was also used (Figure 2-1A) (Isshiki et al., 2002).

To test the effects of membrane tethering, the membrane targeting sequences were fused to the N-GBD-VCA sensor (described in the previous chapter), which is the most fully characterized sensor that I have developed (Seth et al., 2003). The CaaX box was fused to the C-terminus to create N-GBD-VCA-CAAX and the neuromodulin sequence was fused to the N-terminus to create PM-N-GBD-VCA. The FRET responses of the resulting sensors were analyzed in NIH 3T3 cells transfected with sensor and various Rho GTPase mutants. This assay is identical to the one described in the previous chapter for measuring the *in vivo* responses of the original, soluble FRET-based Cdc42 sensors (Seth et al., 2003).

Cells transfected with the N-GBD-VCA-CAAX sensor alone have an average FRET value of 1.32 (Figure 2-1B). The average FRET value decreases to 0.90 in cells cotransfected with CAAX-tagged sensor and Cdc42V12 (Figure 2-1B). The comparable values for the soluble N-GBD-VCA sensor are 1.66 and 0.96, respectively (Figure 2-1B) (Seth et al., 2003). By widefield microscopy, it appears that the sensor is enriched at the plasma membrane (based on higher relative intensity at discernible leading edges) and at internal membranes, but

confocal microscopy has not been performed to establish the precise localization of the CAAX-tagged sensor. Cotransfection of Cdc42N17, a dominant negative mutant, decreases the average FRET value of the CAAX-tagged sensor to 1.10, while it has no significant effect on the soluble sensor (Figure 2-1B) (Seth et al., 2003). Cotransfection of constitutively active Rac1 has no effect on the CAAX-tagged sensor or the soluble sensor (Figure 2-1B) (Seth et al., 2003). Representative images in Figure 2-1C, color-coded for FRET and intensity-normalized for sensor amount, depict cells transfected with CAAX-tagged sensor alone or together with constitutively active GTPase mutants. These results show that the CAAX-tagged sensor, like the soluble sensor, is a specific monitor of Cdc42 *in vivo*.

Another modification was made to the CAAX-tagged sensor to prevent undesired interactions with endogenous cellular components. The VCA domains of WASP and N-WASP interact with Arp2/3 complex and a W500S mutation in WASP blocks this interaction (Higgs and Pollard, 1999; Marchand et al., 2001). To prevent the VCA-moiety of the CAAX-tagged sensor from interacting with endogenous Arp2/3 complex, the analogous N-WASP mutation was introduced into the CAAX-tagged sensor to create N-GBD-VCA-W503S-CAAX. The CAAX-tagged W503S mutant was transfected alone or together with Cdc42V12, Cdc42N17 or RacV12. In all cases, the responses were identical to the wildtype

CAAX-tagged sensor, indicating that the W503S mutation did not affect the FRET properties of the sensor (Figure 2-1B).

The lower FRET value in cells expressing CAAX-tagged sensor alone compared to soluble sensor alone could be due to increased sensitivity of the CAAX-tagged sensor for endogenous Cdc42 activity, which was the originally anticipated outcome of membrane tethering. However, the lower ratio of the CAAX-tagged sensor could also be due to non-specific membrane effects that could alter the inherent FRET efficiency of the sensor. One way to accurately assess sensitivity differences between the soluble and CAAX-tagged sensors would be to measure a dose-response curve for the FRET value as a function of defined amounts of Cdc42 activation. Technically, however, it is not possible to induce defined amounts of GTPase activation. Instead, I have attempted to measure only the end points of the FRET response to Cdc42 activation. Cotransfection of Cdc42V12 is taken as a model for maximal Cdc42 activation and induces similar, low FRET values in both the CAAX-tagged and soluble sensors (Figure 2-1B). Cotransfection of Cdc42N17 was supposed to be a model for complete absence of Cdc42 activity; however, the response of the CAAX-tagged sensor to this mutant suggests that this assumption is incorrect. Indeed, the N17 mutant may have residual affinity for WASP. The soluble sensor does not respond to Cdc42N17, but the strong FRET response of the CAAX-tagged

construct suggests that the N17 mutant can activate the CAAX-tagged sensor either through direct binding or through indirect membrane effects (Figure 2-1B). Given the problematic nature of the N17 mutant, it is unclear what the FRET value for each sensor would be in the absence of Cdc42 activity. Other strategies for inhibiting endogenous Cdc42 activity such as transfection of GAP proteins or silencing by RNA interference could be useful for future FRET calibration studies. Thus, at present, it is unclear if the different FRET values of the CAAX-tagged sensor alone or the soluble sensor alone are due to different sensitivities to basal levels of endogenous Cdc42 activity or to inherent differences in the FRET responses of the two sensors.

Next, I tested the FRET responses of the PM-N-GBD-VCA-W503S sensor. Cells transfected with the PM-N-GBD-VCA-W503S sensor alone have an average FRET value of 1.29 (Figure 2-2A). The average FRET value decreases to 0.84 in cells cotransfected with PM-tagged sensor and Cdc42V12 (Figure 2-2A). As with the CAAX-tagged sensor, confocal microscopy has not been performed to confirm the precise localization of the PM-tagged sensor, although by widefield microscopy it does appear to be concentrated at the plasma membrane. Both the CAAX-tagged sensor and the PM-tagged sensor have similar FRET values in cells expressing sensor alone, but the FRET value, when

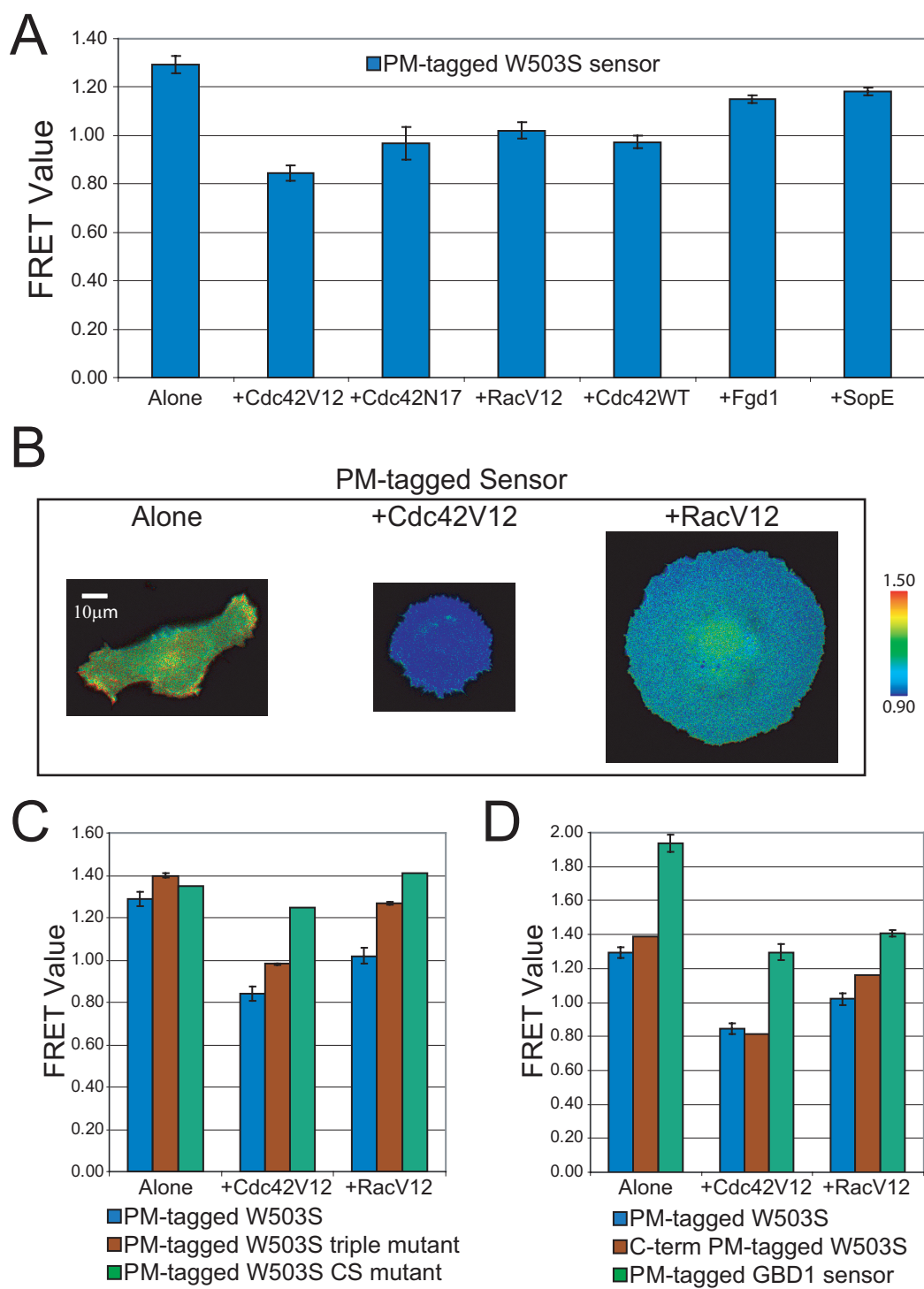


Figure 2-2

Figure 2-2. Characterization of PM-Tagged FRET-Based Cdc42 Sensors.

- (A) Each bar represents the average cellular FRET value ($[\text{YFP channel emission intensity}]/[\text{CFP channel emission intensity}]$ upon CFP excitation) of at least ten cells transfected with the PM-N-GBD-VCA-W503S sensor alone or together with the indicated GTPase or GEF constructs. Error bars represent the standard deviations for a minimum of three different transfections for each condition.
- (B) Images of cells transfected with the PM-N-GBD-VCA-W503S sensor alone or together with the indicated GTPase mutant. Images have been color-coded to represent the sensor concentration and FRET value ($[\text{YFP channel emission intensity}]/[\text{CFP channel emission intensity}]$ upon CFP excitation) distribution throughout the cell. Color hues correspond to the FRET value. The numerical FRET range described by the color hues is depicted in the spectral bar adjacent to the panel of images. Intensity of each pixel is determined by the YFP channel intensity, which correlates with total sensor amount, at that position. Images are representative of the results obtained after analyzing at least ten cells from a minimum of three different experiments for each condition.
- (C-D) Each bar represents the average cellular FRET value ($[\text{YFP channel emission intensity}]/[\text{CFP channel emission intensity}]$ upon CFP excitation) of at least ten cells transfected with the indicated sensor and GTPase mutants. Where shown, error bars represent the standard deviations for a minimum of three different transfections for each condition.

cotransfected with Cdc42V12, is slightly lower for the PM-tagged sensor. As discussed above, it is possible that the differences in FRET values between different sensors are due to differing sensitivities for Cdc42 activity; however, without knowing the *in vivo* FRET response to different defined amounts of Cdc42 activity, this conclusion can not be stated with certainty. In contrast to the soluble sensor (previous chapter) (Seth et al., 2003), coexpression of the PM-tagged sensor and a Cdc42 GEF, either the DH-PH module of Fgd1 or SopE, results in a slight, but reproducible reduction in the FRET value to 1.15 or 1.18, respectively (Figure 2-2A), which suggests that the PM-tagged sensor may be able to detect activation of endogenous Cdc42. Unfortunately, the change in FRET value compared to cells expressing PM-tagged sensor alone is small (~10%). If transfection of Fgd1 or SopE results in physiological levels of Cdc42 activation, then this suggests that the dynamic range of the PM-tagged sensor will be small during biological events mediated by Cdc42; unfortunately there is no reliable data to support or refute this claim. Therefore, experiments with the PM-tagged sensor were continued under the hypothesis that localized activation of GEFs during biological events would produce high local concentrations of activated GTPase that are not achieved simply by overexpression of GEF proteins.

As with the CAAX-tagged sensor, the Cdc42N17 mutant causes an unexpected decrease in the FRET value to 0.97 for the PM-tagged sensor (Figure 2-2A). Coexpression of wildtype Cdc42 and the PM-tagged sensor also reduces the FRET value to 0.97 (Figure 2-2A). In contrast to the CAAX-tagged or soluble sensors, coexpression of PM-tagged sensor and RacV12 also caused a reduced FRET value of 1.02 (Figure 2-2A). The response to Rac was unexpected, but not unexplainable. As shown in the previous chapter, the N-GBD-VCA sensor has a ~ 20 μM affinity for Rac (Seth et al., 2003). Since both Rac and the PM-tagged sensor are enriched at the plasma membrane, it is possible that the high local concentration of both proteins allows them to interact and thereby affects the FRET response of the sensor. Indeed, the unexpected FRET responses to Cdc42N17 and wildtype Cdc42 could also be explained by low affinity interactions that manifest at the high local concentrations achieved by localizing the sensor to the plasma membrane. Alternatively, Cdc42N17, wildtype Cdc42 and RacV12 could all exert indirect membrane effects, of unknown nature, that influence the FRET response of the sensor. Representative images in Figure 2-2B, color-coded for FRET and intensity-normalized for sensor amount, depict cells transfected with PM-tagged sensor alone or together with constitutively active GTPase mutants. Clearly, the PM-tagged sensor is no longer a faithful reporter of Cdc42 activity. However, it may have utility as a joint Rac/Cdc42

sensor when one is interested in knowing if either GTPase is active, but not in the actual identity of the active GTPase.

Mutant PM-tagged sensor constructs were generated to further understand the activation of the PM-tagged sensor by Cdc42V12. In the previous chapter, I described the N-GBD-DD-VCA sensor containing the H211D and H214D CRIB region point mutations as a control construct that does not bind Cdc42 (Seth et al., 2003). In cells, the double mutant sensor still showed a slight FRET response to Cdc42V12, which I attributed to the residual affinity of the mutant sensor for GTPase. To create a better negative control construct, I created two new mutants. In one, I mutated an additional conserved CRIB region residue (F209D) to create a triple mutant sensor called PM-N-GBD-DDD-VCA-W503S. In the second, the sequence of the 16 residue CRIB motif of N-WASP (IGTPSNFQHIGHVGWD, wildtype residues 203-218) was randomly scrambled (QWDVPIHHNGFGTSIG, CRIB-Scrambled sequence) to generate a mutant called PM-N-GBD-CS-VCA-W503S (CS = Crib-Scrambled). Cells expressing the PM-tagged triple mutant sensor have an average FRET value of 1.40, which decreases to 0.98 in cells coexpressing Cdc42V12 (Figure 2-2C). Cells expressing the PM-tagged CS mutant sensor have an average FRET value of 1.35, which decreases to 1.25 in cells coexpressing Cdc42V12 (Figure 2-2C). While both mutants have

diminished Cdc42V12 responses relative to the wildtype PM-tagged sensor, the CS mutant is a much better negative control.

Next, experiments were performed to further understand the activation of the PM-tagged sensor by RacV12. Placement of the PM-tag at the N- or C-terminus of the sensor has no effect on activation by RacV12, indicating that the GTPase effect is independent of orientation to the membrane (Figure 2-2D). PM-tagged GBD1 sensor (comprising only the GBD of WASP, described in the previous chapter) also responds to both Cdc42V12 and RacV12 (Figure 2-2D). Cells coexpressing the PM-tagged N-GBD-DDD-VCA-W503S triple mutant sensor and RacV12 have an average FRET value of 1.27 (Figure 2-2C), while cells coexpressing the PM-tagged CS mutant and RacV12 have a FRET value of 1.41 (Figure 2-2C). Together, these results show that the Rac-induced response of the PM-tagged sensor depends on an intact CRIB motif and therefore, likely depends on a direct interaction with the GTPase. Given these results, it is likely that the responses to Cdc42N17 and wildtype Cdc42 are also mediated by direct sensor-GTPase interactions. However, this hypothesis has not been verified using the types of experiments described above for RacV12.

Based on all the data with the CAAX-tagged and PM-tagged sensors, it appears the CAAX-tagged sensors have greater fidelity for Cdc42 (Figures 2-1, 2-2 and see summary comparison in Figure 2-3). The CAAX-tagged sensors do not

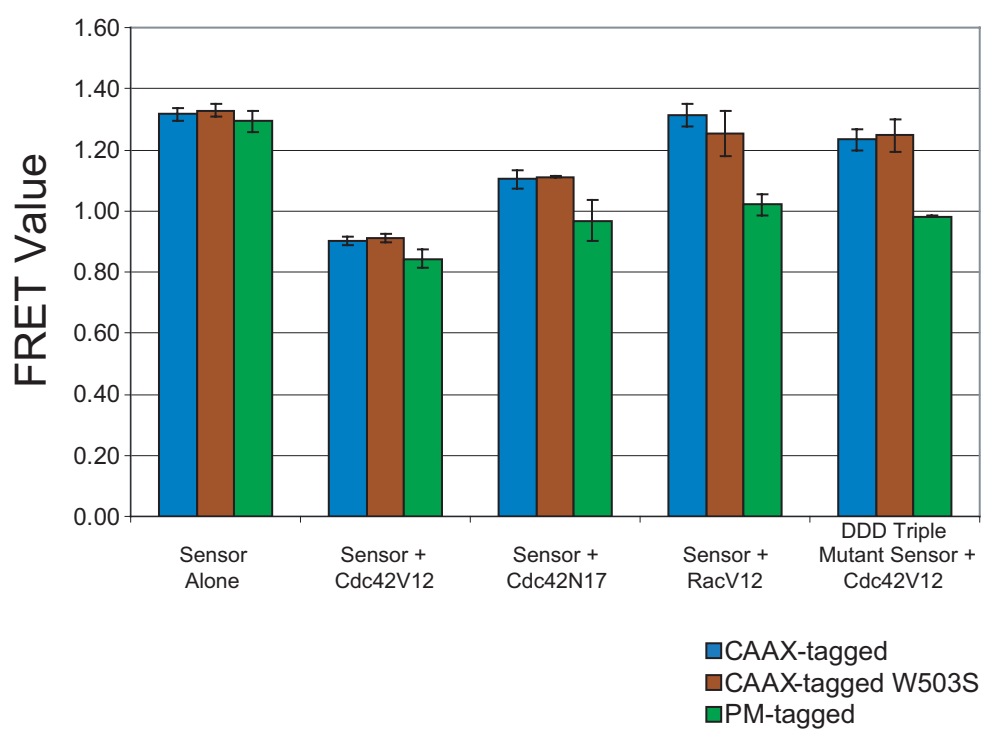


Figure 2-3

Figure 2-3. Comparison of CAAX-Tagged and PM-tagged FRET-Based Cdc42 Sensors.

Each bar represents the average cellular FRET value ($[\text{YFP channel emission intensity}]/[\text{CFP channel emission intensity}]$ upon CFP excitation) of at least ten cells transfected with the indicated sensor and GTPase mutants. Error bars represent the standard deviations for a minimum of three different transfections for each condition. Most of the graph has been compiled from data presented in Figures 2-1 and 2-2.

respond to RacV12 (Figure 2-3). In contrast to the PM-tagged triple mutant that still exhibits substantial response to Cdc42V12, the CAAX-tagged triple mutant sensors have minimal response to Cdc42V12 (Figure 2-3). Since the GTPase-induced FRET responses of the PM-tagged sensors are probably attributable to direct interactions with the GTPases (facilitated by high local concentrations coupled with colocalization at the plasma membrane as discussed above), it is likely that the CAAX-tagged sensors appear to have greater fidelity because they do not colocalize as highly with the GTPases. In other words, the PM-tag may lead to more inappropriate FRET responses than the CAAX-tag by virtue of being a more efficient plasma membrane targeting sequence. Thus, the CAAX-tagged sensors probably have the potential, under the appropriate biological circumstances, to also be activated by Rac, for example, when exposed to very high local concentrations of the GTPase. These issues have not been explored any further experimentally, but should be kept in mind when analyzing FRET data with these sensors. With these caveats and limitations in mind, the CAAX-tagged W503S sensors, nevertheless, represent the most optimized sensors that I have developed thus far. Therefore, these sensors were carried forward to begin FRET-based studies of Cdc42-mediated biological processes.

The results with the different membrane targeting strategies illustrate that membrane tethering is not straightforward and requires extensive optimization

and characterization. As discussed above, one of the major rationales for membrane tethering was to increase probe sensitivity by eliminating cytoplasmic background. An alternative strategy to eliminate background would be to perform FRET imaging using confocal microscopy (Chen et al., 2003). By limiting the fluorescence signal to a single focal plane, confocal imaging would serve to eliminate out-of-focus background fluorescence and thereby help boost the sensitivity of soluble FRET-based probes. Given the technical complexity of developing practical membrane tethers, as described above, the benefits of confocal FRET imaging should be explored.

FRET-based studies of Membrane Ruffling During Cell Spreading

Freshly plated cells will adhere and spread to a given surface over a period of several hours. During this time, cells extend numerous lamellipodia and filopodia to facilitate adhesion and spreading indicating that dynamic cytoskeletal rearrangements are occurring rapidly (Price et al., 1998). Previous work has demonstrated that both Cdc42 and Rac activity are required for adhesion and spreading and that they mediate their effects by controlling the observed cytoskeletal rearrangements (Price et al., 1998). Lamellipodia and filopodia are also important for cell migration suggesting that elucidating the molecular

regulation of cytoskeletal rearrangements during adhesion and spreading may have general applicability to understanding cell motility.

The cell adhesion and spreading model of cell motility was used as an initial biological system for studying the FRET-based Cdc42 sensors. NIH 3T3 cells were transfected with the CAAX-tagged N-GBD-VCA-W503S-CAAX sensor. Approximately 24 hours after transfection cells were trypsinized and replated on glass-bottom dishes. 4 hours after replating, dishes were transferred to the microscope stage where FRET was monitored using timelapse microscopy. Cells were maintained at 37 °C on a heated, humidified stage in CO₂-independent medium. The 100X oil immersion objective was also maintained at 37 °C using an objective heater. To prevent excessive media evaporation during imaging, dishes were covered with autoclaved FoilCovers (Zeiss). This basic set-up routinely and reproducibly allowed extended timelapse microscopy of live cells.

Initial experiments failed to show reproducible endogenous Cdc42 activation during cell spreading. However, upon cotransfection of wildtype Cdc42 with CAAX-tagged sensor, lower FRET ratios (indicating activated Cdc42) were consistently observed in the actively ruffling areas of spreading cells (Figure 2-4). As a negative control, cells were transfected with the N-GBD-DDD-VCA-W503S-CAAX triple mutant sensor. This sensor did not exhibit reduced FRET ratios in ruffling regions of the cell (not shown). However, upon

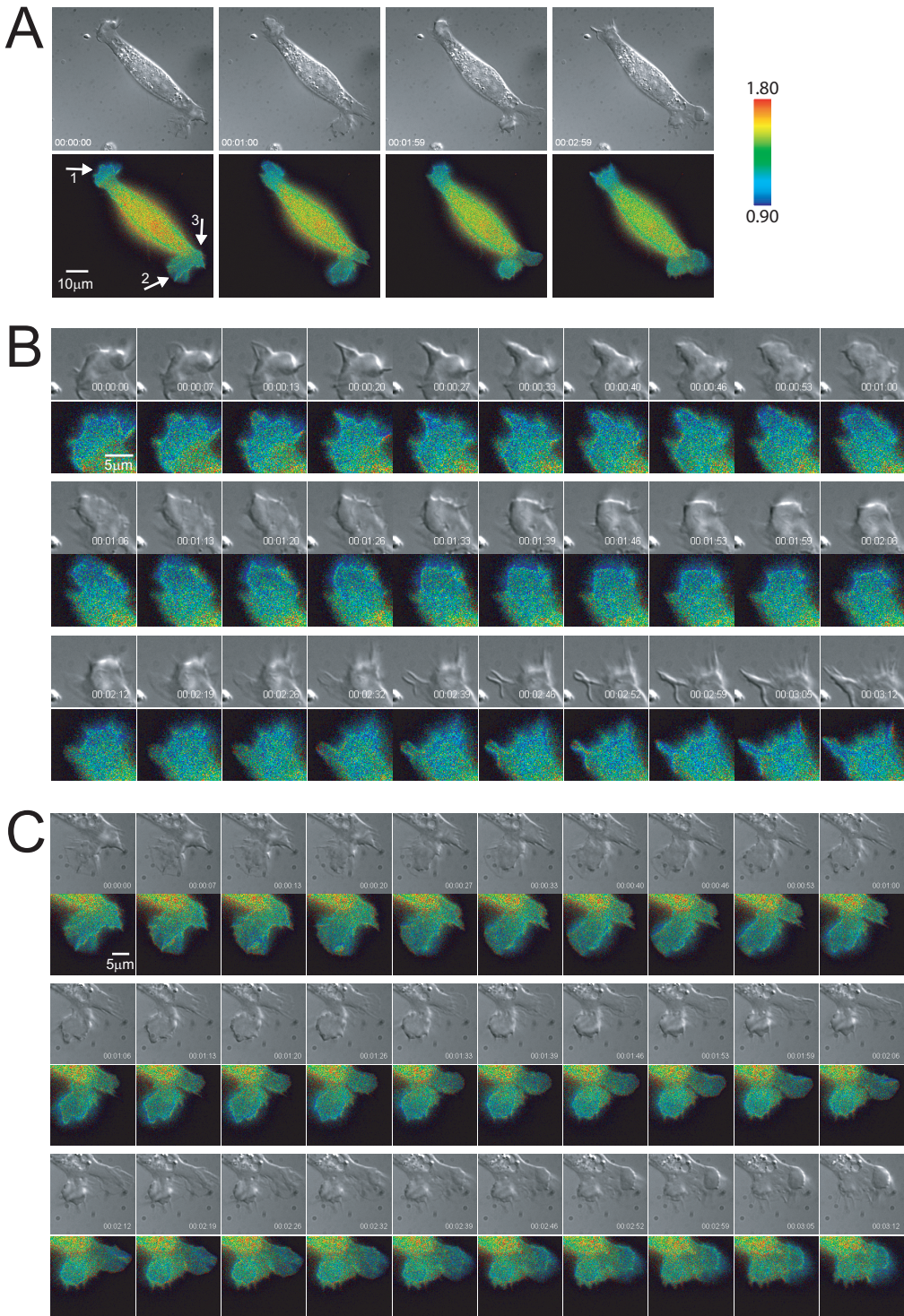


Figure 2-4

Figure 2-4. Cdc42 Activity Monitored with a FRET-based CAAX-tagged Sensor During Membrane Ruffling.

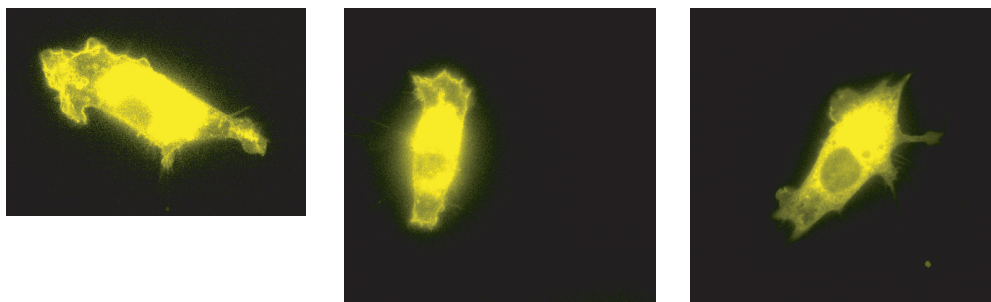
- (A) Selected static images of a ruffling NIH 3T3 cell transfected with the N-GBD-VCA-W503S-CAAX sensor and wildtype Cdc42. The upper row of DIC images shows the elapsed time during the 3 minute series. The lower row of corresponding images has been color-coded to represent the sensor concentration and FRET value ($[\text{YFP channel emission intensity}]/[\text{CFP channel emission intensity}]$ upon CFP excitation) distribution throughout the cell. Color hues correspond to the FRET value. The numerical FRET range described by the color hues is depicted in the spectral bar adjacent to the panel of images. Intensity of each pixel is determined by the YFP channel intensity, which correlates with total sensor amount, at that position. Arrows indicate 3 different regions of the cell which extended or retracted membrane ruffles during image acquisition.
- (B) Magnified DIC and FRET value images of region 1 (as marked in A). Frames were acquired every 6.7 seconds over a total time of 3 minutes 12 seconds.
- (C) Magnified DIC and FRET value images of regions 2 and 3 (as marked in A). Frames were acquired every 6.7 seconds over a total time of 3 minutes 12 seconds.

closer inspection it appears that the CAAX-tagged triple mutant sensor fails to enrich at the leading edges of cells (Figure 2-5). Thus, the absolute fluorescence intensity in CAAX-tagged triple mutant expressing cells is very low in actively ruffling regions, which makes FRET calculations unreliable. The difference in plasma membrane enrichment of the wildtype and triple mutant CAAX-tagged sensors was presumed based on widefield images (Figure 2-5), but was not rigorously confirmed using confocal microscopy.

Others have successfully used ratiometric imaging to study Cdc42 activity in motile 3T3 fibroblast cells without having to transfect supplemental Cdc42 (Nalbant et al., 2004). As discussed in the previous chapter, the studies by Nalbant et. al. used a Cdc42 sensor that is brighter and has a larger dynamic range than the sensors used here. In addition, Nalbant et. al. used cells freshly plated on fibronectin-coated surfaces, while I studied cells freshly plated onto uncoated surfaces. Cell line variations may also explain some of the discrepancies between these experiments. Indeed, I have found that three different aliquots of NIH 3T3 cells obtained from three different sources exhibit different morphologies and growth rates (not shown). Clonal variations in Cdc42 level could make it difficult to use NIH 3T3 cells routinely for these types of experiments. As improved genetically encoded fluorescent proteins are developed and as better FRET pairs

A

N-GBD-VCA-W503S-CAAX Sensor

**B**

N-GBD-DDD-VCA-W503S-CAAX Triple Mutant Sensor

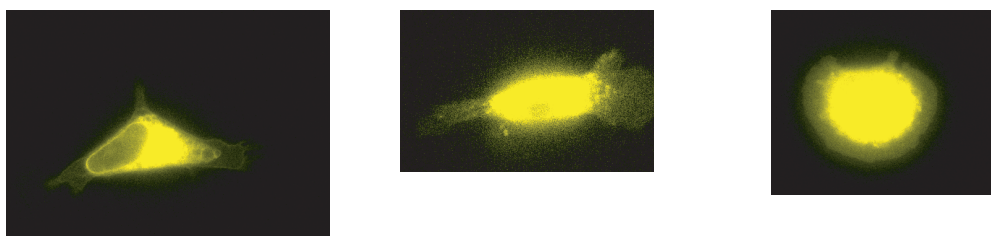


Figure 2-5

Figure 2-5. Wide-field Fluorescence Images of NIH 3T3 cells Expressing CAAX-tagged Sensors.

- (A) Images of 3 different cells expressing the N-GBD-VCA-W503S-CAAX sensor. The images represent the YFP channel intensity for each cell and illustrate the cellular distribution of the sensor.
- (B) Images of 3 different cells expressing the N-GBD-DDD-VCA-W503S-CAAX triple mutant sensor. The images represent the YFP channel intensity for each cell and illustrate the cellular distribution of the sensor. In both panels, the images have been overexposed purposely to facilitate inspection of the cell edges.

are identified (Nguyen and Daugherty, 2005; Shaner et al., 2004; Shaner et al., 2005), it should be possible to determine if the experimental differences observed here are due to inherent limitations in the underlying CFP-YFP technology or to biological variations in the experimental conditions. In any event, this system was not explored further. Rather, efforts were focused on developing model biological systems in which endogenous Cdc42 activity could be observed.

FRET-based studies of T cell Activation

T cells, through their T cell receptors, bind to antigen presenting cells (APCs) that display antigen bound to their MHC receptors (Janeway and Bottomly, 1994; Krogsgaard and Davis, 2005). The T-cell-APC interface is referred to as an immunological synapse and the cytoskeletal organization of the synapse is important for downstream activation of the T cell (Dustin and Cooper, 2000; Tooley et al., 2005). Cdc42 plays an important role in T cell activation and is required for cytoskeletal polarization towards the APC (Cannon and Burkhardt, 2002; Stowers et al., 1995). In collaboration with the Wülfing lab, which routinely performs timelapse fluorescence imaging of T cell activation by APCs (Davis et al., 1999), I attempted to use the FRET-based sensors to further study the role of Cdc42 in this process. In the following description of the T cell work, I contributed to every step, but much of the work including primary T cell

isolation and maintenance, APC maintenance and media preparation was performed largely by Dr. Wülfing or his lab members, including Irina Tskvitaria-Fuller, Nadia Parvaze, Monica Ghosh and Bozidar Purtic.

The basic experimental strategy, as previously reported (Tskvitaria-Fuller et al., 2003), is as follows. Primary T cells are isolated from transgenic mice exclusively expressing the 5C.C7 T cell receptor (TCR), which binds to moth cytochrome C (MCC) peptide (residues 92-103) presented on I-E^k (Seder et al., 1992). The primary, 5C.C7 TCR transgenic T cells are transduced with sensor-encoding retrovirus and primed *in vitro* for APC interactions (Costa et al., 2000). The transduced T cells are then activated by CH27 B cell lymphoma cells, an APC cell line, loaded with 10 μ M MCC. Formation and evolution of the immunological synapse can be monitored by timelapse microscopy. Depending on the nature of the transduced fluorescent probe, different aspects of T cell activation can be studied. This method has been used previously to understand the role of many molecules involved in T cell activation including the T cell receptor, MHC protein, CD4 and actin (Krummel et al., 2000a; Krummel et al., 2000b; Tskvitaria-Fuller et al., 2003; Wülfing et al., 2002). GFP-tagged fusion proteins are routinely studied in this manner in the Wülfing lab and, in principle, the method should be easily transferable to CFP-YFP-based FRET reagents.

The CAAX-tagged N-GBD-VCA-W503S and GBD1 sensors were cloned into retroviral vectors and transfected into the Phoenix-E retrovirus-producing cell line (Costa et al., 2000). Freshly harvested viruses were used to transduce primary T cells. The transfected Phoenix-E cells and transduced T cells were monitored for expression of fluorescent proteins. Expression of the CAAX-tagged GBD1 sensor was higher than the expression of the CAAX-tagged N-GBD-VCA-W503S sensor in Phoenix-E cells (Figure 2-6), but the transfection efficiency of both constructs was lower than other fluorescent constructs routinely used in the Wülfing lab. Sensor-expressing T cells could be isolated by fluorescence activated cell sorting (FACS), however, low sensor expression levels and limitations in the imaging apparatus prevented sensitive detection of the CFP signal from T cells (not shown). The lack of a robust CFP signal prevented reliable FRET calculations. Instrument upgrades in the Wülfing lab may allow CFP-YFP FRET imaging in the future, however, at present, it is unfeasible with these FRET-based Cdc42 sensors.

Cdc42 Activity During T cell Activation

Even though FRET-based studies were not possible in T cells, this biological system represented an important and interesting opportunity to gain insights into Cdc42 function. It was hypothesized that important details about

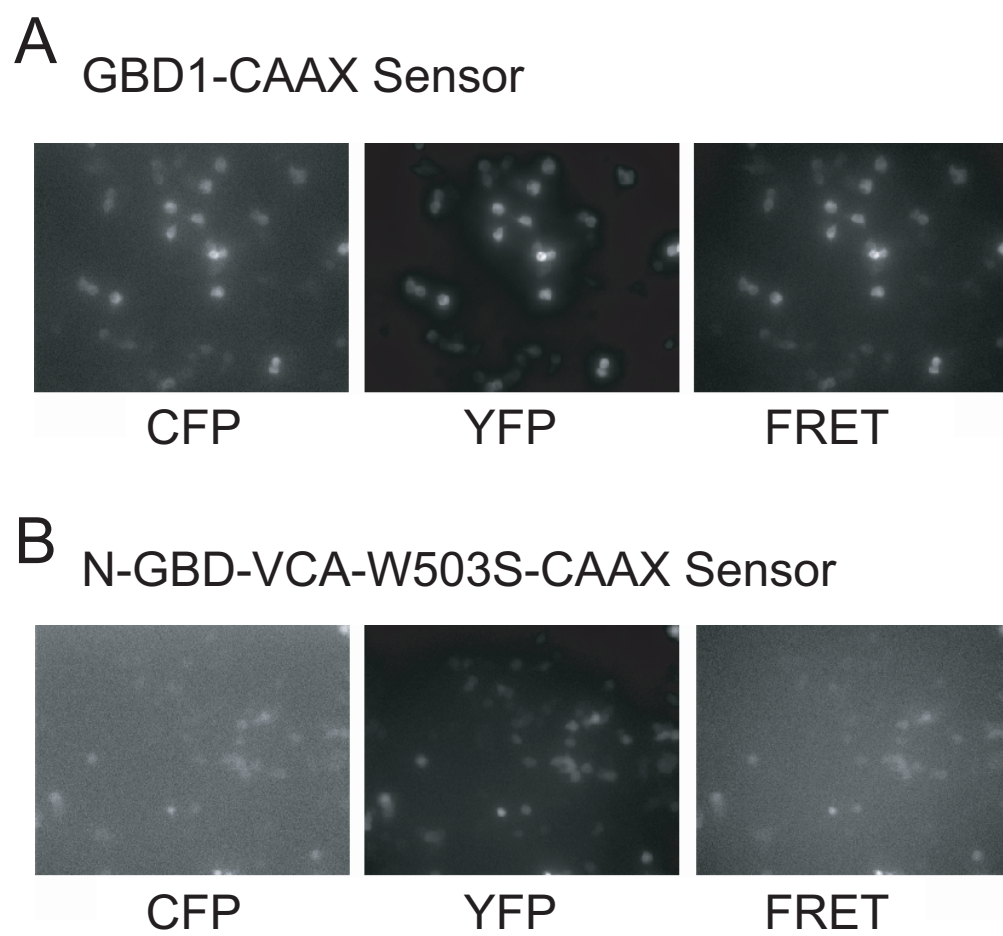


Figure 2-6

Figure 2-6. Wide-field Fluorescence Images of Phoenix-E Cells Expressing CAAX-tagged Sensors.

- (A) CFP, YFP and FRET (YFP Channel Emission Intensity upon CFP excitation) fluorescence intensity images of a field of Phoenix-E retrovirus-producing cells transfected with the GBD1-CAAX sensor.
- (B) CFP, YFP and FRET (YFP Channel Emission Intensity upon CFP excitation) fluorescence intensity images of a field of Phoenix-E retrovirus-producing cells transfected with the N-GBD-VCA-W503S-CAAX sensor. For both sensors, notice the low signal to noise ratio in the channels (CFP and FRET) dependent upon CFP excitation (especially pronounced in panel B).

Cdc42 activity during T cell activation could be elucidated using WASP-based imaging reagents that did not necessarily have to rely on FRET. A fluorescent probe for active Cdc42 was developed by fusing the WASP-GBD (referred to as GBD1 in the previous chapter) to GFP. It was hypothesized that the distribution of the GBD-GFP probe in T cells would correspond to the distribution of active Cdc42. The WASP-GBD has 19 nM affinity for active Cdc42 and a similar reagent has been used to monitor active Cdc42 localization in fixed T cells and live epithelial cells (Cannon et al., 2001; Kim et al., 2000b; Labno et al., 2003; Seth et al., 2003). To further enhance the sensitivity of the probe, a neuromodulin-tag or CAAX-tag was added to the N- or C-terminus, respectively, to create PM-GBD-GFP or GBD-GFP-CAAX.

Transduced T cells expressing PM-GBD-GFP or GBD-GFP-CAAX were activated with APCs and the distribution of the GFP signal was monitored over time. Images were acquired every 20 seconds for 15 minutes during which time T-cell/APC couple formation and evolution were observed. The distribution of GFP signal at the T-cell/APC interface was analyzed at every time point. The percentage of couples exhibiting increased GFP intensity at the T-cell/APC interface was determined. Following previously established criteria (Wulfiging et al., 2002), a couple was scored positive for GFP accumulation if the GFP intensity at the interface was greater than 40% above the cellular background intensity.

Approximately 70% of T-cells expressing GBD-GFP-CAAX and 40% of T cells expressing PM-GBD-GFP show sensor enrichment at the T-cell/APC interface during couple formation and evolution (Figure 2-7A). For both constructs, the increase in accumulation coincided with couple formation (Figure 2-7A). Sensor accumulation is sustained at early time points after couple formation and appears to decrease at the last time point examined, but even then a significant number of couples still show some accumulation (Figure 2-7A). In approximately 20% of the couples, both sensors accumulate preferentially in the center of the T-cell/APC interface (Figure 2-7B). A “central” accumulation pattern, as previously defined (Tskvitaria-Fuller et al., 2003; Wulfig et al., 2002), requires the GFP signal to occupy less than 25% of the interface area. In addition, the concentrated GFP signal must be within the central 60% of the interface (Tskvitaria-Fuller et al., 2003). The functional significance of this “central” accumulation is not clear at present. The reason for the disparity between the percentage of cells showing accumulation with the CAAX-tagged sensor or the PM-tagged sensor is not clear, but may be due to the small number of couples analyzed with the PM-tagged sensor. This small sample size may also contribute to the apparent “central” accumulation observed at later time points with the PM-tagged sensor. A representative series of timelapse images depicting sensor accumulation in a GBD-GFP-CAAX expressing T cell undergoing couple formation is shown in Figure 2-7C. These preliminary results suggest that active Cdc42 accumulates

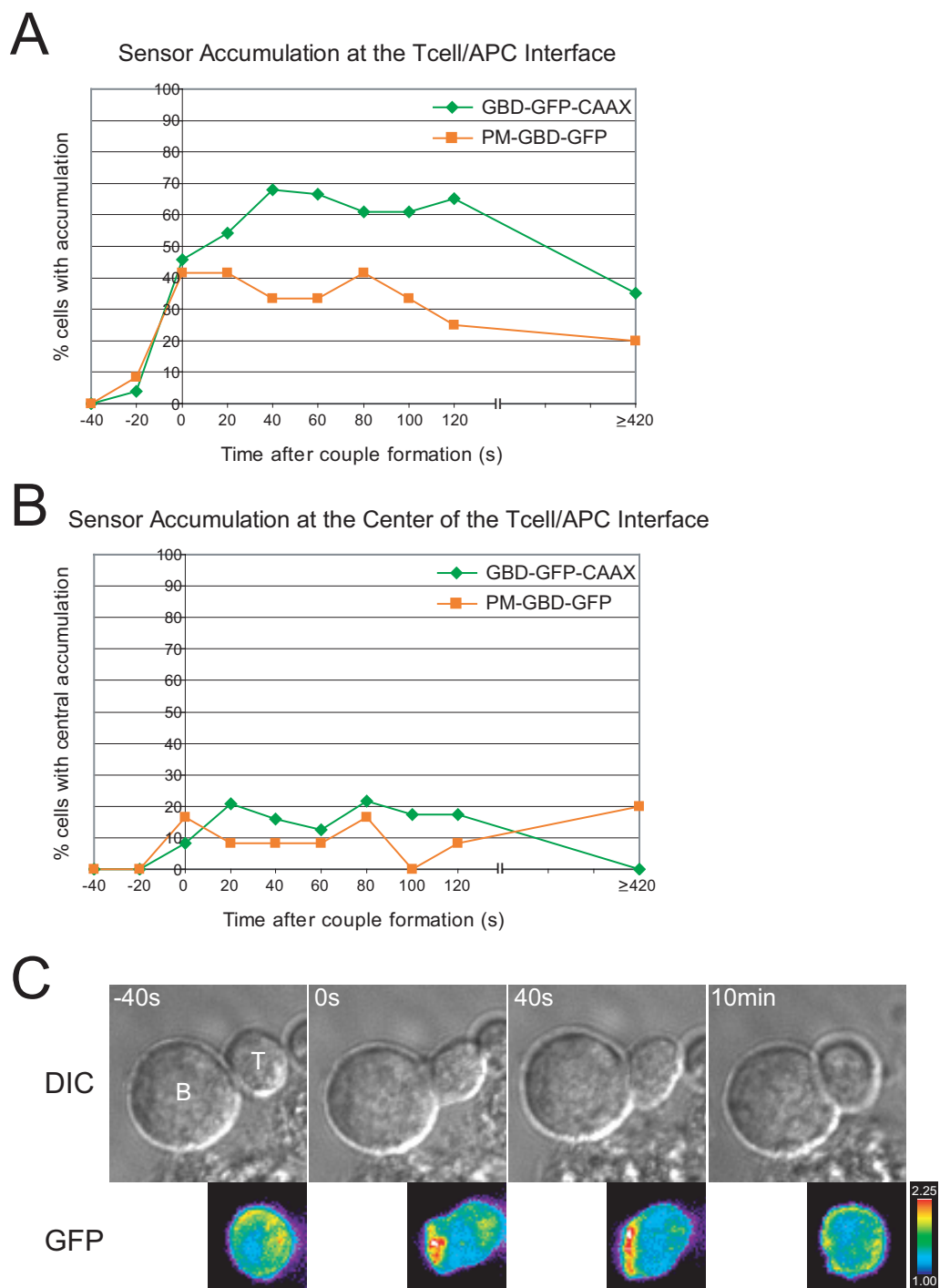


Figure 2-7

Figure 2-7. Localization of Active Cdc42 During T cell Activation by APCs.

- (A) Primary T cells expressing either GBD-GFP-CAAX or PM-GBD-GFP were imaged during activation by APCs. The percentage of cells exhibiting probe enrichment at the T cell/APC interface is shown at different timepoints during couple formation. Data are based on 20-25 couples per timepoint for the CAAX-tagged probe and 9-11 couples per timepoint for the PM-tagged probe.
- (B) Similar to (A) except the data represent the percentage of T cells in which the probe was observed to accumulate at the center of the T cell/APC interface. The criteria for a “central” accumulation pattern are described in the text.
- (C) Static images of a T cell expressing the GBD-GFP-CAAX probe during couple formation. The upper row of DIC images shows the B cell, T cell and time after couple formation. The GFP images show the distribution of the sensor in the T cell at different points during the lifetime of the couple. These images are color-coded to show the relative amount of sensor signal in each pixel. The bar on the right depicts the range of values represented by the color scale. The sensor begins to accumulate at the T cell-APC interface almost simultaneously with couple formation and dissipates within 10 minutes even though the couple persists.

rapidly at the T-cell/APC interface upon couple formation. Even though couple formation persists, Cdc42 accumulation decreases at later time points.

Ongoing experiments in the Wülfing lab are focused on extending the sensor results I have presented here. I have generated a negative control GBD-DDD-GFP-CAAX triple mutant construct containing the three WASP point mutations F244D, H246D, H249D that are analogous to the N-WASP mutations F209D, H211D, H214D described above. In other experiments, the sensors are being used to determine the signaling pathways that govern Cdc42 localization during T cell activation and to identify the specific actin cytoskeletal rearrangements correlated with active Cdc42 accumulation. These studies should shed tremendous insight into the molecular regulation and function of Cdc42 during T cell activation.

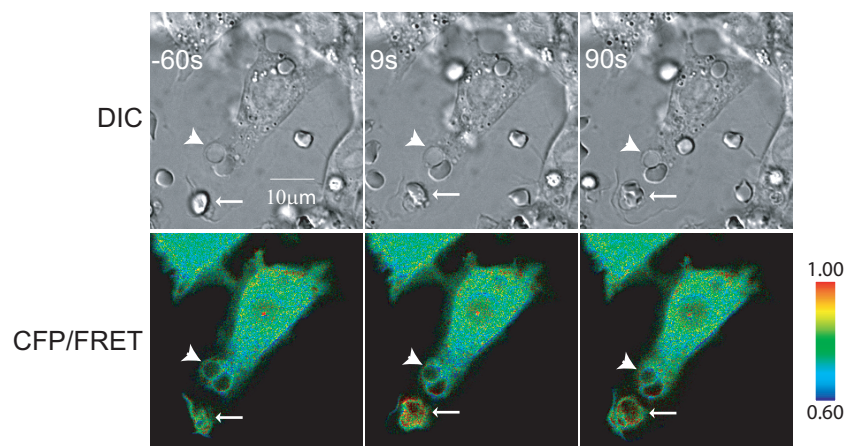
FRET-based studies of Fc- γ receptor mediated phagocytosis

Fc- γ receptor mediated phagocytosis is Cdc42-dependent and requires extensive actin rearrangement at the cell surface of macrophages (Caron and Hall, 1998). The RAW 264.7 murine macrophage cell line has been used extensively to understand the molecular mechanisms of Fc- γ receptor mediated phagocytosis. Fc- γ receptors on the surface of RAW cells will bind to and mediate

internalization of IgG-opsonized red blood cells (RBCs). A previously established protocol for measuring phagocytic efficiency was adapted (as described in Experimental Procedures) to monitor individual phagocytic events in live RAW macrophages incubated at 37 °C using timelapse microscopy. Early experiments indicated that macrophages readily phagocytose the RBCs and each phagocytic event requires ~90 seconds to complete from the time of cell-cell contact until the RBC is clearly internalized as judged by light microscopy. For RBCs that encounter macrophages from the side, as opposed to landing on top of them, the extension of macrophage pseudopods around the RBC is readily observable in fluorescently labeled cells. The extending pseudopod structure is referred to as the phagocytic cup. The pseudopods eventually meet at the top of the RBC and fuse to close the phagosome, which is then internalized into the main cell body.

RAW cells transfected with the N-GBD-VCA-W503S-CAAX sensor were used to examine the spatial and temporal patterns of Cdc42 activation during Fc- γ receptor mediated phagocytosis. Initial FRET experiments revealed that Cdc42 activity may be transiently enhanced at the developing phagosome (Figure 2-8A). However, two primary technical issues, which became apparent in these initial experiments, needed to be resolved before further data analysis and interpretation. First, after analyzing a number of images, it became clear that different phagocytic events occurred in different focal planes. Further, as phagocytic

A



B

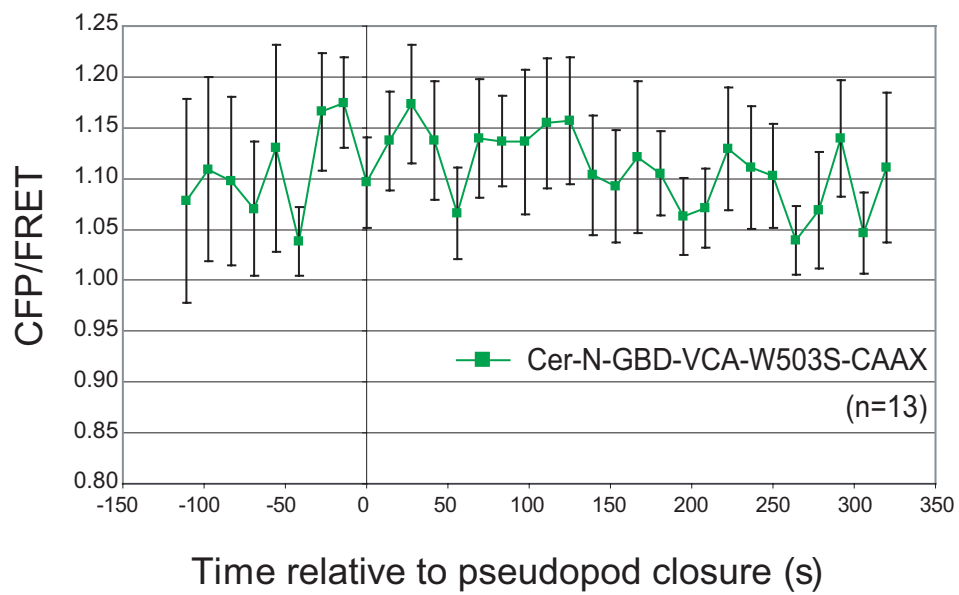


Figure 2-8

Figure 2-8. FRET-based Imaging of Cdc42 Activity During Fc- γ Receptor Mediated Phagocytosis.

- (A) Images show phagocytosis of RBCs by a macrophage expressing the N-GBD-VCA-W503S-CAAX sensor. Pseudopod fusion around the RBC indicated by arrows occurs at time 0 (not shown). The DIC images show progressive internalization of the RBC and the CFP/FRET images show the relative Cdc42 activity at the corresponding times. Two RBCs, indicated by arrowheads, are already phagocytosed at -60s and show minimal Cdc42 activation throughout the timelapse. The bar on the right shows the range of ratios represented by the color scale. Note that in the CFP/FRET images, warmer colors represent higher Cdc42 activity, in contrast to previous figures in which the inverse FRET/CFP ratio is presented.
- (B) Timecourse of FRET changes reported by the Cer-N-GBD-VCA-W503S-CAAX sensor during Fc- γ Receptor Mediated Phagocytosis. For each timepoint, the CFP/FRET ratio was averaged over the portion of the cell surface in contact with the RBC. Data points are the average values calculated for 13 different phagocytic events. Error bars represent the standard error of the mean.

events evolved over time they were observed to drift into different focal planes as a result of movement during the internalization process. To ensure a high chance of acquiring an in-focus phagocytic event that could be analyzed for several minutes, multiple different focal planes would have to be acquired at each timepoint. A z-stack of 4 planes spaced 1.5 μm apart was found to be optimal. Second, sensor-expression in RAW cells was low relative to the expression in NIH 3T3 cells. Thus, longer exposure times had to be used for the CFP and FRET channels to capture a suitable image. Empirically, exposure times of 1 second had to be used for each of these channels compared to 200 milliseconds for the YFP channel. The 2.2 total seconds required to capture one set of fluorescence images could potentially introduce errors into the FRET calculation since the CFP and FRET images required for the analysis would be temporally offset by more than 1 second. Coupled with the need to image multiple planes for every timepoint, the total time to acquire one timepoint would be ~20 seconds (including the delays introduced by switching between fluorescence filters and between fluorescence and brightfield light sources). Given that phagocytosis can be completed within 90 seconds, it seemed that the technical limitations imposed by the imaging system would not allow for sufficient temporal resolution of the phagocytic process.

Even though the acquisition delay is largely imposed by switching times within the hardware of the imaging system, it seemed reasonable that higher

sensitivity detection of CFP could help increase the achievable temporal resolution. Towards this end, it was hypothesized that a recently reported brighter mutant of CFP, called cerulean, could be useful (Rizzo et al., 2004). The excitation and emission wavelengths of cerulean and CFP are identical, but cerulean is 2.5X brighter (Rizzo et al., 2004). Cerulean, like CFP, is also a good FRET partner with YFP (Rizzo et al., 2004). Thus, a new sensor construct was generated in which the CFP moiety was replaced with cerulean to generate Cer-N-GBD-VCA-W503S-CAAX. RAW cells transfected with the CAAX-tagged cerulean-based sensor have increased fluorescence intensities compared to the original CFP-based sensor (not shown). The CFP and FRET channels can be collected in 400 milliseconds each with the cerulean-based sensor, compared to 1 second each for the CFP-based sensor. The decrease in acquisition time corresponds exactly to the published 2.5X brighter fluorescence of cerulean compared to CFP.

Next, the CAAX-tagged cerulean-based sensor was used to monitor Cdc42 activation during Fc- γ receptor mediated phagocytosis. For each cell imaged, a z-stack containing 3 planes spaced 2 μm apart was acquired at every timepoint (the optimal z-stack of 4 planes spaced 1.5 μm apart was not acquired due to acquisition time considerations). These imaging parameters resulted in one timepoint being acquired every 14 seconds. Ideally, however, one would like to achieve even higher temporal resolution. In any event, FRET signals were

analyzed during phagocytosis in cells expressing the CAAX-tagged cerulean-based sensor. For each timepoint, the plane in which the phagosome was best in-focus was chosen for analysis. The average FRET value (ratio of CFP channel emission intensity to FRET channel emission intensity) around the phagosome was calculated at every time point for each phagocytic event. However, after analysis of several events, no consistent or reproducible FRET change was observed during the course of phagocytosis (Figure 2-8B). There is likely some unresolved problem with the imaging or the analysis because Cdc42 is known to be involved in this process. In addition, recent FRET-based studies of ectopically expressed Cdc42 show that it is selectively activated at the phagocytic cup (Hoppe and Swanson, 2004).

The remaining unresolved technical issues preventing reliable FRET imaging have not been definitely determined. Some problems may arise from incomplete membrane localization of the CAAX-tagged probe. If there is residual sensor in the cytosol, then this will reduce the sensitivity of the FRET-based probe and could potentially eliminate the signal during phagocytosis. Confocal imaging should be performed to map the precise localization of the CAAX-tagged sensor in RAW cells. There could also be a problem with the actual quantitation of the FRET data. In most of the work here, fluorophore bleed-through into different filter sets was not considered since for many FRET applications this is not necessary (Gordon et al., 1998). However, explicitly accounting for bleed-

through in the analysis of FRET during phagocytosis did not improve the results (not shown). Initial experiments with a CAAX-tagged cerulean-based GBD1 sensor (GBD1 sensor discussed in the previous chapter), which has 10-fold higher affinity for active Cdc42 than N-GBD-VCA, also did not show promising results (not shown). As discussed above, using confocal microscopy for FRET-imaging could be a viable alternative to membrane tethering in terms of reducing out-of-focus background signal. Although, laser scanning confocal microscopy would be too slow for imaging phagocytosis in real-time, spinning disk confocal microscopy would probably be well-suited for this application. Thus, spinning disk confocal microscopy might be helpful if the unresolved FRET imaging issues are due to insufficient sensitivity. Regardless of the source, technical difficulties still prevent reliable FRET-imaging under the conditions that would most likely be useful for understanding interesting biological systems. The suggestions outlined above may help resolve these issues in the future.

A valuable lesson from the T cell studies was that useful experiments can still be conducted even if the methodology of choice does not work as expected. Since the non-FRET GBD-GFP probe had already proved useful in the T cell system, my attention turned towards using the GBD-GFP sensor to understand the role of Cdc42 during Fc- γ receptor mediated phagocytosis. The results from these experiments will be described in the next chapter.

Discussion

The experiments presented here were aimed at achieving two important objectives. The first goal was to increase the sensitivity of the FRET-based Cdc42 probes to be able to detect endogenous Cdc42 activity. The second goal was to develop a robust imaging assay for a Cdc42-dependent biological process. Although a number of suitable biological systems were established, technical issues related to probe sensitivity and FRET-analysis need to be resolved before the Cdc42 sensors can be used routinely and reproducibly to monitor the spatial and temporal activity of endogenous GTPase.

The use of membrane tethering to increase the sensitivity of the FRET-based probes proved to be non-trivial. The palmitoylated plasma membrane tether derived from neuromodulin caused the sensors to become unfaithful reporters of Cdc42 activity. The membrane tether derived from the CAAX sequence of Cdc42 did not cause such fidelity problems. However, a negative control sensor fused to the CAAX-tag did not localize in the same pattern as the wildtype CAAX-tagged sensor. The dependence of the specific localization pattern on non-CAAX sequences is surprising and highlights another complication of membrane targeting. Clearly, a better membrane tethering sequence is needed in the future. Given the results with the current membrane tethers, any future sequence needs to be carefully selected, optimized and tested in a variety of control experiments before it is adopted as the new standard.

Both T cell activation by APCs and Fc- γ receptor mediated phagocytosis are processes that require significant Cdc42-mediated actin cytoskeletal rearrangements. Technical improvements in reagents, imaging equipment and image analysis will likely be needed to allow robust FRET-based experiments for both of these systems. New fluorescent proteins are being developed rapidly as are more optimized FRET pairs, including the currently favored CFP-YFP derivatives, CyPet and YPet (Nguyen and Daugherty, 2005; Shaner et al., 2005; Zhang et al., 2002). In the near future, optimized GFP and mRFP derivatives may also be useful for FRET (Shaner et al., 2004; Zhang et al., 2002). Each new generation of fluorescent proteins has its own advantages and drawbacks. Until the general utility of these new FRET pairs is demonstrated, users will have to determine empirically whether they provide substantial advantages in their particular system or application (Shaner et al., 2005). Spinning disk confocal imaging is an emerging technology that could also prove useful for extending these studies in the future (Nakano, 2002). Confocal imaging will help the sensitivity problem of the soluble FRET-based sensors without requiring the introduction of potentially problematic membrane tethers and the spinning disk technology will support imaging with high temporal resolution (Chen et al., 2003; Nakano, 2002). In the meantime, non-FRET based imaging experiments are being used to elucidate the molecular function and regulation of Cdc42 signaling

during T cell activation (described above) and during Fc- γ receptor mediated phagocytosis (described in the following chapter).

CHAPTER 3

Autoinhibition Regulates the Actin Assembly Activity and Cellular Localization of the Diaphanous-Related Formins FRL α and mDia1

Abstract

Diaphanous-Related Formins (DRFs) are key regulators of actin cytoskeletal dynamics. DRFs are characterized by a C-terminal Diaphanous Autoregulatory Domain (DAD) that is postulated to regulate the actin assembly activity of the adjacent formin homology 2 (FH2) domain through autoinhibitory interactions with an N-terminal regulatory region, although this has only been shown directly for the DRF mDia1. Here, I show that the actin assembly activity of FRL α , a macrophage-specific DRF, is also autoinhibited by its N-terminal domain. In cells, autoinhibitory interactions also block a novel GTPase-independent membrane localization activity of the N-terminal domain in both FRL α and mDia1. The Rho-family GTPase Cdc42 relieves autoinhibition of

FRL α actin assembly activity and cellular localization. FRL α is required for efficient Fc- γ receptor mediated phagocytosis and is recruited to the phagocytic cup by Cdc42. These results suggest mutual autoinhibition of biochemical activity and cellular localization may be a general regulatory principle for DRFs and demonstrate a novel role for formins in immune function.

Introduction

Dynamic control of the actin cytoskeleton is essential for cell polarization, migration and division (Evangelista et al., 2003; Pollard and Borisy, 2003). Proper actin remodeling involves activation of different eukaryotic nucleation factors that can generate specific types of new actin filaments. Arp2/3 complex nucleates new actin filaments while remaining anchored to the sides of existing filaments. This activity creates branched actin networks associated with actin patches, actin comets and lamellipodia which are important for cell polarization, intracellular vesicle/pathogen motility and cell motility (Higgs and Pollard, 2001; Machesky and Gould, 1999). Formin proteins generate long, unbranched actin filaments creating actin cables, contractile rings and stress fibers which are involved in budding, cytokinesis and maintenance of cell morphology (Chang et al., 1997; Evangelista et al., 2002; Sagot et al., 2002; Sharpless and Harris, 2002; Zigmond, 2004). It is presently unclear if and how the distinct activities of these actin nucleation machines are coordinated during the cytoskeletal remodeling required for complex biological processes.

The general importance of formins for regulating cell polarization and tissue morphogenesis is exemplified by mutations in Formin, DRF1 and DRF2 which result in malformation of limbs and kidneys, deafness and premature ovarian failure, respectively (Bione et al., 1998; Lynch et al., 1997). Especially in

mammals, the specific formin-mediated cytoskeletal functions important for these morphogenetic effects have not been well characterized. At least 15 different formins have been identified in humans and mice and it is likely that novel formin functions have yet to be discovered (Higgs and Peterson, 2005). Compared to the solitary Arp2/3 complex, whose molecular regulation by upstream signals is understood in some detail (Higgs and Pollard, 2001), much less is known about the regulation and function of the much larger formin family.

The formins are defined by a conserved C-terminal formin homology 2 (FH2) domain that mediates effects on actin (Higgs, 2005; Higgs and Peterson, 2005; Wallar and Alberts, 2003; Watanabe and Higashida, 2004; Zigmond, 2004). The FH2 domain functions as a dimer and has varying effects in different formins, including actin filament nucleation, filament severing and barbed-end binding with elongation (anti-capping effect) or without elongation (capping effect) (Evangelista et al., 2002; Harris et al., 2004; Kovar et al., 2003; Kovar and Pollard, 2004; Li and Higgs, 2003; Pring et al., 2003; Romero et al., 2004; Xu et al., 2004). The proline rich FH1 domain, found immediately N-terminal to the FH2 domain, mediates interactions with profilin, which helps deliver actin monomers to the FH2 domain, and also with WW and SH3 domains (Bedford et al., 1997; Chan et al., 1996; Evangelista et al., 2003; Kovar et al., 2003; Romero et al., 2004).

The function of the conserved N-terminal region found in most formins is still unclear. *In vitro* and *in vivo* studies with mDia1 have demonstrated a role for its N-terminus in mediating autoinhibition of FH2 activity (see below) (Alberts, 2001; Ishizaki et al., 2001; Li and Higgs, 2003; Li and Higgs, 2005; Watanabe et al., 1999). Other studies with the fungal formins Bni1p, Fus1 and SepA have implicated their N-termini in regulating localization *in vivo* (Ozaki-Kuroda et al., 2001; Petersen et al., 1998; Sharpless and Harris, 2002). For both Bni1p and Fus1, perturbation of cellular localization disrupts biological activity (Ozaki-Kuroda et al., 2001; Petersen et al., 1998). It is unclear if the effects of the N-terminus on FH2 activity and cellular localization are linked or if the N-terminus simply serves different roles in different formins. Elucidating the general regulation of formin localization and activity in higher eukaryotes will be important for understanding the biological activities of these molecules.

In the DRF subfamily a short (~20 residue) conserved region called the Diaphanous Autoregulatory Domain, or DAD, follows the FH2 domain in sequence (Alberts, 2001; Higgs and Peterson, 2005). In mDia1, the DAD binds to the N-terminus to inhibit the actin assembly activity of the FH2 domain through an unknown mechanism (Alberts, 2001; Li and Higgs, 2003). The DAD binding element in the N-terminus is called the Diaphanous Inhibitory Domain (DID) (Li and Higgs, 2005). Rho binds to the mDia1 N-terminus through a region that spans a portion of the DID and an adjacent sequence element termed the G-region

(for GTPase binding) (Otomo et al., 2005a; Rose et al., 2005). Rho binding destabilizes interactions between the N- and C-termini leading to partial activation of the mDia1 FH2 domain (Li and Higgs, 2003; Watanabe et al., 1999). The mDia1 N-terminus forms a dimer through its Dimerization Domain (DD) and Coiled Coil region (CC) (Otomo et al., 2005a; Rose et al., 2005). Based on sequence similarity, the G-DID-DD-CC architecture of the mDia1 N-terminus is likely to hold for other DRF family members (Higgs, 2005). The formins Bni1p and FHOD1 are also likely to be autoinhibited based on cytoskeletal effects of mutant proteins studied *in vivo* (Koka et al., 2003; Sagot et al., 2002). However, the generality of FH2 domain autoinhibition through a DAD-DID interaction and activation by Rho GTPases has yet to be established directly for DRFs other than mDia1.

FRL α is a macrophage-specific DRF whose FH2 domain can nucleate new actin filaments and sever existing filaments *in vitro* (Harris et al., 2004; Yayoshi-Yamamoto et al., 2000). FRL α has been reported to bind to Rac and modulate cell adhesion, migration and survival, but its molecular function in macrophages has not been explored in detail. (Yayoshi-Yamamoto et al., 2000). Due to its unique expression profile, it was hypothesized that understanding FRL α may reveal new aspects of formin biology in higher eukaryotes as well as elucidate general principles governing the biological and biochemical regulation of formin proteins.

The data show that the FRL α N-terminus binds to the C-terminus in a DAD-dependent manner and inhibits the actin assembly activity of the FH2 domain. The isolated N-terminal regions of both FRL α and mDia1 are localized to the plasma membrane in transfected cells. In both cases, the full length proteins are sequestered in the cytosol because DAD binding prevents the plasma membrane association “activity” of the N-terminus. For FRL α , the data show that active Cdc42 relieves autoinhibition of FH2 activity *in vitro* and relieves DAD-mediated autoinhibition of N-terminus localization in macrophages. Knockdown experiments reveal that FRL α is required for efficient Fc- γ receptor mediated phagocytosis, consistent with its role as a macrophage-specific Cdc42 effector. Live cell imaging shows that FRL α is transiently recruited to the phagocytic cup and that recruitment depends on its ability to interact with Cdc42. These studies reveal a general mechanism of DRF regulation in which autoinhibition controls actin assembly activity and cellular localization. In addition, the data demonstrate a new biological function for DRFs in the immune system of higher eukaryotes.

Experimental Procedures

Constructs

FRL α and mDia1 constructs were generated by PCR and standard cloning techniques. Murine FRL α template was provided by Dr. Takeshi Watanabe (Kyushu University). Full length FRL α (residues 1-1094), the FRL α N-terminus (residues 1-450), the FRL α C-terminus (residues 612-1094) and the FRL α Δ FH2-C-terminus (residues 994-1094) were cloned into pET vectors containing N-terminal, TEV protease-cleavable Glutathione-S-Transferase (GST) or Maltose Binding Protein (MBP) affinity tags. Full length mDia1 (residues 1-1255), the mDia1 N-terminus (residues 1-570) and the mDia1 Δ G-N-terminus (residues 131-570) were cloned by PCR for mammalian expression. All FRL α and mDia1 constructs were cloned into a modified pCMV-Script vector containing C-terminal EGFP or mRFP (template provided by Dr. Roger Y. Tsien, UCSD). Mini-FRL α (residues 1-536 and 994-1094 tethered by a GGSGGS linker) and mini-mDia1 (residues 1-457 and 1168-1255 tethered by a GGSGGS linker) were generated using overlap extension PCR. Point mutations were introduced using the QuikChange Site Directed Mutagenesis protocol (Stratagene). Myc-tagged GTPase constructs were provided by Dr. Melanie H. Cobb (UT Southwestern). The WASP-GBD comprises residues 230-288 of the human protein. The WASP-GBDmut was generated by randomly scrambling the amino acid sequence of the

internal CRIB (Cdc42/Rac interactive binding) motif, which is necessary for high-affinity interactions with Cdc42 (Rudolph et al., 1998). The 16 residue wildtype sequence, IGAPSGFKHVSHVGWD, was mutated to KWDVPIHHGGFGASVS using PCR. This strategy was adopted since mutants containing multiple point mutations of conserved residues still show residual Cdc42 affinity in cells (described in the previous chapter).

The following siRNA oligonucleotides were used for RNA interference experiments:

- 1) FRL2614sense: CAGACGUUGUUGCACUACUTT
- 2) FRL2614antisense: AGUAGUGCAACAACGUCUGTT
- 3) GFPsense: GCAGAAGAACGGCAUCAAGTT
- 4) GFPantisense: CUUGAUGCCGUUCUUCUGCTT

Bacterial Expression and Protein Purification

All proteins were expressed in *E. coli* strain BL21(DE3). FRL α N-terminus constructs were expressed as GST-fusion proteins while C-terminus constructs were expressed as MBP-fusions. N-terminal constructs were purified using glutathione sepharose beads (Amersham), anion exchange chromatography and gel filtration. C-terminal constructs were purified using two steps of cation exchange chromatography followed by gel filtration. Prior to some assays, the

affinity tags were cleaved using TEV protease and the tag-free proteins were purified either with anion or cation exchange chromatography.

Cdc42 (residues 1-179) was prepared and loaded with guanosine 5'-[β , γ -imido]triphosphate (GMPPNP) as previously described (Abdul-Manan et al., 1999; Kim et al., 2000a).

Actin was purified from rabbit skeletal muscle and labeled with pyrene as described (Pollard and Cooper, 1984; Spudich and Watt, 1971).

Biochemical Assays

Pull Down Experiments

To examine interactions between the FRL α N- and C-termini, 600 pmol of GST-N-terminus was loaded onto glutathione sepharose beads (Amersham) and incubated with 600 pmol of C-terminus in 200 μ L of binding buffer (20 mM Tris [pH 8.0], 100 mM NaCl and 1 mM DTT). Beads were washed 3 times with 200 μ L binding buffer containing 0.1% TritonX-100 and then washed 2 times with 200 μ L binding buffer without detergent. Samples were then boiled in 2x SDS sample buffer and analyzed by SDS-PAGE and Coomassie staining. Alternatively, the same protocol was carried out with 600 pmol of MBP-C-terminus loaded onto amylose resin (New England Biolabs) and incubated with 600 pmol of GST-N-terminus.

Actin Assembly Assays

Experiments were performed as described previously (Higgs and Pollard, 1999). Briefly, reactions contained 4 μ M actin (5% pyrene labeled), 10 mM imidazole (pH 7.0), 50 mM KCl, 1 mM EGTA and 1 mM $MgCl_2$. Pyrene fluorescence ($\lambda_{ex} = 365$ nm, $\lambda_{em} = 407$ nm) was recorded over time to monitor actin assembly.

Cell Culture and Transfection

RAW 264.7 cells were purchased from the ATCC and maintained in DMEM containing 10% FBS and 1 mM sodium pyruvate (Invitrogen). Cells were transfected with 5 μ g total DNA using Lipofectamine 2000 according to the manufacturer's protocol (Invitrogen). Cells were seeded into 6-well plates at a density of 1×10^6 cells/well one day prior to transfection. For siRNA transfection, cells were seeded into 24-well plates at a density of 2×10^5 cells/well one day prior to transfection. Cells were transfected with siRNAs using 1.5 μ L siQuest reagent (Mirus Bio Corporation) and 250 nM siRNAs (final concentration per well) according to the manufacturer's protocol. To determine the efficiency of FRL α knockdown, cell lysates were prepared in lysis buffer (described below) 48 hours after siRNA transfection. Western blotting was performed as described below using polyclonal rabbit anti-FRL α antibodies generously provided by Dr. Henry N. Higgs (Dartmouth).

HEK293t cells were maintained in 10% calf serum (ATCC) and 1 mM penicillin/streptomycin (Invitrogen). For co-immunoprecipitation, cells were transfected with 10 µg total DNA using a calcium phosphate precipitation method. Cells were seeded into 10 cm dishes at a density of 1×10^6 cells/plate one day prior to transfection.

Co-Immunoprecipitation

To examine interactions between FRL α constructs and Rho GTPases, HEK293t cells were cotransfected with expression vectors for each formin-GFP and myc-GTPase construct (5 µg each). 36 hours after transfection, cell lysates were prepared in lysis buffer (20 mM Tris [pH 7.4], 100 mM NaCl, 1 mM DTT, 1 mM MgCl₂, 0.2% NP-40, 1 mM PMSF, 1 mM benzamidine 1 µg/mL leupeptin, 1 µg/mL antipain, 0.5 µg/mL pepstatin, 20 mM NaF and 0.5 mM NaVO₃). After centrifugation, the protein concentration in the supernatant was measured using the Coomassie Plus reagent (Pierce) and adjusted to 1 µg/µL and incubated with anti-GFP antibody (Molecular Probes, Invitrogen) for 1 hour at 4 °C. Immune complexes were precipitated with UltraLink Immobilized Protein A/G beads (Pierce) by incubation for 1 hour at 4 °C. Beads were washed 3 times with 1 mL lysis buffer without protease and phosphatase inhibitors. Proteins were eluted off

the beads by boiling in 2x SDS sample buffer and analyzed by Western blotting with either primary anti-GFP (Invitrogen) or anti-myc (Covance) antibodies. Alkaline phosphatase conjugated secondary antibodies (Promega) were used to visualize the protein bands.

Confocal Microscopy

24 hours after transfection, RAW cells were washed and scraped into 1 mL of fresh medium. Depending on cell density, 200-500 μ L of the resuspended cells were placed into 12-well dishes containing 1 mL of medium and a 12 mm glass coverslip (Fisher) in each well. After allowing the cells to adhere for 6-8 hours, the cells were fixed in 3.7% formaldehyde, washed with phosphate-buffered saline (PBS) and mounted on glass slides. Confocal imaging was performed on a Zeiss LSM 510META laser scanning microscope using a 63X oil immersion objective. Images were converted to TIFF files and analyzed using Slidebook software (Intelligent Imaging Innovations). Background correction was performed based on cell-free regions of each image. In order to allow comparison between cells with different expression levels of fluorescent proteins, the channel intensities in each cell were normalized using the maximum intensity value in that cell.

Phagocytosis Assays for Live Cell Imaging

Opsonization of Red Blood Cells

IgG-opsonized sheep red blood cells (RBCs) (Colorado Serum Company) were prepared for Fc- γ receptor mediated phagocytosis essentially as described previously (Greenberg et al., 1990). RBCs (80-100 μ L packed cell volume) were washed with 1 mL BWD buffer (20 mM HEPES [pH7.4], 125 mM NaCl, 5 mM KCl, 5 mM glucose, 10 mM NaHCO₃, 1 mM KH₂PO₄, 1 mM MgCl₂, 1 mM CaCl₂) 2 times and opsonized with subagglutinating concentrations of rabbit anti-sheep RBC IgG (ICN Pharmaceuticals) for 20 minutes at 37 °C, followed by a 20 minute incubation at 4 °C. Opsonized RBCs were pelleted by centrifugation at 2500 rpm for 5 minutes. The RBCs were washed 3 times with 1 mL BWD buffer and then resuspended in 1 mL BWD and stored at 4 °C. For complement mediated phagocytosis, RBCs were first opsonized with rabbit anti-sheep RBC IgM (Cederlane Laboratories) following the IgG opsonization protocol above. The IgM opsonized RBCs were then incubated with 10% (volume::volume) Complement C5 deficient human serum (Sigma) for 20 minutes at 37°C, followed by 20 minutes at 4°C. The RBCs were then washed 3 x 1 mL BWD buffer and then stored at 4°C.

Image Acquisition

24 hours after transfection, RAW cells were washed and scraped into 1 mL of fresh medium. The resuspended cells were plated onto 35 mm glass-bottom dishes (MatTek) and allowed to adhere for 6-8 hours. 1 hour prior to imaging, cells were washed with BWD 3 times and returned to the 37 °C incubator in 1 mL of BWD. For complement mediated phagocytosis, cells were treated with 100 nM PMA 30 minutes prior to imaging to activate complement receptors. For imaging, cells were incubated at 37 °C on a heated stage connected to a humidifier module (Zeiss). To further prevent media evaporation, the cells were covered with an optically clear FoilCover (Zeiss). To start phagocytosis, 1 mL of 50-fold diluted opsonized RBCs was added dropwise to the macrophages on the microscope stage. In the next 5-10 minutes, a fluorescent macrophage was selected for observation and then image acquisition was started. For each imaging run, 61 timepoints were collected over a total duration of 13.7 minutes. For each timepoint, a 4 plane z-stack of fluorescent images, spaced 1.5 μm apart, was acquired. In each plane, a GFP channel and an mRFP channel was collected. In addition, one DIC image (50 ms exposure time) was acquired at each timepoint. The total of 9 images per timepoint was collected at maximum speed, which resulted in 1 timepoint acquired per 13.7 seconds.

Imaging was performed using a 63X oil immersion objective on a Zeiss Axiovert 200M inverted microscope equipped with a 75 W xenon lamp. Fluorescence images were acquired using FITC and Cy3 filter sets (Chroma Technology) to acquire GFP and mRFP signals, respectively, using 200 ms exposure times, 2X2 binning and a 10% ND filter. Images were collected using a Sensicam CCD camera (PCO Computer Optics). Slidebook software (Intelligent Imaging Innovations) was used to acquire and analyze the images.

Image Analysis

Each fluorescent image was background corrected based on cell-free regions of the image. For each phagocytic event, the optimal plane (where the phagocytic cup was in best focus as judged by eye) was determined at each timepoint. The best planes were then stitched together to create a 2D timelapse imaging series for each phagocytic event. For each event, the timepoint at which pseudopod fusion occurred, visualized most easily in the fluorescent images, was set as the zero time reference (Marshall et al., 2001). Only events in which the macrophage and RBC could be observed 8 timepoints before fusion and 23 timepoints after fusion were further analyzed. Thus, for each phagocytic event, 32 timepoints covering a span of 438 seconds were analyzed. Although arbitrarily chosen, this timescale allows for complete analysis of the FRL α and Cdc42 dynamics that are observed.

To analyze fusion protein accumulation during phagocytosis, I averaged the GFP/mRFP ratio at the site of phagocytosis (R_p) and normalized it to the GFP/mRFP ratio in the cell cytoplasm (R_c) for each timepoint. This normalization accounts for different levels of fusion protein expression in different cells and thereby allows comparisons between phagocytic events occurring in different cells. This method of analysis is conceptually similar to previously described methods (Hoppe and Swanson, 2004). In the implementation used here, R_p was calculated by creating a mask, one for every timepoint, around the region of contact between the macrophage and the RBC. For early timepoints, the R_p mask is flat and represents the binding site of the RBC on the macrophage. As the pseudopods advance along the perimeter of the RBC, the R_p mask becomes U-shaped and encompasses the two pseudopods as well as the base of the phagocytic cup. At fusion and subsequent timepoints, the R_p mask forms a circle around the RBC. Similarly, an R_c mask was also created at every timepoint. The R_c mask was positioned in a region of the cell cytoplasm away from the nucleus and distant from any phagocytic events. For each pixel in each mask at each timepoint, the ratio of GFP intensity to mRFP intensity was calculated. The ratios for each mask were then averaged. Thus, for every timepoint, the average GFP/mRFP ratio at the site of phagocytosis and the average GFP/mRFP ratio in the cell cytoplasm were generated. These ratios were

used to generate the pseudocolored images and graphical data shown in Figures 3-6, 3-7, 3-8 and 3-9.

Phagocytosis Assays for siRNA Transfected Cells

24 hours after transfection, RAW cells were scraped and plated onto a 12 mm glass coverslip (Fisher) in a fresh well of a 24-well plate and allowed to adhere overnight. 48 hours after transfection, cells were washed with BWD 2 times and returned to the 37 °C incubator in 0.2 mL of BWD. After 1 hour, 20 µL of 10-fold diluted opsonized RBCs were added to each well and incubated at 37 °C. After 1 hour, cells were washed 2 times with BWD and then incubated for 1 minute in 1 mL distilled water to lyse extracellular RBCs. Cells were washed 2 times with PBS and then fixed in 3.7% formaldehyde for 20 minutes. Cells were then washed 3 times with PBS and then permeabilized with PSG buffer (PBS, 0.01% saponin, 0.25% gelatin, 0.02% NaN₃) for 30 minutes. Intracellular RBCs were then stained with FITC-conjugated anti-Rabbit antibodies (Jackson ImmunoResearch) diluted 1:200 in PSG. After 1 hour, cells were washed 3 times with PSG and coverslips were mounted on glass slides. Imaging was performed on a Zeiss Axiovert 200M inverted microscope using a 63X oil immersion objective. In each field, the number of internalized RBCs was counted using the FITC fluorescence signal and the number of macrophages was counted using the autofluorescence of the cells. The phagocytic index (defined as the number of

RBCs/100 macrophages) was calculated from these values (Botelho et al., 2000). Each experiment was performed in duplicate and a minimum of 300 macrophages was counted for every condition.

Results

Autoinhibition Regulates the Actin Assembly Activity and Intracellular Localization of FRL α

To investigate the biochemical regulation of FRL α , recombinant N and C terminal fragments were separately expressed and purified. Most previous *in vivo* studies of DRF N-terminus function have used fragments based on the conserved GBD-FH3 sequence elements. However, recent structural studies of the mDia1 N-terminus have demonstrated these conserved sequence elements do not demarcate structural elements of the protein. Therefore, the results from previous studies using constructs representing divided structural domains are difficult to interpret. Here, the predicted structural domains of FRL α , based on sequence alignments with mDia1, have been used to examine the function of its N-terminus (Otomo et al., 2005a). The N-terminal construct (residues 1-450) contains the regions of FRL α that align with the G, DID and DD elements of mDia1 (the alignment suggests that FRL α lacks a CC region), while the C-terminal construct (residues 612-1094) contains the FH2 and DAD domains (Figure 3-1A). Pull

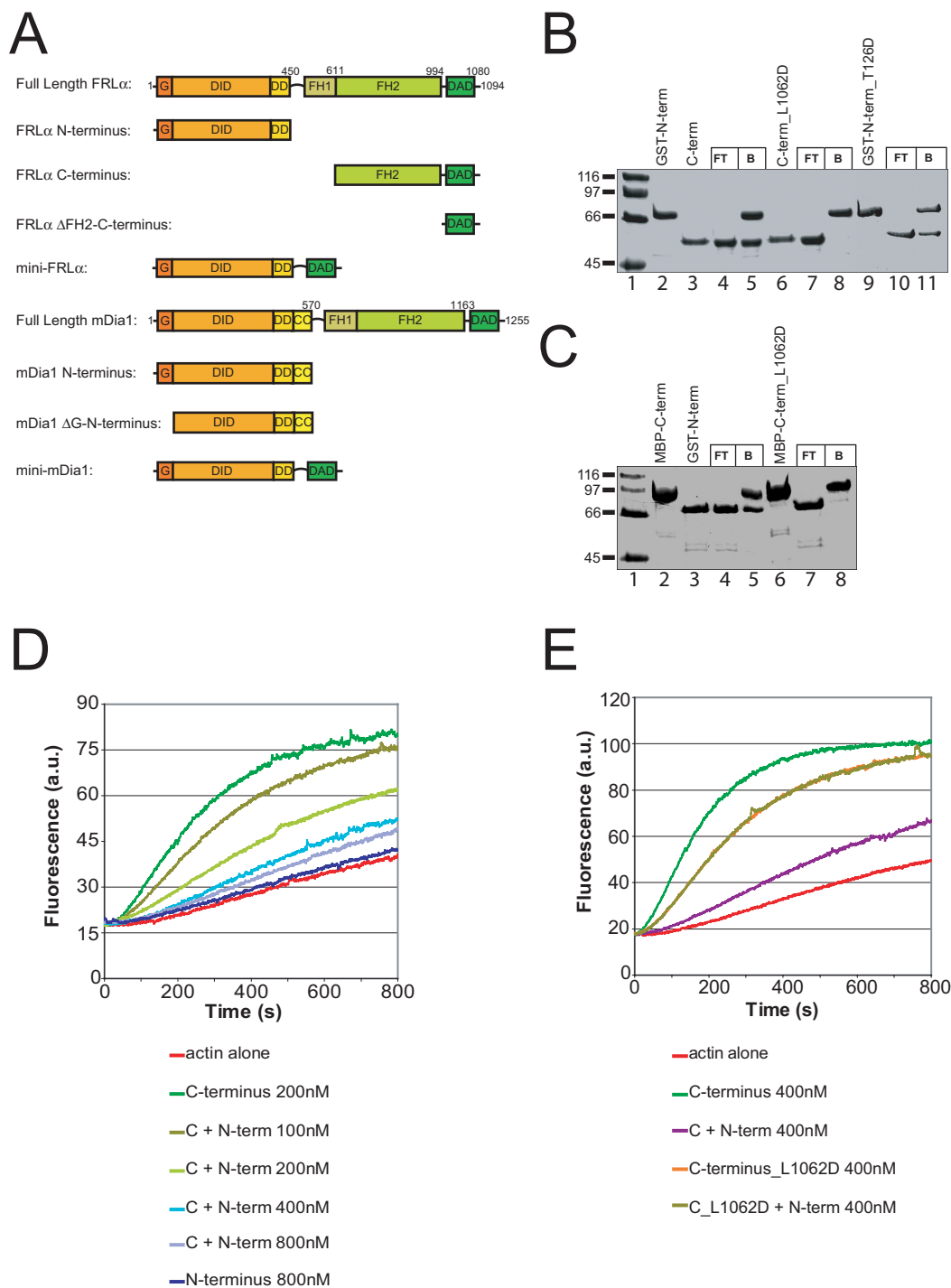


Figure 3-1

Figure 3-1. The N-terminus of FRL α Negatively Regulates the Actin Assembly Activity of the C-terminal FH2 Domain.

- (A) Schematic diagrams of FRL α , mDia1 and the primary constructs used in this study.
- (B) Interaction between the N- and C-termini of FRL α . 3 μ M GST-tagged N-terminus proteins were immobilized on glutathione sepharose beads and used to pull down 3 μ M C-terminal constructs. Aliquots of the purified proteins used are shown in lanes 2, 3, 6 and 9. Unbound proteins in the flow-through (FT) and proteins remaining on the beads after five washes (B) are shown for each experiment. GST-N-terminus was used to pull down wildtype C-terminus (lanes 4 and 5) or C-terminus_L1062D containing a point mutation in the DAD domain (lanes 7 and 8). GST-N-terminus_T126D (Cdc42 binding mutant) was used to pull down wildtype C-terminus (lanes 10 and 11). For each experiment, the volumes loaded on the SDS-PAGE gel were adjusted to equalize protein concentrations in the FT and B lanes. Gels are stained with Coomassie Blue.
- (C) Similar to (B) except MBP-tagged wildtype C-terminus (lane 2) or mutant C-terminus (lane 6) was immobilized on amylose resin and used to pull down GST-N-terminus (lane 3). FT and B samples from the wildtype C-terminus pull down (lanes 4 and 5) or the mutant C-terminus pull down (lanes 7 and 8) are shown.
- (D) Dose-dependent inhibition of actin assembly activity of the FRL α C-terminus (200 nM) in the presence of the indicated amount of N-terminus monitored by the increase in fluorescence of pyrene-actin (4 μ M, 5% labeled) upon incorporation into filaments.
- (E) Effect of the L1062D DAD motif mutation on the ability of 400 nM N-terminus to inhibit actin assembly (4 μ M, 5% pyrene-labeled) by 400 nM wildtype or mutant C-terminus.

down assays show that immobilized GST-tagged N-terminus can interact directly with untagged C-terminus (Figure 3-1B). Binding is also observed when immobilized MBP-tagged C-terminus is used to pull down GST-tagged N-terminus (Figure 3-1C). The DAD motif is required for binding since a C-terminal construct mutated at a single conserved leucine residue within the DAD motif (L1062D) can not interact with the N-terminal fragment (Figure 3-1B,C). Mutation of the same residue in mDia1 (Takanori Otomo and MKR, unpublished data) or mDia2 (Alberts, 2001) also prevents interactions between N- and C-terminal fragments.

A well characterized actin assembly assay (Higgs and Pollard, 1999) was used to determine the functional consequences of the interaction between the N- and C-termini. As previously described, the FH2 domain of FRL α can stimulate actin filament assembly, although it is approximately 50-fold less potent than the FH2 domain of mDia1 (Figure 3-1D) (Harris et al., 2004; Li and Higgs, 2003). Addition of increasing amounts of N-terminus inhibits the activity of the C-terminus in a dose-dependent manner, but has no effect on FH2-independent actin assembly (Figure 3-1D). The N-terminus is unable to inhibit the activity of the L1062D DAD mutant C-terminus, thereby demonstrating that binding of the N-terminus to the C-terminus is required for inhibition (Figure 3-1E). These results demonstrate that the biochemical activity of the FRL α FH2 domain is regulated by DAD-mediated autoinhibitory interactions with the N-terminus.

To examine how interactions between the N- and C-terminal elements affect the biological function of FRL α , RAW 264.7 cells, a murine macrophage cell line, were transfected with GFP-tagged FRL α . Full length FRL α is cytoplasmic and is excluded from the nucleus as shown by confocal images of cells coexpressing FRL α -GFP and mRFP, a uniformly distributed fluorescent control (Figure 3-2A). In contrast, the N-terminal fragment of FRL α is located primarily at the plasma membrane, suggesting that in the full length protein the cellular localization of the N-terminus may be controlled by binding to the C-terminus (Figure 3-2B). To test this hypothesis, the cellular localization of FRL α -GFP proteins with mutations that would impair the N+C interaction was determined. Introduction of the L1062D DAD mutation, which blocks the N+C interaction *in vitro* (Figure 3-1B,C), results in plasma membrane localization of full length FRL α (Figure 3-2C). In mDia1, an L260E mutation in the N-terminal DID region blocks DAD binding without affecting Rho interactions (Otomo et al., 2005a). The analogous mutation in full length FRL α (V281E) causes the protein to localize at the plasma membrane (Figure 3-2D).

Next, I constructed a truncated FRL α protein, called mini-FRL α , containing the N-terminal 536 residues (G-DID-DD regions plus sequence elements which do not align with mDia1) tethered by a (Gly-Gly-Ser)₂ linker to the DAD-containing C-terminal 101 residues (Figure 3-1A). Like full length

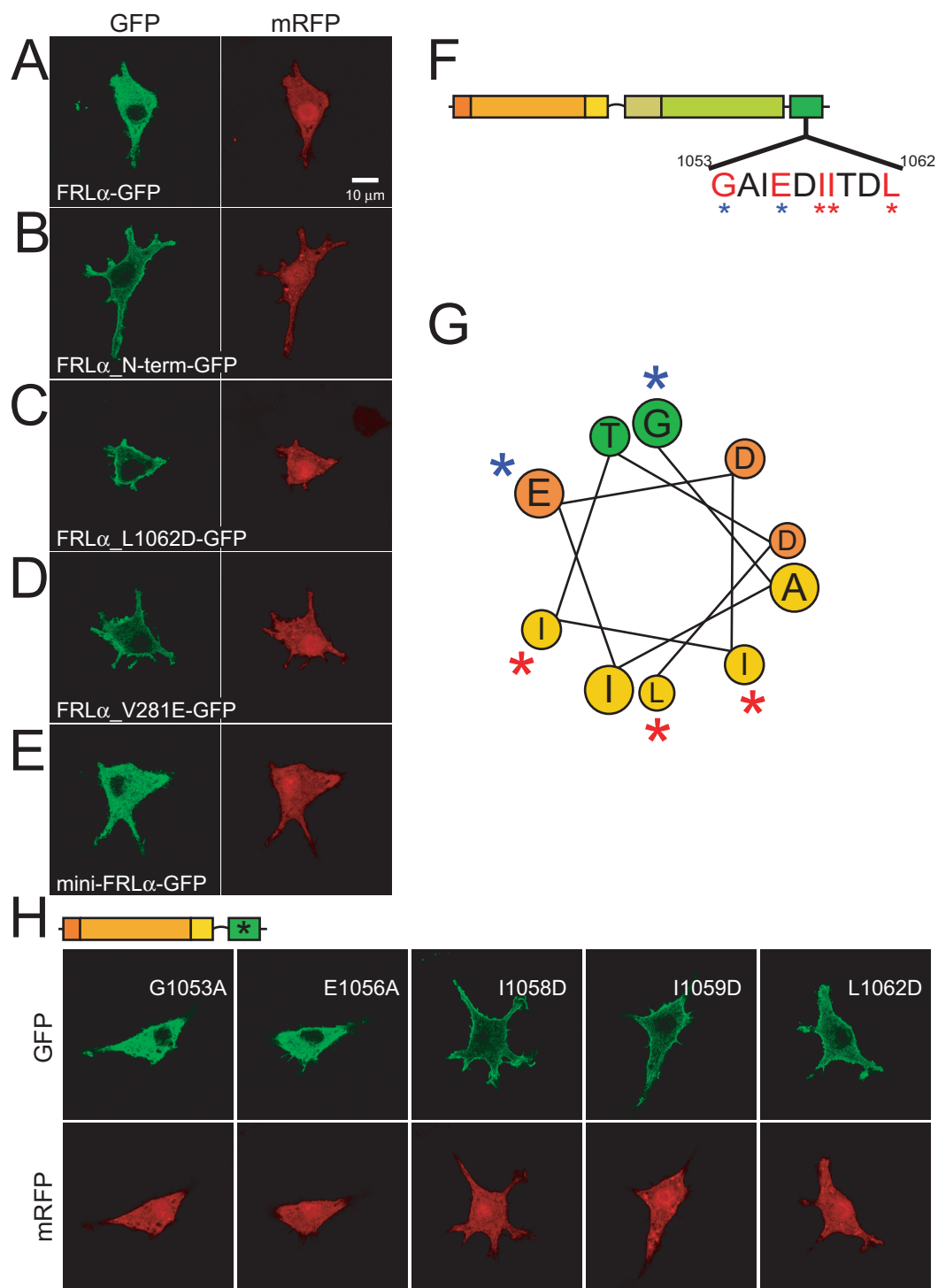


Figure 3-2

Figure 3-2. Autoinhibition Regulates FRL α Localization.

Confocal images of RAW cells co-expressing GFP fusion proteins and mRFP. The mRFP serves as an evenly distributed control fluorophore in these cells. For these and all subsequent confocal images the intensities for each channel have been normalized against the maximum value in the cell depicted in each image. The GFP fusion proteins are:

- (A) Full length FRL α -GFP.
- (B) FRL α N-terminus-GFP.
- (C) Full length FRL α -GFP containing an L1062D mutation in the DAD region of the C-terminus.
- (D) Full length FRL α -GFP containing a V281E mutation in the DID region of the N-terminus.
- (E) mini-FRL α -GFP consisting of the N-terminus of FRL α fused directly to the DAD domain with an artificial (Gly-Gly-Ser)₂ linker.
- (F) A schematic diagram of FRL α showing a portion of the DAD motif (conserved residues are in red). Residues that effect autoinhibitory control of FRL α localization are marked with a red asterisk, while residues that have no effect are indicated with blue asterisks.
- (G) A helical wheel depicting the FRL α DAD motif. Residues involved in autoinhibitory control of localization are marked with asterisks as in (F).
- (H) Confocal images of cells co-expressing mRFP and the indicated mutant mini-FRL α -GFP fusion protein.

FRL α , mini-FRL α -GFP is located in the cytoplasm of transfected cells (Figure 3-2E). The DAD motif contains five highly conserved residues (Figure 3-2F) (Alberts, 2001) and is predicted to form an amphipathic helix (Figure 3-2G) when bound to the DID based on NMR analyses of mDia1 (Takanori Otomo and MKR, unpublished data). Mutation of the conserved residues G1053 or E1056 on one face of the putative FRL α DAD helix has no effect on mini-FRL α localization (Figure 3-2H). In contrast, mutation of any one of the conserved hydrophobic residues I1058, I1059 or L1062 on the opposite face of the helix results in plasma membrane localization of mini-FRL α (Figure 3-2H). These results demonstrate that binding of the hydrophobic face of the putative amphipathic DAD helix is necessary and sufficient to block membrane localization mediated by the FRL α N-terminus. The combined *in vitro* and *in vivo* data show that the interactions between the N- and C-termini are mutually autoinhibitory with the N-terminus blocking the actin assembly activity of the FH2 domain and the C-terminus blocking the plasma membrane localization “activity” of the N-terminus.

Cdc42 Relieves FRL α Autoinhibition in vitro and in vivo

Following the model of mDia1, I next sought to determine if Rho GTPases could relieve autoinhibition of FRL α . Previously reported pull down assays indicated that an N-terminal fragment of FRL α can specifically associate with

Rac1 in a nucleotide-independent manner (Yayoshi-Yamamoto et al., 2000). However, I could not detect an interaction between recombinant Cdc42 or Rac1 loaded with a GTP analogue, GMPPNP, and GST-tagged N-terminus using similar assays (data not shown). Unexpectedly, high concentrations of Cdc42-GMPPNP can relieve N-terminal inhibition of the FRL α FH2 domain (Figure 3-3A). The Cdc42 effect is dose-dependent and saturates at ~ 400 μ M GTPase, a concentration that slightly decreases the activity of the isolated C-terminus (Figure 3-3A). Under these conditions, even though Cdc42-GMPPNP exhibits low potency, it essentially fully relieves inhibition by the N-terminus. Cdc42-GDP is a much weaker activator compared to Cdc42-GMPPNP (Figure 3-3B); activation saturates at 430 μ M Cdc42-GDP, but at a level below that achieved with 10-fold less Cdc42-GMPPNP. Rac-GMPPNP only modestly relieves autoinhibition of FRL α actin assembly activity (at a level comparable to Cdc42-GDP, data not shown). The results for Cdc42-mediated activation of FRL α are in contrast to Rho-mediated activation of mDia1 where the potency of activation is higher (single-digit micromolar range), but where the degree of activation at saturation and the nucleotide-dependence are much less (Li and Higgs, 2003; Otomo et al., 2005a).

Recent biochemical analyses have identified residues in both the G and DID regions of mDia1 that are important for the interaction with GTPase (Otomo et al., 2005a; Rose et al., 2005). A V161D mutation in the mDia1 DID decreases

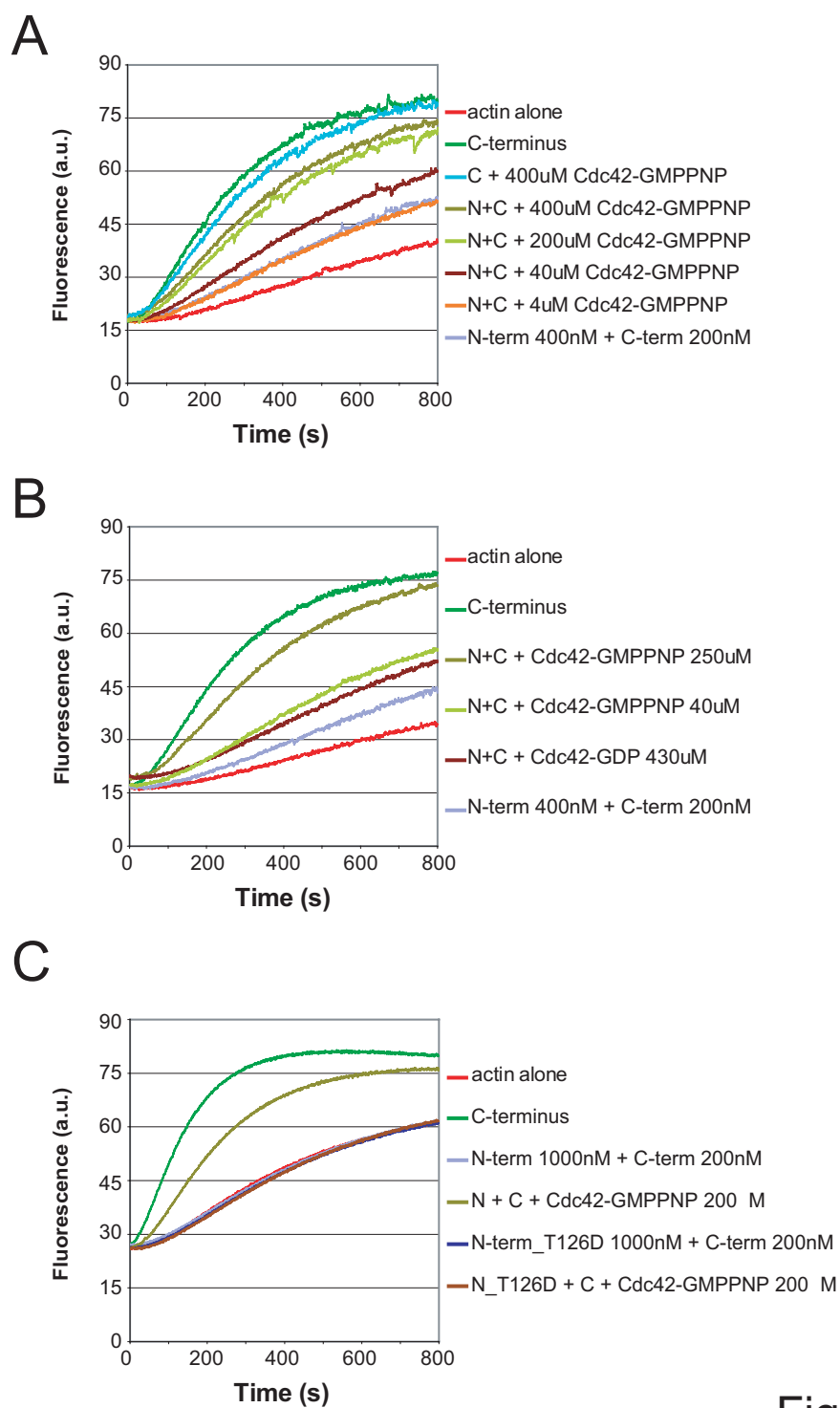


Figure 3-3

Figure 3-3. Active Cdc42 Relieves Autoinhibition of FRL α Actin Assembly Activity.

Actin assembly assays were performed with 4 μ M actin, 5% pyrene-labeled.

- (A) Effect on inhibition of actin assembly by 200 nM C-terminus in the presence of 400 nM N-terminus by the addition of the indicated amount of Cdc42-GMPPNP.
- (B) Similar to (A) except using Cdc42-GDP.
- (C) Actin assembly by 200 nM C-terminus in the presence of 1 μ M wildtype N-terminus or 1 μ M T126D N-terminus, with or without 200 μ M Cdc42-GMPPNP.

Rho binding without affecting DAD binding (Otomo et al., 2005a). The analogous T126D mutation in the FRL α N-terminus does not affect binding to the C-terminus (Figure 3-1B) or inhibition of FH2-mediated actin assembly (Figure 3-3C), but blocks the ability of Cdc42-GMPPNP to relieve inhibition (Figure 3-3C).

The effects of Cdc42 on FRL α biochemical activity *in vitro* are mirrored by its effects on FRL α localization in macrophages. When cotransfected with constitutively active Cdc42, both FRL α -GFP and mini-FRL α -GFP localize at the plasma membrane (Figure 3-4A,B). Localization of FRL α is nucleotide and GTPase-specific as the protein remains primarily cytosolic in cells coexpressing dominant negative Cdc42 or constitutively active Rac1 or RhoA (Figure 3-4C,D,E).

Since Cdc42 is membrane-anchored through prenylation of its C-terminal CAAX motif (Ziman et al., 1993), it was tested whether Cdc42 was directly recruiting FRL α to the plasma membrane of RAW cells. The T126D mutant FRL α N-terminus, which is unresponsive to Cdc42 in actin assembly assays, is primarily cytosolic relative to the wildtype N-terminus (Figure 3-4F, upper row). In some cells, however, the T126D mutant does show partial accumulation at the plasma membrane (Figure 3-4F, lower row). To test if the plasma membrane localization of the wildtype FRL α N-terminus depends on endogenous Cdc42, I

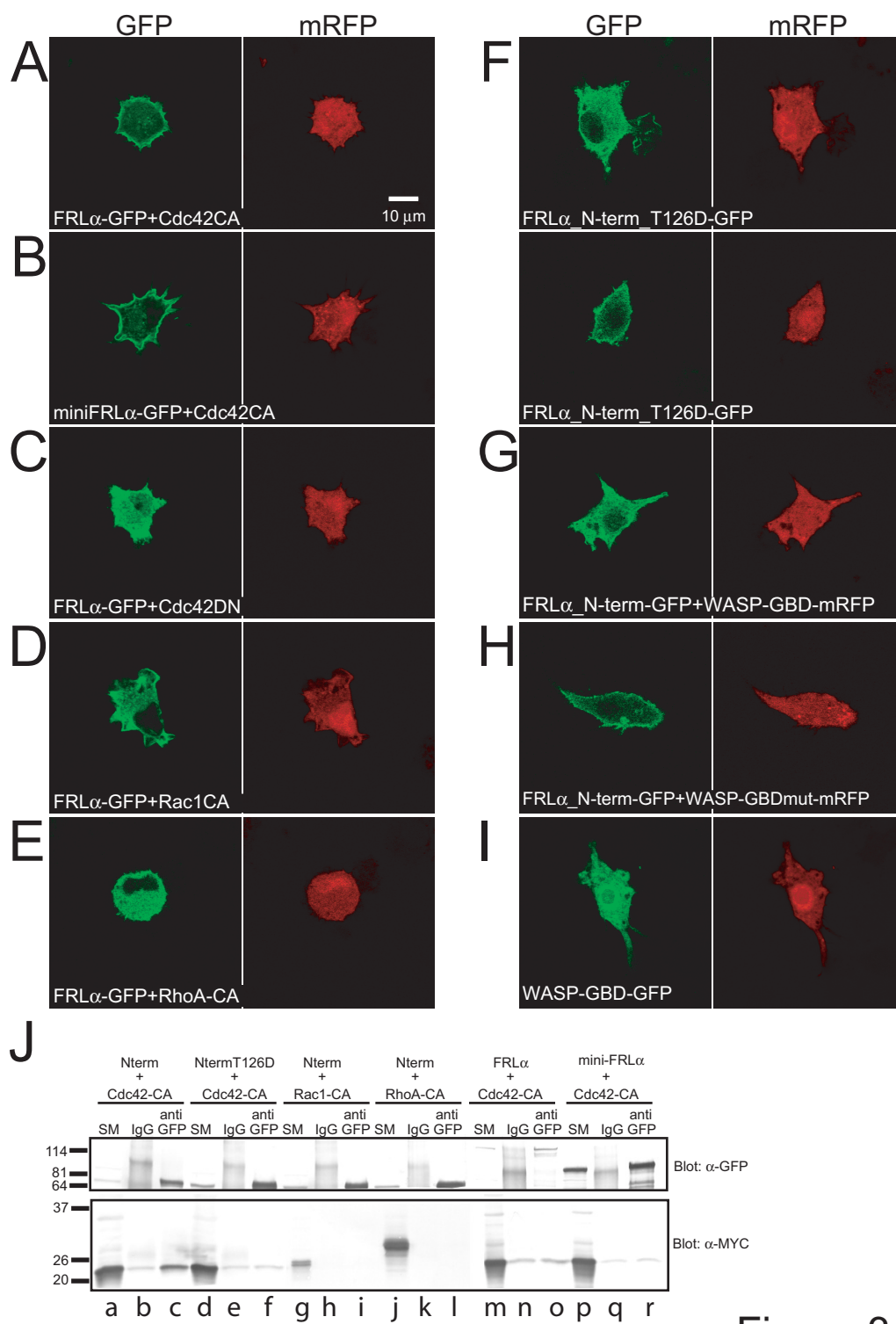


Figure 3-4

Figure 3-4. Active Cdc42 Relieves Autoinhibition of FRL α Localization.

- (A-B) Confocal images of RAW cells co-expressing mRFP, constitutively active Cdc42 and (A) full length FRL α -GFP or (B) mini-FRL α -GFP.
- (C-E) Confocal images of RAW cells expressing mRFP, full length FRL α -GFP and (C) dominant negative Cdc42, (D) constitutively active Rac1, or (E) constitutively active RhoA.
- (F) Confocal images of two different cells expressing mRFP and the FRL α N-terminus_T126D-GFP mutant. Although primarily cytosolic, the mutant is partially localized at the plasma membrane in some cells (seen more clearly in the lower panel).
- (G-H) Confocal images of cells co-expressing N-terminus-GFP and an mRFP fusion of (G) the WASP-GBD or (H) a mutant WASP-GBD that does not bind Cdc42.
- (I) Confocal images of a cell co-expressing mRFP and WASP-GBD-GFP.
- (J) Co-immunoprecipitation experiments using lysates from 293t cells co-expressing myc-tagged Rho GTPase mutants and different FRL α -GFP constructs. Lysates were immunoprecipitated using anti-GFP or control IgG antibodies and blotted with anti-GFP or anti-myc antibodies. For each experiment (lanes a-c, d-f, g-i, j-l, m-o, and p-r), the lysate (starting material) is shown in the first lane followed by the material bound to control IgG beads or anti-GFP beads in the next two lanes.

coexpressed it with the GBD of WASP, a nanomolar binding partner of active Cdc42 that should sequester the active GTPase. The wildtype FRL α N-terminus is cytoplasmic in cells coexpressing GBD-mRFP (Figure 3-4G). In contrast, the plasma membrane localization of the FRL α N-terminus is unperturbed in cells coexpressing a mutant WASP GBD that has no detectable binding affinity for Cdc42, indicating that competition for Cdc42 binding prevents FRL α membrane localization (Figure 3-4H). Together, the T126D mutant N-terminus data and the WASP-GBD data suggest that Cdc42 binding is necessary for efficient plasma membrane localization of FRL α . The WASP-GBD itself is cytoplasmic and does not show any accumulation at the plasma membrane whether expressed at low or high levels (Figure 3-4I). Since the WASP-GBD is a high affinity Cdc42 binding partner, this result suggests that Cdc42 binding is not sufficient to mediate membrane localization of its effectors. This result plus the partial membrane localization of the T126D mutant N-terminus, which shows no detectable response to Cdc42 *in vitro*, implies that an additional, presently unknown, factor may contribute to FRL α localization at the plasma membrane. Thus, Cdc42 is likely necessary but not sufficient for membrane localization of FRL α .

Although the data suggest a direct interaction between Cdc42 and the N-terminus of FRL α , I have been unsuccessful in demonstrating a direct interaction in pull down or fluorescence-based binding assays using bacterially expressed,

recombinant proteins (data not shown). However, when cotransfected into mammalian 293t cells, constitutively active Cdc42 and the wildtype FRL α N-terminus can be co-immunoprecipitated (Figure 3-4J, lanes a-c). The N-terminus does not co-immunoprecipitate with constitutively active Rac1 or RhoA, which indicates the GTPase specificity of FRL α (Figure 3-4J, lanes g-i and j-l, respectively). The T126D mutant N-terminus does not co-immunoprecipitate with Cdc42, suggesting that, *in vitro* and in cells, the Cdc42-responsiveness of FRL α is mediated by the same set of interactions (Figure 3-4J, lanes d-f). Further, full length FRL α and mini-FRL α do not co-immunoprecipitate with Cdc42, even though they localize at the plasma membrane when coexpressed with constitutively active Cdc42 (Figure 3-4J, lanes m-o and p-r, respectively). These results rule out the possibility that Cdc42 and the FRL α N-terminus are co-immunoprecipitating simply because they are both localized at the plasma membrane. Rather, they suggest that Cdc42 has higher affinity for the FRL α N-terminus as compared to an autoinhibited FRL α molecule, which is consistent with the idea that Cdc42 must compete with the autoinhibitory interactions present in full length or mini-FRL α . It is presently unclear why pull down experiments with mammalian cell lysates show an interaction between the FRL α N-terminus and active Cdc42, while similar experiments using purified, bacterially-expressed proteins do not.

The *in vitro* and *in vivo* data suggest that FRL α is a direct effector of Cdc42 and that the interactions between FRL α and Cdc42 may be similar to those between mDia1 and Rho. Cdc42 relieves autoinhibition of FRL α actin assembly activity *in vitro* and relieves autoinhibition of FRL α membrane localization in macrophages. The affinity of Cdc42 for FRL α is likely to be relatively low, compared to the nanomolar affinity of Cdc42 for the GBD regions of effectors such as WASP or PAK (Rudolph et al., 2001; Thompson et al., 1998), which suggests that Cdc42 may have to cooperate with other factors to regulate FRL α *in vivo*.

Autoinhibitory Control of mDia1 Intracellular Localization

To determine whether autoinhibitory control of localization is unique to FRL α or is a general feature of DRF biology, parallel experiments using mDia1 were performed. The results of recent biochemical and structural studies of autoinhibition and activation of mDia1 allowed the construction of GFP fusion proteins with defined structural domains of the protein (Figure 3-1A) (Li and Higgs, 2005; Otomo et al., 2005a; Rose et al., 2005). A GFP fusion of the N-terminus of mDia1 (residues 1-570) is localized at the plasma membrane (Figure 3-5A). Both full length mDia1-GFP and mini-mDia1-GFP, analogous to the mini-FRL α construct, are cytoplasmic and excluded from the nucleus of RAW

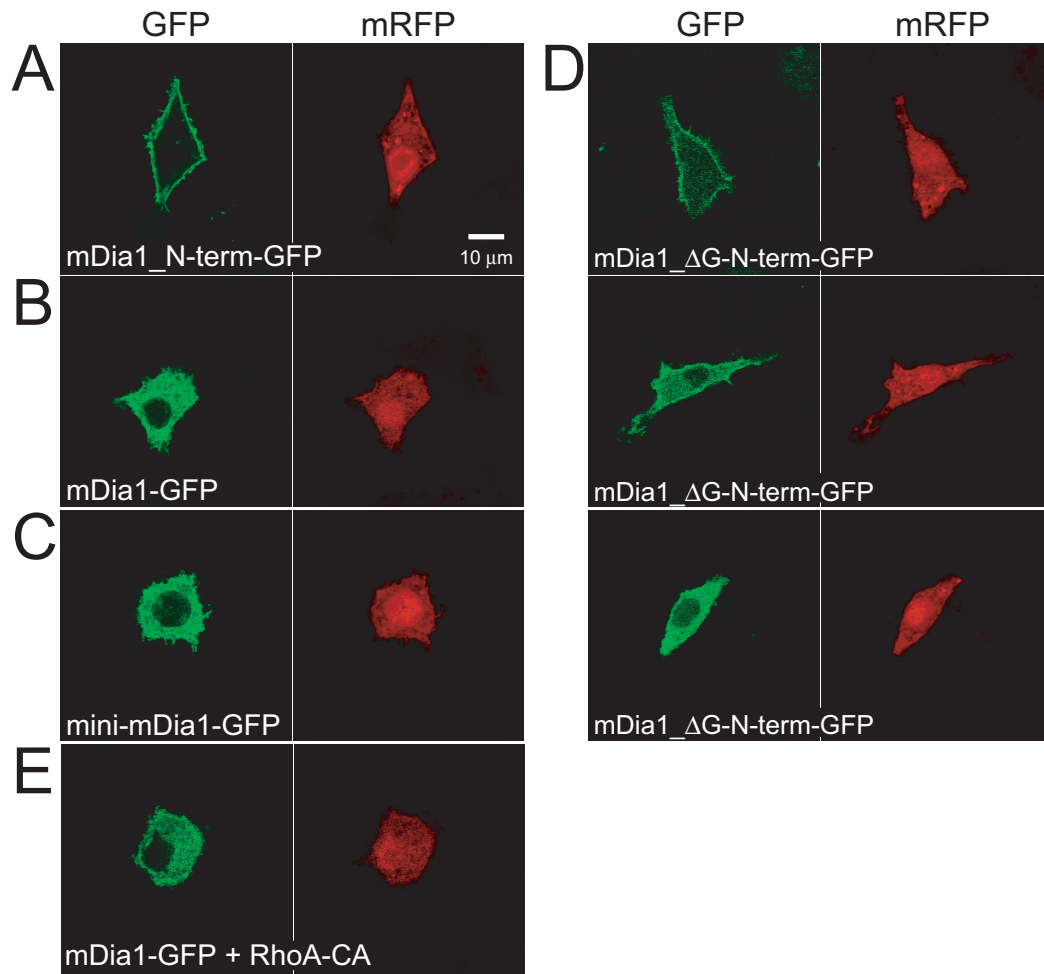


Figure 3-5

Figure 3-5. Autoinhibition Controls the Localization of the Rho-regulated DRF mDia1.

Confocal images of RAW cells co-expressing mRFP and

- (A) mDia1 N-terminus-GFP,
- (B) Full length mDia1-GFP,
- (C) mini-mDia1-GFP, or
- (D) mDia1 Δ G-N-terminus-GFP. Three different cells are shown to illustrate the different localization patterns observed with this construct. The GFP fusion is localized at the plasma membrane in the first cell (upper panel) and in the cytosol of the third cell (lower panel). The second cell (middle panel) has an intermediate distribution between membrane and cytosol. As discussed in the text, this variable localization pattern correlates with the absolute level of GFP signal in each cell. At low GFP levels, the fusion protein is primarily at the plasma membrane while at higher levels it is primarily cytosolic.
- (E) Confocal images of a cell expressing mRFP, full length mDia1-GFP + constitutively active RhoA.

cells (Figure 3-5B,C). These results show that autoinhibition controls localization of mDia1 in a manner analogous to FRL α , where the plasma membrane localization of the N-terminus is prevented by DAD-binding.

Next, the role of Rho in regulating the membrane localization of mDia1 was tested. Deletion of the G region (residues 1-130) of the mDia1 N-terminus has previously been shown to prevent interactions with Rho (Li and Higgs, 2003; Otomo et al., 2005a; Rose et al., 2005). In cells expressing low concentrations of Δ G-N-terminus-GFP, the fusion protein is plasma membrane localized (Figure 3-5D, upper panel). However, as the expression level of the fusion protein increases, the GFP signal becomes relatively more intense in the cytosol suggesting that the membrane binding site becomes saturated. (Figure 3-5D, middle and lower panels). While coexpression of constitutively active Cdc42 causes relocalization of FRL α -GFP from the cytoplasm to the plasma membrane (Figure 3-4A), coexpression of constitutively active RhoA has no effect on the cytoplasmic localization of mDia1-GFP (Figure 3-5E). The results with the Δ G-N-terminus suggest that there is a saturable, GTPase-independent interaction that is sufficient to mediate membrane localization of the N-terminus at low levels of expression. At higher levels of expression, the G region is necessary for efficient membrane localization. Thus, for both FRL α and mDia1, the data suggest that efficient plasma membrane localization of the N-terminus is GTPase-dependent,

but that there is a GTPase-independent component important for localization as well.

FRL α is Required for Fc- γ Receptor Mediated Phagocytosis and is Recruited to the Phagocytic Cup by Cdc42

Next, it was determined if FRL α is involved in Fc- γ receptor mediated phagocytosis. This process is Cdc42-dependent and requires extensive actin rearrangement at the cell surface of macrophages (Caron and Hall, 1998). Using siRNAs directed against FRL α , significant knockdown of endogenous FRL α in RAW macrophages was achieved (Figure 3-6A). Fc- γ receptor mediated phagocytosis of IgG opsonized red blood cells (RBCs) was reduced in these cells by $45 \pm 4\%$ compared to cells expressing control siRNAs (Figure 3-6B), demonstrating an important role for FRL α in this process.

To better understand the function of FRL α in phagocytosis, timelapse microscopy was used to analyze phagocytic events in live RAW macrophages incubated with IgG opsonized RBCs at 37 °C. Under the assay conditions, macrophages readily phagocytose the RBCs and each phagocytic event requires ~90 seconds to complete from the time of cell-cell contact until the RBC is clearly internalized as judged by light microscopy. For RBCs that encounter macrophages from the side, as opposed to landing on top of them, the extension of

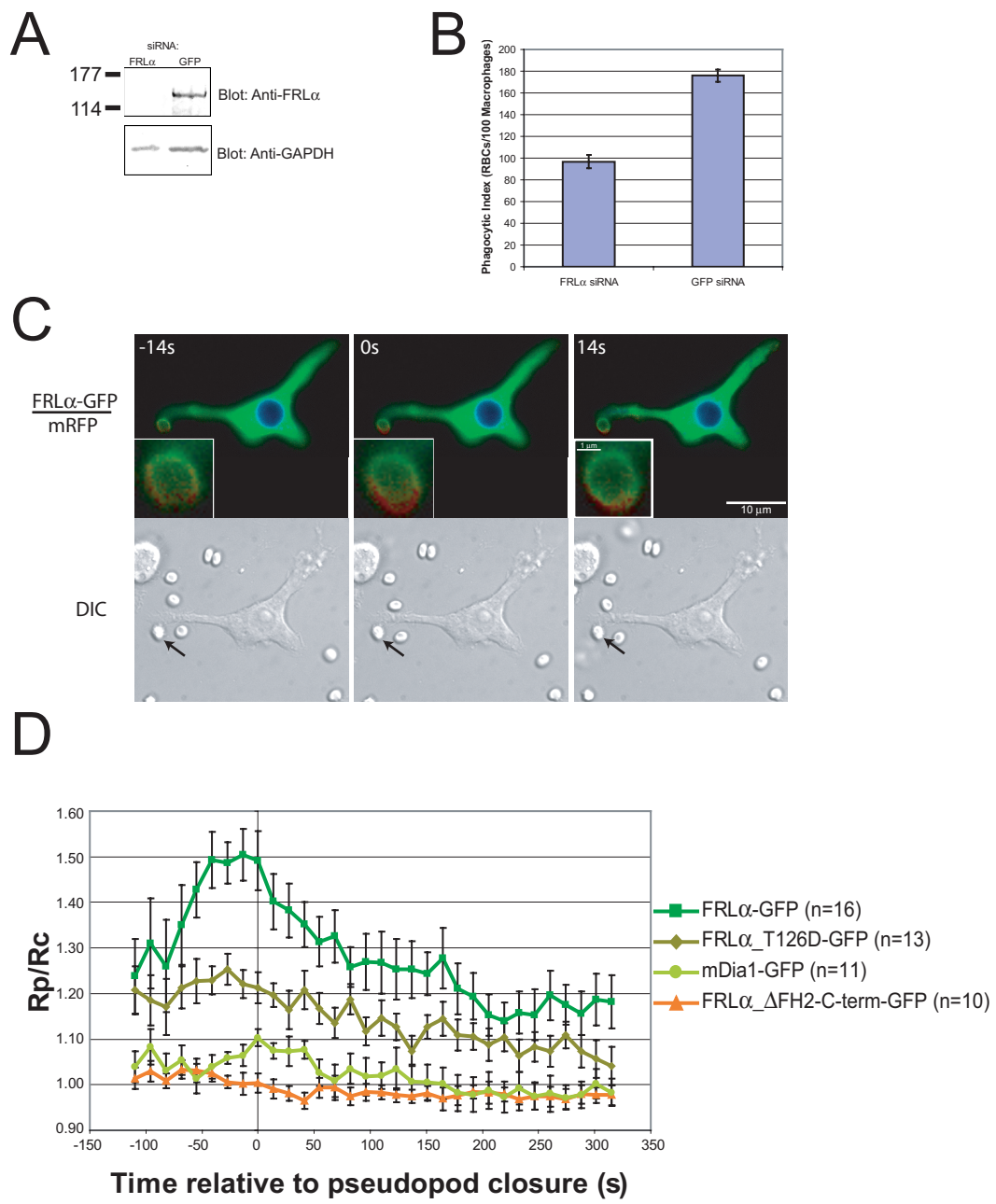


Figure 3-6

Figure 3-6. Cdc42 recruits FRL α to the Phagocytic Cup During Fc- γ Receptor Mediated Phagocytosis.

- (A) Western blot of lysates prepared from cells transfected with siRNAs directed against FRL α or GFP (control) and probed with anti-FRL α or anti-GAPDH (loading control) antibodies.
- (B) Phagocytic index (defined as the number of RBCs/100 macrophages) of siRNA transfected RAW macrophages. Experiments were performed in duplicate and repeated 3 times. Data are the averages based on counting at least 300 macrophages per experiment. Error bars represent the standard error of the mean.
- (C) FRL α -GFP expressing cell undergoing Fc- γ Receptor Mediated Phagocytosis. The zero timepoint is a reference for when the phagosome closes around the RBC being engulfed. The upper panels are pseudocolored to represent the GFP/mRFP ratio at each pixel in the cell. Higher ratios are represented by warmer colors and represent an increased accumulation of GFP relative to mRFP. The lower panel is the corresponding DIC image for each timepoint. The ingested RBC is indicated by the arrow. The insets depict an additional 4x magnification of the phagocytic cup.
- (D) Timecourse of formin accumulation during Fc- γ Receptor Mediated Phagocytosis. N indicates the number of phagocytic events analyzed for each construct. For each timepoint, the GFP/mRFP ratio at the cell surface in contact with the RBC (R_p) was divided by the ratio in the cell cytoplasm (R_c). Error bars represent the standard error of the mean.

macrophage pseudopods around the RBC is readily observable in fluorescently labeled cells. The pseudopods eventually meet at the top of the RBC and fuse to close the phagosome, which is then internalized into the main cell body.

In cells coexpressing FRL α -GFP and mRFP, ratiometric imaging was used to determine specific sites of FRL α accumulation. During phagocytosis, FRL α -GFP accumulates in the developing phagocytic cup and appears to concentrate at the tips of the extending pseudopods (Figure 3-6C, Supplemental Movies 1,2,3, see Appendix). FRL α -GFP accumulation is maximal immediately prior to pseudopod fusion, which was set as a reference timepoint in order to compare multiple phagocytic events (Marshall et al., 2001), and rapidly dissipates as the RBC is internalized (Figure 3-6C,D). A control GFP construct fused to the C-terminal 101 residues of FRL α does not accumulate at the phagocytic cup (Figure 3-6D). Consistent with previous findings that Rho is not involved in Fc- γ receptor mediated phagocytosis, mDia1-GFP does not localize to the cup during this process (Figure 3-6D). The T126D mutant of FRL α also does not localize to the cup, demonstrating that FRL α recruitment likely requires interaction with Cdc42 (Figure 3-6D).

Unexpectedly, a GFP fusion of the C-terminus of FRL α also localizes to the phagocytic cup during Fc- γ receptor mediated phagocytosis (Figure 3-7). The FH2 and DAD domains in the C-terminus have not previously been identified as

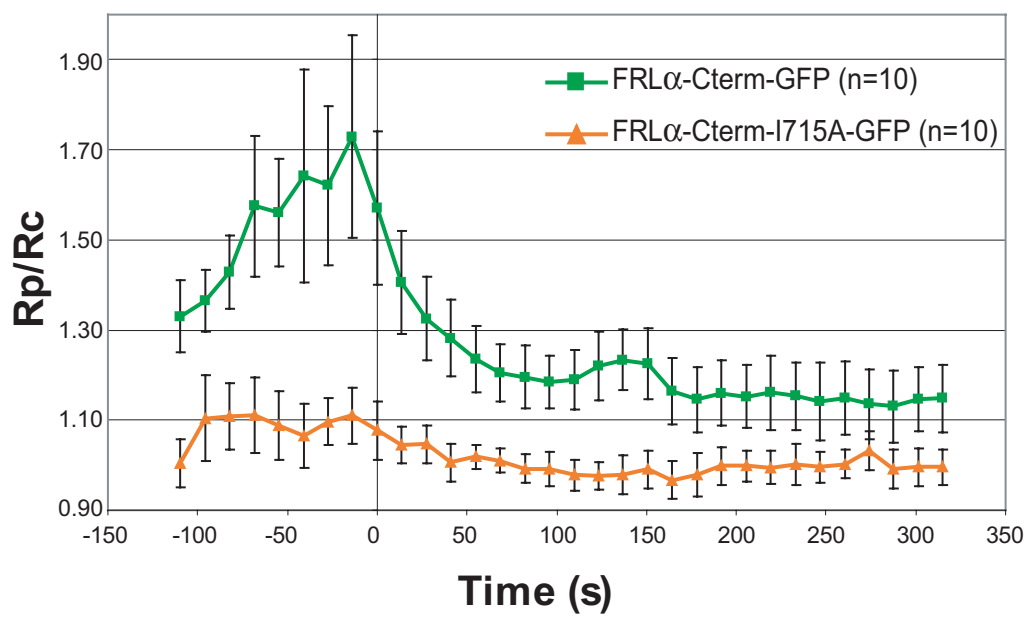


Figure 3-7

Figure 3-7. The Isolated C-terminus of FRL α is Recruited to the Phagocytic Cup During Fc- γ Receptor Mediated Phagocytosis Through its Interaction with Actin.

Timecourse of wildtype or mutant FRL α -C-terminus-GFP accumulation during Fc- γ Receptor Mediated Phagocytosis. The I715A mutant is unable to interact with actin. N indicates the number of phagocytic events analyzed for each construct. For each timepoint, the GFP/mRFP ratio at the cell surface in contact with the RBC (R_p) was divided by the ratio in the cell cytoplasm (R_c). Error bars represent the standard error of the mean.

important for DRF localization. Since the FH2 domain can interact strongly with actin and since the phagocytic cup is rich in actin, it was hypothesized that the observed localization of the C-terminus is due to FH2-mediated actin binding. To test this hypothesis, an I715A mutant C-terminus-GFP fusion construct was generated. The analogous I1431A mutation in the Bni1p FH2 domain prevents its association with actin (Otomo et al., 2005b; Xu et al., 2004). The I715A mutant C-terminus does not localize to the phagocytic cup during Fc- γ receptor mediated phagocytosis (Figure 3-7). These results suggest that the isolated C-terminus of FRL α can be recruited to the phagocytic cup by actin. The data also suggest that this actin-mediated recruitment is not sufficient to recruit autoinhibited FRL α as the T126D mutant full length molecule is not recruited to the cup. Thus, the recruitment of the isolated C-terminus is probably not physiologically relevant and is most likely an experimental artifact caused by its high affinity for actin. Further, the inability of the T126D mutant to be recruited to the phagocytic cup suggests that the interaction with Cdc42 is more important for the localization of full length FRL α .

Active Cdc42 has also been shown to accumulate transiently at the extending pseudopod tips of the phagocytic cup (Hoppe and Swanson, 2004). To compare the temporal and spatial pattern of Cdc42 accumulation with that of FRL α , the localization of active Cdc42 was monitored during phagocytosis using the WASP-GBD fused to GFP. The WASP-GBD has 19 nM affinity for active

Cdc42 and a similar reagent has been used to monitor active Cdc42 localization in T cells and epithelial cells (Cannon et al., 2001; Kim et al., 2000b; Labno et al., 2003; Seth et al., 2003). As a control, a mutant GBD-GFP construct that is unable to bind Cdc42 was used. The data show that Cdc42, like FRL α , is recruited transiently to the phagocytic cup and that its accumulation peaks immediately prior to pseudopod fusion (Figure 3-8A,B, Supplemental Movies 4,5, see Appendix). However, in some phagocytic events, the FRL α concentration gradient from the base of the phagocytic cup to the pseudopod tip appears to be steeper than the gradient for Cdc42 (more intermediate colored pixels in the insets of Figure 3-8A compared to the insets in Figures 3-6C). In these images, it appears that the FRL α localization pattern is actually a subset of the Cdc42 pattern. In general though, the timing and localization of Cdc42 and wildtype FRL α are largely coincident supporting the idea that FRL α function during phagocytosis is linked to Cdc42 signaling.

DRF Localization During Complement Receptor Mediated Phagocytosis

Complement receptor phagocytosis is a Rho-dependent process that also occurs in macrophages. However, using assays similar to those for Fc- γ receptor mediated phagocytosis, mDia1-GFP was not observed to accumulate at sites of complement receptor mediated phagocytosis (Figure 3-9). FRL α -GFP does not

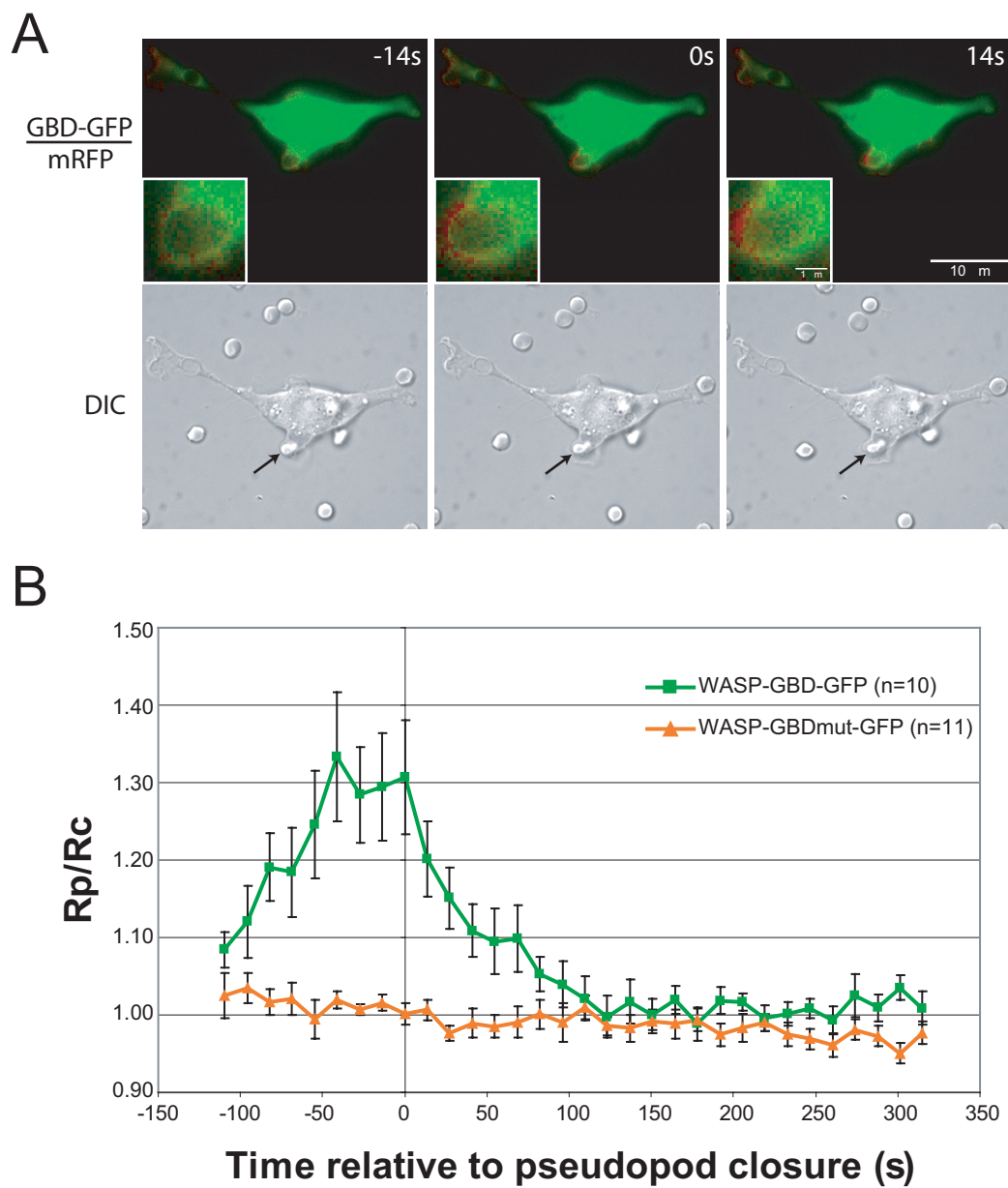


Figure 3-8

Figure 3-8. Recruitment of Active Cdc42 to the Phagocytic Cup During Fc- γ Receptor Mediated Phagocytosis.

- (A) GBD-GFP expressing cell undergoing Fc- γ Receptor Mediated Phagocytosis. As in Figure 3-6A, the GFP/mRFP ratio is pseudocolored in the top panel to reflect the relative accumulation of GBD-GFP over mRFP. The localization of the GBD-GFP protein reflects the distribution of Cdc42-GTP during phagocytosis. The arrow in the lower panel of DIC images indicates the ingested RBC. The insets depict an additional 4x magnification of the phagocytic cup.
- (B) Timecourse of active Cdc42 accumulation during Fc- γ Receptor Mediated Phagocytosis. Multiple phagocytic events were analyzed, as in Figure 3-6B, in cells expressing mRFP and GBD-GFP or the mutant GBD-GFP (as a negative control). Error bars represent the standard error of the mean.

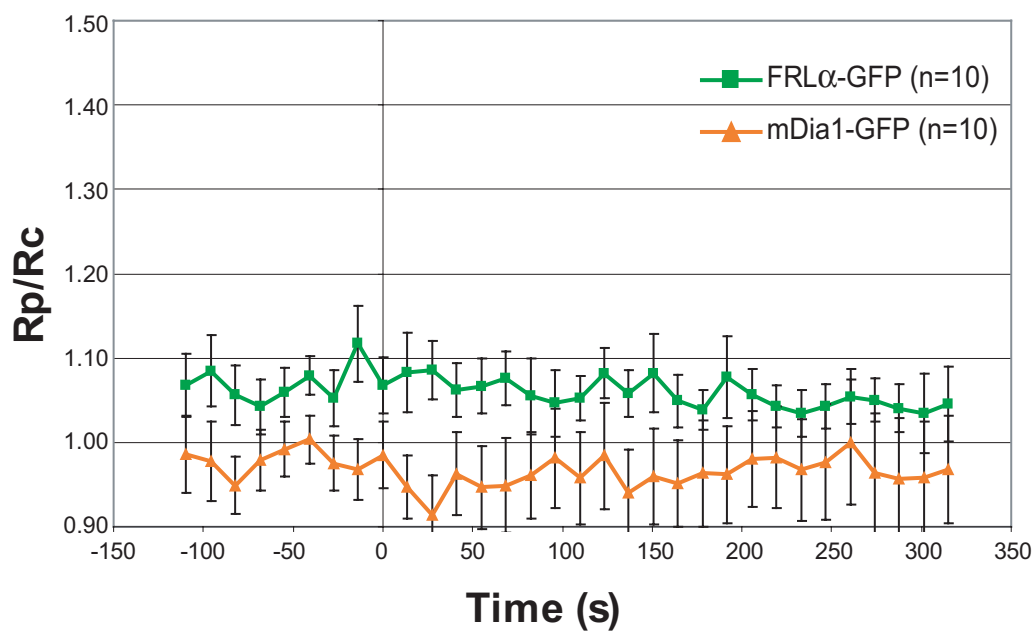


Figure 3-9

Figure 3-9. Localization of DRFs During Complement Receptor Mediated Phagocytosis.

Timecourse of formin accumulation during Complement Receptor Mediated Phagocytosis. N indicates the number of phagocytic events analyzed for each construct. For each timepoint, the GFP/mRFP ratio at the cell surface in contact with the RBC (R_p) was divided by the ratio in the cell cytoplasm (R_c). Error bars represent the standard error of the mean.

accumulate during complement mediated phagocytosis either which indicates its specificity for the Fc- γ receptor process (Figure 3-9). However, there is a potential complication in interpreting these data. During complement phagocytosis, particles simply sink into the cell whereas in Fc- γ phagocytosis, the cell actively extends pseudopods to capture and internalize particles (Allen and Aderem, 1996; May and Machesky, 2001). Therefore, it is easy to observe side-on views of Fc- γ phagocytosis. In these side-on events, cellular background fluorescence does not interfere with pseudopod fluorescence and, therefore, it is relatively easy to determine localization patterns for various proteins. In contrast, most complement mediated phagocytic events occur at the surface of the cell and the lack of cellular protrusions away from the cell body means that the fluorescence at the site of phagocytosis will be obscured by cellular background fluorescence. Therefore, complement mediated phagocytosis is probably better suited for study by confocal microscopy rather than the wide-field technique used here. Indeed, a recent study has found that mDia1 is required for complement receptor mediated phagocytosis (Colucci-Guyon et al., 2005). In static images from this study (Colucci-Guyon et al., 2005), it appears that the enrichment of mDia1 at the phagosome is relatively modest. This modest accumulation coupled with the background fluorescence problem discussed above probably explains why the wide-field experiments presented here did not detect mDia1-GFP localization during complement mediated phagocytosis. In the future, studies

could be aimed at studying mDia1-GFP localization during complement receptor mediated phagocytosis using spinning disk confocal microscopy. This technique should afford the high temporal resolution required to study phagocytosis in real-time as well as eliminate the background problem.

Discussion

Formins are important regulators of the actin cytoskeleton whose activity is required for cytokinesis, cell polarization and tissue morphogenesis. The DRF subfamily is particularly interesting because of its potential to mediate signals by Rho GTPases, which are known to play central roles in cytoskeletal biology. The DRF mDia1, the most extensively studied family member, is regulated by autoinhibition and partially activated by Rho. To extend the current understanding of DRF function, the *in vitro* and cellular regulation of the macrophage-specific DRF FRL α were studied. The results presented here show that FRL α , like mDia1, is autoinhibited through binding of its N- and C-termini. Autoinhibition regulates both the actin assembly activity of the C-terminal FH2 domain *in vitro* and the plasma membrane localization of the N-terminus in cells. Biochemical, knockdown and imaging studies reveal that FRL α is a direct effector of Cdc42 that plays an important role in Fc- γ receptor mediated phagocytosis. The results demonstrate a new cytoskeletal function for DRFs and define a new paradigm of DRF regulation in which binding of the N- and C-

termini mediates mutual autoinhibition of biochemical activity as well as cellular localization.

Autoinhibition of DRF Actin Assembly Activity

Autoinhibition is a common regulatory mechanism for many Rho GTPase effectors and has been characterized in detail for several GTPase-effector pairs, including Cdc42-WASP, Cdc42-PAK and Rho-mDia1 (Kim et al., 2000a; Lei et al., 2000; Otomo et al., 2005a; Rose et al., 2005). Sequence comparisons with mDia1 suggest that many DRFs, including the FRL and DAAM families, are also autoinhibited Rho GTPase effectors (Higgs, 2005; Higgs and Peterson, 2005). As with mDia1, the DAD motif of FRL α is required for the autoinhibitory binding interaction between the N- and C-termini.

N-terminal fragments of FRL α , based on recent crystal structures of the mDia1 N-terminus (Otomo et al., 2005a; Rose et al., 2005), were generated to investigate the mechanisms of autoinhibition and activation in FRL α . As with mDia1, some conserved residues in the FRL α DID are required for autoinhibitory binding to the DAD and others are required for activation by GTPase. Based on fragmented DID constructs, earlier work suggested that FRL α may bind Rac (Yayoshi-Yamamoto et al., 2000). However, using constructs containing intact structural domains that are biochemically well-behaved, the data now show that FRL α is a Cdc42-specific effector. Several lines of evidence support this

assertion. Cdc42 is able to relieve autoinhibition of FH2-mediated actin assembly by the wildtype N-terminus but not by the T126D mutant N-terminus. Mutation of the analogous residue in mDia1, prevents direct Rho binding and Rho-mediated activation (Otomo et al., 2005a). Further, the wildtype FRL α N-terminus co-immunoprecipitates with active Cdc42 from cell lysates, but the point mutant does not. In addition, the timing and localization of Cdc42 and wildtype FRL α are largely coincident during phagocytosis, and the recruitment of FRL α to the phagocytic cup is blocked by the T126D mutation. Thus, Cdc42 can bind FRL α and stimulate its biochemical activity, and likely controls its localization during phagocytosis. However, the interaction between Cdc42 and FRL α appears to be of low affinity, based on the dose-response in actin assembly assays and the inability to detect binding in GST pull down assays using recombinant, bacterially expressed proteins. The interaction between Cdc42 and FRL α may be modulated by cellular factors, a point of ongoing investigation in the Rosen laboratory.

RhoA and Cdc42 can activate autoinhibited mDia1 and FRL α , respectively. However, there are significant differences in the properties of activation in the two systems. For Rho-mDia1, relief of autoinhibition saturates at ~10-25% activation, but requires only low micromolar concentrations of GTPase (Li and Higgs, 2003; Otomo et al., 2005a). In contrast, Cdc42 can fully activate FRL α , but only at high micromolar concentrations. In pharmacological terms,

RhoA is a more potent, but less efficacious activator of mDia1 than Cdc42 is of FRL α . This is in direct analogy, for example, to the pharmacological descriptions of agonist-mediated activation of G protein coupled receptors (GPCRs). For GPCRs, full and partial agonists exemplify differing efficacy, and high and low affinity ligands exemplify differing potency. Importantly, efficacy and potency are uncoupled parameters. These issues can be understood conceptually in the context of two-state models of allostery, where a receptor is postulated to exist in equilibrium between an inactive and active state and stimulatory ligands bias the equilibrium towards the latter (Buck et al., 2004; Kenakin, 2004; Leff, 1995; Leung and Rosen, 2005). Efficacy arises from the differing relative affinities of a ligand for the active and inactive state (regardless of absolute affinities). Potency is governed largely by the absolute affinity for the inactive state. As applied here, Rho would have high, but similar affinities for the active and inactive states of mDia1 (hence high potency, but low efficacy), while Cdc42 would have low, but different affinities for the two states of FRL α (hence low potency, but high efficacy). While the simple two-state framework is useful, more biophysical studies on mDia1 and FRL α will be required to develop a quantitative model of DRF activation.

Both Cdc42-GTP and Cdc42-GDP show dose-dependent activation of FRL α . However, maximal activation is much greater in the GTP bound state. Therefore, the nucleotide state does not merely modulate the affinity of GTPase

for FRL α (if that were the case than Cdc42-GDP should fully activate FRL α at high enough concentrations). Rather the two nucleotide states of the GTPase have intrinsically different abilities to activate. In the pharmacological terms discussed above, the two nucleotide states of Cdc42 display markedly different efficacies in activation of FRL α . A similar nucleotide-dependent efficacy has recently been described for Cdc42-mediated activation of WASP (Leung and Rosen, 2005). Thus, it may be a general principle that the GTPase nucleotide switch modulates both the affinity for effectors (potency) and the ability of the GTPase to activate effectors (efficacy). As previously noted (Leung and Rosen, 2005), this property ensures that effectors are not spuriously activated even in the presence of high local concentrations of GDP-GTPase. This is an important concern for GTPase signaling cascades where GTPases and effectors are independently recruited to their sites of action (typically membrane surfaces). Modulating efficacy with the nucleotide switch ensures that even at high local concentrations effectors will only be activated in the presence of GTP-GTPase, thereby preserving the fidelity of GTPase signaling cascades.

Autoinhibition of DRF Localization: A Membrane Factor X?

The functional significance of the N-terminus of DRFs has been thought to be limited to mediating autoinhibition of the C-terminus (Evangelista et al., 2003; Higgs, 2005; Wallar and Alberts, 2003). The data presented here show that

the N-terminal domains of the DRFs FRL α and mDia1 are plasma membrane localized when expressed in tissue culture cells. Fusion to a functional DAD motif blocks this activity of the N-terminus and both the full-length and mini-DRFs are cytoplasmic. Thus, plasma membrane localization of DRFs is also regulated by autoinhibition. Interactions between the N-terminus and C-terminus, therefore, mediate mutual autoinhibition of DRF localization and biochemical activity. A similar mechanism of mutual autoinhibition regulating plasma membrane localization and F-actin binding has been proposed for the ERM family of cytoskeletal proteins (Pufall and Graves, 2002).

Since the N-terminal domains of FRL α and mDia1 bind Rho GTPases, which are membrane localized themselves, it is reasonable to suspect that GTPase binding mediates membrane localization. Mutations of FRL α or mDia1, which disrupt Rho GTPase effects *in vitro*, also impair membrane localization of their N-termini. However, these mutants still show significant enrichment at the plasma membrane and, at least for mDia1, this enrichment appears saturable. Other GTPase binding proteins, such as the WASP GBD, are not plasma membrane localized. These results suggest that GTPases are necessary but not sufficient for membrane localization of DRFs and that other factors are likely to be involved.

Upon coexpression of constitutively active Cdc42, full length FRL α is recruited to the plasma membrane. Coexpression of constitutively active Cdc42

also causes mini-FRL α to relocate to the plasma membrane. The results with mini-FRL α suggest that membrane localization in the presence of active Cdc42 is mediated by the N-terminus of FRL α and that the role of Cdc42 is to disrupt the autoinhibitory interaction between the N- and C-termini. This is in contrast to WASP which is recruited to the plasma membrane during T cell signaling by binding of the SH3 domain of Nck to its polyproline region, rather than by Cdc42-mediated relief of autoinhibition (Cannon et al., 2001; Zeng et al., 2003). For mDia1, coexpression of constitutively active RhoA does not result in relocation to the plasma membrane. Thus, relief of autoinhibitory control of cellular localization does not correlate with potency of GTPase-mediated relief of autoinhibitory control of actin assembly activity, but rather with efficacy and, therefore, with the ability of the GTPase to disrupt autoinhibitory interactions between the N- and C-termini. These results further support the idea, stated above, that GTPases are not the only factors involved in regulating membrane localization of the DRF N-terminus, otherwise the high affinity GTPase would be expected to be more effective in mediating membrane relocation. The mechanistic basis for this intriguing observation is unclear at present. Further experiments are needed to better define the role of different GTPases in DRF membrane localization.

The hypothesis that other factors contribute to DRF activation was first suggested when Rho was found to have low efficacy in activating mDia1 *in vitro*

(Li and Higgs, 2003). The results presented here support this hypothesis and add the further prediction that the additional factor is membrane-associated. *In vitro*, Cdc42 only activates FRL α at very high concentrations. A cooperatively acting factor could help overcome the low potency of Cdc42-mediated activation. Based on the data presented here, an additional factor involved in membrane localization would bind to the DID and, therefore, could compete with DAD binding. Thus, like GTPases, this additional factor could also act to bias the autoinhibitory equilibrium toward the active state, cooperatively increasing the efficacy of activation. Since several actin regulatory proteins are activated by phospholipids, I have tested several candidate phosphoinositides for an ability to activate FRL α actin assembly activity *in vitro*, but have had no positive results. Thus, the nature and identify of Factor X remains elusive and, for now, remains a speculative hypothesis.

Coordinated Cytoskeletal Remodeling During Fc- γ Receptor Mediated Phagocytosis

Cdc42 plays an essential role in Fc- γ receptor mediated phagocytosis (Caron and Hall, 1998). Formins have not previously been implicated in this process, although mDia1 has been shown to accumulate at sites of integrin crosslinking by fibronectin-coated beads, an experimental model of phagocytosis (Watanabe et al., 1997). The identification of FRL α as a Cdc42-effector led me

to test whether this macrophage-specific DRF is involved in Fc- γ receptor mediated phagocytosis. Knockdown of FRL α below detectable levels inhibits Fc- γ receptor phagocytosis by ~45%. Two previous studies on Fc receptor mediated phagocytosis reported that dominant negative Cdc42 inhibits phagocytosis by 40-75% (Caron and Hall, 1998; Massol et al., 1998). The variable results are probably due to different experimental conditions and data analysis methods between the different studies. However, the data are consistent with the hypothesis that a Cdc42-FRL α pathway is important for Fc- γ receptor mediated phagocytosis.

It is useful to distinguish three phases of Fc- γ receptor mediated phagocytosis: pseudopod extension, pseudopod fusion and particle internalization (Castellano et al., 2001; May and Machesky, 2001; Swanson and Hoppe, 2004). These phases represent functional steps during phagocytosis and do not necessarily occur sequentially (as evident from images showing partial internalization before fusion is complete). Early experiments with actin polymerization inhibitors demonstrated the essential role of growing actin filaments in mediating many types of phagocytosis (Aderem and Underhill, 1999; Allen and Aderem, 1996; Greenberg et al., 1991). Timelapse imaging of live macrophages shows that fluorescently labeled actin accumulates at the base and extending pseudopods of the phagocytic cup (Araki et al., 2003; Scott et al., 2005). At closure, actin forms a continuous, homogenous sphere around the

phagosome (Scott et al., 2005). Following closure, actin dissipates from the phagosome starting at the base, resulting in a short-lived actin “cap” structure at the top of the phagosome (Scott et al., 2005). The molecular architecture of the actin structures at each phase of phagocytosis and the specific signaling pathways that control their formation have yet to be determined.

Recent studies have started to define the spatio-temporal localization patterns and functional roles of different actin-regulatory proteins during Fc- γ receptor mediated phagocytosis. Much work in this area has focused on Cdc42 and Rac. Either dominant negative Cdc42 or Rac can inhibit Fc- γ receptor mediated phagocytosis in macrophages or the highly related process of Fc- ϵ receptor mediated phagocytosis in mast cells (Caron and Hall, 1998; Massol et al., 1998). Electron microscopy (EM) based structural studies in mast cells reveal intriguing morphological differences between the aberrant phagocytic cups produced in the presence of dominant negative Cdc42 or Rac (Massol et al., 1998). In the Cdc42 mutant cells, the aberrant phagocytic cups lack extended pseudopods and resemble pedestals (Massol et al., 1998). In the Rac mutant cells, pseudopods extend up and around the beads but they do not fuse and the beads are not internalized (Massol et al., 1998). Taken together, these results suggest that during Fc receptor mediated phagocytosis, Cdc42 mediates pseudopod extension and that Rac controls fusion and internalization. Consistent with this model, this work and previous studies have shown that activated Cdc42 localizes primarily at

the tips of the extending pseudopods and dissipates rapidly after pseudopod fusion (Hoppe and Swanson, 2004). In addition, active Rac1 is localized at the base and throughout the pseudopods during extension and then concentrates at the base during fusion and internalization (Hoppe and Swanson, 2004). Further, in an engineered phagocytic mast cell line, membrane clustering of active Cdc42 with antibody coated beads is sufficient to trigger the extension of membrane protrusions that do not fuse (Castellano and Chavrier, 2000; Castellano et al., 1999). Clustering of active Rac in these cells results in significant bead internalization via a phagocytic mechanism in which the bead simply sinks into the cell (Castellano et al., 2000). These results highlight the different roles of Cdc42 and Rac during Fc receptor mediated phagocytosis.

In contrast to the Rho GTPases, the actions of downstream signaling molecules during phagocytosis have been studied less extensively. WASP family proteins are important for Arp2/3 complex activation during cell migration (Pollard and Borisy, 2003), and static images reveal that WASP and Arp2/3 complex are recruited to the phagocytic cup (Coppolino et al., 2001; May et al., 2000). However, the detailed spatio-temporal patterns of these molecules during phagocytosis have not been reported. Ena/VASP family proteins are anti-capping proteins that are required for efficient cell migration, where the balance of capping and anti-capping activities is important for regulating leading edge extension (Pollard and Borisy, 2003). Fluorescently labeled VASP in live

macrophages is recruited transiently to the base and pseudopods of the phagocytic cup (Coppolino et al., 2001). However, the spatial distribution of VASP within the phagocytic cup and the timing of VASP recruitment/departure have not been determined with high resolution.

Fc- γ receptor mediated phagocytosis represents one of the first isolated cytoskeletal systems in higher eukaryotes where both Arp2/3 (May et al., 2000) and formins (this work) have essential functions. Why might two different actin nucleation machines be required for Fc- γ phagocytosis? While both Arp2/3 complex and FRL α can nucleate actin filaments, there are important differences in their resulting actin networks. Arp2/3 networks are branched and sensitive to capping proteins and, therefore, behavior of the Arp2/3 network depends on the balance of capping and nucleation. FRL α generated filaments are unbranched and resistant to capping proteins. Based on its localization pattern and linkage to Cdc42 signaling, FRL α function may only be important for pseudopod extension, while Arp2/3 complex may be required for the other phases of phagocytosis. In addition to nucleating new filaments, the FRL α FH2 domain can also sever actin filaments (Harris et al., 2004). This activity could lead to an increase in ATP-capped filament ends, which, at least for cofilin-severed filaments, appear to be preferential sites of Arp2/3-mediated branching (Ichetovkin et al., 2002). Indeed, FRL α may not serve a nucleation function during phagocytosis at all, but rather

may serve to facilitate pseudopod extension by functioning as an anti-capping or severing protein to modify the Arp2/3 actin network. In this context, the demonstration that FRL α is a Cdc42-effector is particularly intriguing considering that actin filaments generated by Cdc42-GTP in neutrophil extracts are protected from capping proteins (Huang et al., 1999). Beyond these types of speculation, the specific biochemical and biological roles of FRL α and Arp2/3 complex during Fc- γ receptor mediated phagocytosis remain elusive.

An important future goal is to develop a detailed understanding of the molecular relationships between the core cytoskeletal components, including actin, Arp2/3 complex, FRL α , WASP, Rho GTPases, VASP and phospholipids, involved in Fc- γ phagocytosis. Due to the different methodologies and experimental conditions used in prior studies, it is difficult to accurately and meaningfully compare the existing data on all these factors. However, with high-speed, multi-color imaging techniques using fluorescent chimeras and activity-based probes it should be possible to determine the spatio-temporal correlation of signaling molecules with each other and with specific phases of phagocytosis. Perturbations of specific signaling molecules using RNA interference, dominant negative constructs or pharmacological agents should allow elucidation of the epistatic relationships governing the spatio-temporal accumulation patterns of individual molecules. In addition, higher resolution imaging techniques such as EM tomography should be able to reveal spatial relationships between signaling

molecules and the actin filament architecture. Understanding the detailed molecular mechanisms of phagocytosis will shed important insight into this essential function of the immune system and will help determine the relative contributions of different actin regulatory engines to cytoskeletal dynamics in higher eukaryotes.

CONCLUSIONS

Actin will slowly, but spontaneously start to polymerize at a certain, critical concentration (Pollard and Borisy, 2003). The polymerizing filament will exhibit an interesting phenomenon called treadmilling where the filament polymerizes at one end and depolymerizes at the other. At high enough concentrations, the actin filament will eventually start to grow from both ends.

However, on its own, actin can not grow fast enough to meet the speeds required for efficient cell migration (Pollard and Borisy, 2003). It does not spontaneously form the network structures required to generate the force needed to push the leading edge forward during lamellipodial protrusion. A group of filaments will not suddenly orient themselves in a uniform direction to serve as guidance cues for cellular cargo.

Cytoskeletal signaling pathways bridge the gap between the inherent polymerization properties of actin and actual cellular utility (Pollard and Borisy, 2003). They accelerate the rate of filament nucleation. They regulate the speed of filament elongation. They can bundle filaments or sever them. They control where, when and how a filament elongates in order to fulfill the cytoskeletal needs of the cell.

Rho GTPases are at the heart of these cytoskeletal signaling pathways. Therefore, to understand the molecular basis for cytoskeletal regulation it is necessary to uncover the molecular mechanisms controlling and coordinating Rho GTPases, their upstream regulators and their downstream effectors.

Cytoskeletal Imaging

The FRET-based sensors I describe in Chapters 1 and 2 are aimed at understanding just one component of the aforementioned signaling pathways, the Rho GTPase Cdc42. The data suggest that these sensors may become valuable tools for studying endogenous Cdc42 activity during a variety of cytoskeletal processes. However, as discussed in the previous chapters, further sensor optimization and the use of different imaging technologies (i.e. spinning disk confocal microscopy) may be required before the sensors can be used robustly and reproducibly. FRET-based probes have the potential to quantitatively measure the level and timecourse of activated Cdc42 in different regions of the cell during a given process. As such, the continued development of FRET-based imaging remains a worthy technical challenge.

In contrast to the FRET-based sensors, the GFP-based probes for active Cdc42 were easier to implement and produced interesting results on Cdc42 activity during T cell activation and Fc- γ receptor mediated phagocytosis. For Fc- γ phagocytosis, where the analysis is more complete, the imaging data, in

combination with previous analysis of Cdc42 function during phagocytosis (Caron and Hall, 1998; Castellano et al., 1999; Massol et al., 1998), supports a model in which Cdc42 activity is required for the pseudopod extension phase.

As discussed in the previous chapter, other molecules have also been implicated in phagocytosis using GFP-based strategies similar to the one described here (Botelho et al., 2000; Coppolino et al., 2001; Marshall et al., 2001; Scott et al., 2005). A comprehensive analysis of all the cytoskeletal regulatory molecules implicated in phagocytosis should now be attempted. The important goals will be to determine the epistatic relationships between signaling molecules and the specific functions of each. Multiple genetically encoded fluorophores are now available which will facilitate the imaging of several proteins simultaneously (Shaner et al., 2005). In this manner, it should be possible to deconstruct systematically a complicated cytoskeletal process into its component molecular steps.

Fc- γ receptor mediated phagocytosis is particularly well suited for these types of studies because it is a relatively fast process which means many individual events can be analyzed. The morphology of the phagocytic cup is fairly stereotypical facilitating comparison between multiple events. In addition, the assay is robust and can be initiated at will on the microscope stage. Finally, Fc- γ receptor mediated phagocytosis is an important process in the immune

system (Aderem and Underhill, 1999). A better understanding of how it works at a molecular level should have important medical implications.

Formin Biology

Many molecules have been implicated in a variety of different cytoskeletal processes. Understanding their molecular functions using live cell imaging is a powerful approach. However, it is possible that key cytoskeletal regulatory components have yet to be identified or appreciated. In this regard, further investigation regarding the cytoskeletal functions of formin proteins is warranted. This large family of proteins can have many effects on actin including nucleation of new actin filaments (Zigmond, 2004). Many members of the DRF subfamily are thought to be regulated by Rho GTPases and thus, probably play important roles in many of the cytoskeletal processes mentioned throughout this text. The physiological functions of most of the mammalian DRFs remain largely unexplored.

The comprehensive biochemical and biological analysis of FRL α , presented in Chapter 3, led to the discoveries that FRL α is a Cdc42 effector and that it plays an important role in Fc- γ receptor mediated phagocytosis. Immediately, FRL α , by virtue of its direct interactions with actin, joined the group of cytoskeletal regulatory factors that should be studied in any analysis of the cytoskeletal processes occurring during Fc- γ receptor mediated phagocytosis.

The analysis of FRL α was aided immensely by the extensive structural and biochemical analyses of the related DRF mDia1 (Li and Higgs, 2003; Li and Higgs, 2005; Otomo et al., 2005a; Rose et al., 2005).

The remaining uncharacterized DRFs should now be subjected to the same sort of biochemical and biological analysis that was performed on FRL α . First, these molecules should be tested for actin assembly activity. Second, they should be tested for regulation by autoinhibition. To determine GTPase specificity, the N-termini of these DRFs should be subjected to pull down assays with all the known Rho family members. In case the affinity for GTPase is low (as is the situation for FRL α and Cdc42), the ability of GTPases to relieve autoinhibition of actin assembly should also be tested. In this manner, the DRFs can be paired with their appropriate regulatory GTPases. Some of these formins may not be autoinhibited and some may not be regulated by Rho GTPases (Higgs, 2005), but some of them will be and it is important to determine these points experimentally.

The regulation of cellular localization by autoinhibition and/or by GTPases should also be investigated for the other DRFs. There are already hints in the literature that GTPase-mediated membrane localization, as observed for FRL α , may be important for some DRFs. The DRF mDia2 has been shown to bind Rif, a recently identified Rho family member (Pellegrin and Mellor, 2005). In NIH 3T3 cells, mDia2 is cytoplasmic, but when coexpressed with constitutively active Rif, it localizes to the plasma membrane where it generates

long filopodia (Pellegrin and Mellor, 2005). Similarly, the DRF hDia2C is normally cytoplasmic in HeLa cells, but when co-expressed with constitutively active RhoD, it is recruited to early endosomes where it functions to regulate endosome dynamics (Gasman et al., 2003). It will be interesting to determine the generality of GTPase-mediated membrane localization. Also, the specific localization patterns for each DRF may provide insights into the potential biological functions of those DRFs.

For FRL α , simply knowing its GTPase specificity and tissue expression profile was sufficient to accurately guess its biological function. For other DRFs, this may not be so easy. But other information in the literature may help to form reasonable hypotheses as to the biological roles of these DRFs. For those DRFs where biological functions can be reasonably hypothesized, functional assays and live cell imaging should be performed to confirm those predictions. In this manner, the breadth of formin biology can be systematically better understood.

It is becoming increasingly evident that the formins are important cytoskeletal regulators. Thus, any complete analysis of cytoskeletal dynamics during a given process should address the potential role of formins in that process. By explicitly trying to determine the universe of formin cytoskeletal effects, the strategies outlined here will help make future studies of cytoskeletal dynamics more comprehensive and accurate. As the cast of characters becomes more

complete, new imaging reagents and technologies will be better able to define the molecular mechanisms regulating cellular actin dynamics.

Molecular Basis of Cytoskeletal Dynamics

Overexpressed individually in fibroblasts, the Rho GTPases, Rho, Rac and Cdc42, produce stress fibers, lamellipodia or filopodia, respectively. The molecular basis for these distinct effects is not completely known, but is thought to be due to the unique spectrum of downstream effectors engaged by each GTPase. Even when working in a concerted fashion during physiological cytoskeletal processes, Rho GTPase signaling pathways produce a diverse array of distinct cytoskeletal patterns. For example, consider three essential cytoskeletal processes that occur in the immune system: Fc- γ phagocytosis, T cell activation (a specialized form of cell adhesion and polarization) and chemotaxis (a specialized form of cell migration). All of these processes require Rho GTPase signaling. Despite the similarities, these three processes exhibit quite different morphological and cytoskeletal features. Why?

To understand the molecular basis for differing cytoskeletal dynamics, it will be necessary to identify all of the cytoskeletal regulators that are important for a given process. Imaging the localization and activities of these factors during the process is the most direct route towards understanding their functions. Strategies for identifying new regulators and for comprehensive imaging

approaches, particularly as applied to Fc- γ phagocytosis, have been described above and in the previous chapters. Similar strategies should be applied towards studying T cell activation and chemotaxis as well. The goal will be to develop a comprehensive understanding of the molecular mechanisms governing the cytoskeletal dynamics during each of the three processes. Since many molecules are shared between these processes, it will be possible to compare the different systems and determine which epistatic relationships and molecular functions are generally conserved and which ones are process-specific. The process-specific relationships and functions will probably represent the keys to understanding the molecular basis for the distinct cytoskeletal patterns observed in each of these processes.

While this conceptual approach can also be applied towards studying and comparing other important physiological cytoskeletal processes, the insights gained into the three immune functions will be particularly valuable. Once the molecular differences between Fc- γ phagocytosis, T cell activation and chemotaxis are known, it will be possible to design strategies to selectively interfere with or control a specific process. Selective inhibition of different effector arms of the immune system will have basic science applications towards understanding how the immune system functions and will have medical applications for modulating the immune response either to restore health or to combat disease.

APPENDIX

Legends for Supplemental Movies

Supplemental Movie 1. DIC Timelapse Movie of FRL α -GFP Expressing Macrophage Undergoing Fc- γ Receptor Mediated Phagocytosis.

The timelapse movie depicts the macrophage and phagocytic event shown in Figure 3-6C.

Supplemental Movie 2. Fluorescence Timelapse Movie of FRL α -GFP Expressing Macrophage Undergoing Fc- γ Receptor Mediated Phagocytosis.

The timelapse movie depicts the cell from Figure 3-6C and is pseudocolored to represent the GFP/mRFP ratio at every pixel.

Supplemental Movie 3. Magnified Phagocytic Cup from Supplemental Movie 2.

Supplemental Movie 4. DIC Timelapse Movie of GBD-GFP Expressing Macrophage Undergoing Fc- γ Receptor Mediated Phagocytosis.

The timelapse movie depicts the macrophage and phagocytic event shown in Figure 3-8A.

Supplemental Movie 5. Fluorescence Timelapse Movie of GBD-GFP Expressing Macrophage Undergoing Fc- γ Receptor Mediated Phagocytosis.

The timelapse movie depicts the cell from Figure 3-8A and is pseudocolored to represent the GFP/mRFP ratio at every pixel.

REFERENCES

- Abdul-Manan, N., Aghazadeh, B., Liu, G. A., Majumdar, A., Ouerfelli, O., Siminovitch, K. A., and Rosen, M. K. (1999). Structure of Cdc42 in complex with the GTPase-binding domain of the 'Wiskott-Aldrich syndrome' protein. *Nature* **399**, 379-383.
- Aderem, A., and Underhill, D. M. (1999). Mechanisms of phagocytosis in macrophages. *Annu Rev Immunol* **17**, 593-623.
- Alberts, A. S. (2001). Identification of a carboxyl-terminal diaphanous-related formin homology protein autoregulatory domain. *J Biol Chem* **276**, 2824-2830.
- Allen, L. A., and Aderem, A. (1996). Molecular definition of distinct cytoskeletal structures involved in complement- and Fc receptor-mediated phagocytosis in macrophages. *J Exp Med* **184**, 627-637.
- Araki, N., Hatae, T., Furukawa, A., and Swanson, J. A. (2003). Phosphoinositide-3-kinase-independent contractile activities associated with Fcγ-receptor-mediated phagocytosis and macropinocytosis in macrophages. *J Cell Sci* **116**, 247-257.
- Aspenstrom, P. (1999). Effectors for the Rho GTPases. *Curr Opin Cell Biol* **11**, 95-102.
- Bedford, M. T., Chan, D. C., and Leder, P. (1997). FBP WW domains and the Abl SH3 domain bind to a specific class of proline-rich ligands. *Embo J* **16**, 2376-2383.
- Benard, V., Bohl, B. P., and Bokoch, G. M. (1999). Characterization of rac and cdc42 activation in chemoattractant-stimulated human neutrophils using a novel assay for active GTPases. *J Biol Chem* **274**, 13198-13204.
- Bione, S., Sala, C., Manzini, C., Arrigo, G., Zuffardi, O., Banfi, S., Borsani, G., Jonveaux, P., Philippe, C., Zuccotti, M., *et al.* (1998). A human homologue of the *Drosophila melanogaster* diaphanous gene is disrupted in a patient with premature ovarian failure: evidence for conserved function in oogenesis and implications for human sterility. *Am J Hum Genet* **62**, 533-541.
- Bishop, A. L., and Hall, A. (2000). Rho GTPases and their effector proteins. *Biochem J* **348 Pt 2**, 241-255.

Boettner, B., and Van Aelst, L. (2002). The role of Rho GTPases in disease development. *Gene* 286, 155-174.

Botelho, R. J., Teruel, M., Dierckman, R., Anderson, R., Wells, A., York, J. D., Meyer, T., and Grinstein, S. (2000). Localized biphasic changes in phosphatidylinositol-4,5-bisphosphate at sites of phagocytosis. *J Cell Biol* 151, 1353-1368.

Bretschneider, T., Diez, S., Anderson, K., Heuser, J., Clarke, M., Muller-Taubenberger, A., Kohler, J., and Gerisch, G. (2004). Dynamic actin patterns and Arp2/3 assembly at the substrate-attached surface of motile cells. *Curr Biol* 14, 1-10.

Buck, M., Xu, W., and Rosen, M. K. (2001). Global disruption of the WASP autoinhibited structure on Cdc42 binding. Ligand displacement as a novel method for monitoring amide hydrogen exchange. *Biochemistry* 40, 14115-14122.

Buck, M., Xu, W., and Rosen, M. K. (2004). A two-state allosteric model for autoinhibition rationalizes WASP signal integration and targeting. *J Mol Biol* 338, 271-285.

Cannon, J. L., and Burkhardt, J. K. (2002). The regulation of actin remodeling during T-cell-APC conjugate formation. *Immunol Rev* 186, 90-99.

Cannon, J. L., Labno, C. M., Bosco, G., Seth, A., McGavin, M. H., Siminovitch, K. A., Rosen, M. K., and Burkhardt, J. K. (2001). Wasp recruitment to the T cell:APC contact site occurs independently of Cdc42 activation. *Immunity* 15, 249-259.

Caron, E., and Hall, A. (1998). Identification of two distinct mechanisms of phagocytosis controlled by different Rho GTPases. *Science* 282, 1717-1721.

Carson, M. J. (1991). Ribbons 2.0. *J Appl Crystallogr* 24, 958-961.

Castellano, F., and Chavrier, P. (2000). Inducible membrane recruitment of small GTP-binding proteins by rapamycin-based system in living cells. *Methods Enzymol* 325, 285-295.

Castellano, F., Chavrier, P., and Caron, E. (2001). Actin dynamics during phagocytosis. *Semin Immunol* 13, 347-355.

Castellano, F., Montcourrier, P., and Chavrier, P. (2000). Membrane recruitment of Rac1 triggers phagocytosis. *J Cell Sci* 113 (Pt 17), 2955-2961.

Castellano, F., Montcourrier, P., Guillemot, J. C., Gouin, E., Machesky, L., Cossart, P., and Chavrier, P. (1999). Inducible recruitment of Cdc42 or WASP to a cell-surface receptor triggers actin polymerization and filopodium formation. *Curr Biol* 9, 351-360.

Chan, D. C., Bedford, M. T., and Leder, P. (1996). Formin binding proteins bear WWP/WW domains that bind proline-rich peptides and functionally resemble SH3 domains. *Embo J* 15, 1045-1054.

Chang, F., Drubin, D., and Nurse, P. (1997). cdc12p, a protein required for cytokinesis in fission yeast, is a component of the cell division ring and interacts with profilin. *J Cell Biol* 137, 169-182.

Chen, Y., Mills, J. D., and Periasamy, A. (2003). Protein localization in living cells and tissues using FRET and FLIM. *Differentiation* 71, 528-541.

Chiu, V. K., Bivona, T., Hach, A., Sajous, J. B., Silletti, J., Wiener, H., Johnson, R. L., Cox, A. D., and Philips, M. R. (2002). Ras signalling on the endoplasmic reticulum and the Golgi. *Nat Cell Biol* 4, 343-350.

Choy, E., Chiu, V. K., Silletti, J., Feoktistov, M., Morimoto, T., Michaelson, D., Ivanov, I. E., and Philips, M. R. (1999). Endomembrane trafficking of ras: the CAAX motif targets proteins to the ER and Golgi. *Cell* 98, 69-80.

Clarke, S. (1992). Protein isoprenylation and methylation at carboxyl-terminal cysteine residues. *Annu Rev Biochem* 61, 355-386.

Colucci-Guyon, E., Niedergang, F., Wallar, B. J., Peng, J., Alberts, A. S., and Chavrier, P. (2005). A Role for Mammalian Diaphanous-Related Formins in Complement Receptor (CR3)-Mediated Phagocytosis in Macrophages. *Curr Biol* 15, 2007-2012.

Coppolino, M. G., Krause, M., Hagendorff, P., Monner, D. A., Trimble, W., Grinstein, S., Wehland, J., and Sechi, A. S. (2001). Evidence for a molecular complex consisting of Fyb/SLAP, SLP-76, Nck, VASP and WASP that links the actin cytoskeleton to Fcgamma receptor signalling during phagocytosis. *J Cell Sci* 114, 4307-4318.

Costa, G. L., Benson, J. M., Seroogy, C. M., Achacoso, P., Fathman, C. G., and Nolan, G. P. (2000). Targeting rare populations of murine antigen-specific T lymphocytes by retroviral transduction for potential application in gene therapy for autoimmune disease. *J Immunol* 164, 3581-3590.

Davis, M. M., Wulfig, C., Krummel, M. F., Savage, P. A., Xu, J., Sumen, C., Dustin, M. L., and Chien, Y. H. (1999). Visualizing T-cell recognition. *Cold Spring Harb Symp Quant Biol* 64, 243-251.

Del Pozo, M. A., Kiosses, W. B., Alderson, N. B., Meller, N., Hahn, K. M., and Schwartz, M. A. (2002). Integrins regulate GTP-Rac localized effector interactions through dissociation of Rho-GDI. *Nat Cell Biol* 4, 232-239.

del Pozo, M. A., Price, L. S., Alderson, N. B., Ren, X. D., and Schwartz, M. A. (2000). Adhesion to the extracellular matrix regulates the coupling of the small GTPase Rac to its effector PAK. *Embo J* 19, 2008-2014.

Dustin, M. L., and Cooper, J. A. (2000). The immunological synapse and the actin cytoskeleton: molecular hardware for T cell signaling. *Nat Immunol* 1, 23-29.

Erickson, J. W., and Cerione, R. A. (2001). Multiple roles for Cdc42 in cell regulation. *Curr Opin Cell Biol* 13, 153-157.

Erickson, J. W., Zhang, C., Kahn, R. A., Evans, T., and Cerione, R. A. (1996). Mammalian Cdc42 is a brefeldin A-sensitive component of the Golgi apparatus. *J Biol Chem* 271, 26850-26854.

Etienne-Manneville, S., and Hall, A. (2001). Integrin-mediated activation of Cdc42 controls cell polarity in migrating astrocytes through PKCzeta. *Cell* 106, 489-498.

Etienne-Manneville, S., and Hall, A. (2002). Rho GTPases in cell biology. *Nature* 420, 629-635.

Evangelista, M., Pruyne, D., Amberg, D. C., Boone, C., and Bretscher, A. (2002). Formins direct Arp2/3-independent actin filament assembly to polarize cell growth in yeast. *Nat Cell Biol* 4, 260-269.

Evangelista, M., Zigmond, S., and Boone, C. (2003). Formins: signaling effectors for assembly and polarization of actin filaments. *J Cell Sci* 116, 2603-2611.

Feig, L. A. (1999). Tools of the trade: use of dominant-inhibitory mutants of Ras-family GTPases. *Nat Cell Biol* 1, E25-27.

Gardiner, E. M., Pestonjamasp, K. N., Bohl, B. P., Chamberlain, C., Hahn, K. M., and Bokoch, G. M. (2002). Spatial and temporal analysis of Rac activation during live neutrophil chemotaxis. *Curr Biol* 12, 2029-2034.

- Gasman, S., Kalaidzidis, Y., and Zerial, M. (2003). RhoD regulates endosome dynamics through Diaphanous-related Formin and Src tyrosine kinase. *Nat Cell Biol* 5, 195-204.
- Gordon, G. W., Berry, G., Liang, X. H., Levine, B., and Herman, B. (1998). Quantitative fluorescence resonance energy transfer measurements using fluorescence microscopy. *Biophys J* 74, 2702-2713.
- Greenberg, S., Burridge, K., and Silverstein, S. C. (1990). Colocalization of F-actin and talin during Fc receptor-mediated phagocytosis in mouse macrophages. *J Exp Med* 172, 1853-1856.
- Greenberg, S., el Khoury, J., di Virgilio, F., Kaplan, E. M., and Silverstein, S. C. (1991). Ca(2+)-independent F-actin assembly and disassembly during Fc receptor-mediated phagocytosis in mouse macrophages. *J Cell Biol* 113, 757-767.
- Hall, A. (1998). Rho GTPases and the actin cytoskeleton. *Science* 279, 509-514.
- Hardt, W. D., Chen, L. M., Schuebel, K. E., Bustelo, X. R., and Galan, J. E. (1998). *S. typhimurium* encodes an activator of Rho GTPases that induces membrane ruffling and nuclear responses in host cells. *Cell* 93, 815-826.
- Harris, E. S., Li, F., and Higgs, H. N. (2004). The mouse formin, FRLalpha, slows actin filament barbed end elongation, competes with capping protein, accelerates polymerization from monomers, and severs filaments. *J Biol Chem* 279, 20076-20087.
- Higgs, H. N. (2005). Formin proteins: a domain-based approach. *Trends Biochem Sci* 30, 342-353.
- Higgs, H. N., and Peterson, K. J. (2005). Phylogenetic analysis of the formin homology 2 domain. *Mol Biol Cell* 16, 1-13.
- Higgs, H. N., and Pollard, T. D. (1999). Regulation of actin polymerization by Arp2/3 complex and WASp/Scar proteins. *J Biol Chem* 274, 32531-32534.
- Higgs, H. N., and Pollard, T. D. (2001). Regulation of actin filament network formation through ARP2/3 complex: activation by a diverse array of proteins. *Annu Rev Biochem* 70, 649-676.
- Hoppe, A. D., and Swanson, J. A. (2004). Cdc42, Rac1, and Rac2 display distinct patterns of activation during phagocytosis. *Mol Biol Cell* 15, 3509-3519.

Huang, M., Yang, C., Schafer, D. A., Cooper, J. A., Higgs, H. N., and Zigmond, S. H. (1999). Cdc42-induced actin filaments are protected from capping protein. *Curr Biol* 9, 979-982.

Ichetovkin, I., Grant, W., and Condeelis, J. (2002). Cofilin produces newly polymerized actin filaments that are preferred for dendritic nucleation by the Arp2/3 complex. *Curr Biol* 12, 79-84.

Ishizaki, T., Morishima, Y., Okamoto, M., Furuyashiki, T., Kato, T., and Narumiya, S. (2001). Coordination of microtubules and the actin cytoskeleton by the Rho effector mDia1. *Nat Cell Biol* 3, 8-14.

Isshiki, M., Ying, Y. S., Fujita, T., and Anderson, R. G. (2002). A molecular sensor detects signal transduction from caveolae in living cells. *J Biol Chem* 277, 43389-43398.

Itoh, R. E., Kurokawa, K., Ohba, Y., Yoshizaki, H., Mochizuki, N., and Matsuda, M. (2002). Activation of rac and cdc42 video imaged by fluorescent resonance energy transfer-based single-molecule probes in the membrane of living cells. *Mol Cell Biol* 22, 6582-6591.

Janeway, C. A., Jr., and Bottomly, K. (1994). Signals and signs for lymphocyte responses. *Cell* 76, 275-285.

Katsumi, A., Milanini, J., Kiosses, W. B., Del Pozo, M. A., Kaunas, R., Chien, S., Hahn, K. M., and Schwartz, M. A. (2002). Effects of cell tension on the small GTPase Rac. *J Cell Biol* 158, 153-164.

Kenakin, T. (2004). Principles: receptor theory in pharmacology. *Trends Pharmacol Sci* 25, 186-192.

Kim, A. S., Kakalis, L. T., Abdul-Manan, N., Liu, G. A., and Rosen, M. K. (2000a). Autoinhibition and activation mechanisms of the Wiskott-Aldrich syndrome protein. *Nature* 404, 151-158.

Kim, S. H., Li, Z., and Sacks, D. B. (2000b). E-cadherin-mediated cell-cell attachment activates Cdc42. *J Biol Chem* 275, 36999-37005.

Koka, S., Neudauer, C. L., Li, X., Lewis, R. E., McCarthy, J. B., and Westendorf, J. J. (2003). The formin-homology-domain-containing protein FHOD1 enhances cell migration. *J Cell Sci* 116, 1745-1755.

Kovar, D. R., Kuhn, J. R., Tichy, A. L., and Pollard, T. D. (2003). The fission yeast cytokinesis formin Cdc12p is a barbed end actin filament capping protein gated by profilin. *J Cell Biol* *161*, 875-887.

Kovar, D. R., and Pollard, T. D. (2004). Insertional assembly of actin filament barbed ends in association with formins produces piconewton forces. *Proc Natl Acad Sci U S A* *101*, 14725-14730.

Kraynov, V. S., Chamberlain, C., Bokoch, G. M., Schwartz, M. A., Slabaugh, S., and Hahn, K. M. (2000). Localized Rac activation dynamics visualized in living cells. *Science* *290*, 333-337.

Krogsgaard, M., and Davis, M. M. (2005). How T cells 'see' antigen. *Nat Immunol* *6*, 239-245.

Kroschewski, R., Hall, A., and Mellman, I. (1999). Cdc42 controls secretory and endocytic transport to the basolateral plasma membrane of MDCK cells. *Nat Cell Biol* *1*, 8-13.

Krummel, M., Wulfing, C., Sumen, C., and Davis, M. M. (2000a). Thirty-six views of T-cell recognition. *Philos Trans R Soc Lond B Biol Sci* *355*, 1071-1076.

Krummel, M. F., Sjaastad, M. D., Wulfing, C., and Davis, M. M. (2000b). Differential clustering of CD4 and CD3zeta during T cell recognition. *Science* *289*, 1349-1352.

Kurokawa, K., Itoh, R. E., Yoshizaki, H., Nakamura, Y. O., and Matsuda, M. (2004). Coactivation of Rac1 and Cdc42 at lamellipodia and membrane ruffles induced by epidermal growth factor. *Mol Biol Cell* *15*, 1003-1010.

Labno, C. M., Lewis, C. M., You, D., Leung, D. W., Takesono, A., Kamberos, N., Seth, A., Finkelstein, L. D., Rosen, M. K., Schwartzberg, P. L., and Burkhardt, J. K. (2003). Itk functions to control actin polymerization at the immune synapse through localized activation of Cdc42 and WASP. *Curr Biol* *13*, 1619-1624.

Leff, P. (1995). The two-state model of receptor activation. *Trends Pharmacol Sci* *16*, 89-97.

Lei, M., Lu, W., Meng, W., Parrini, M. C., Eck, M. J., Mayer, B. J., and Harrison, S. C. (2000). Structure of PAK1 in an autoinhibited conformation reveals a multistage activation switch. *Cell* *102*, 387-397.

Leung, D. W., and Rosen, M. K. (2005). The nucleotide switch in Cdc42 modulates coupling between the GTPase-binding and allosteric equilibria of Wiskott-Aldrich syndrome protein. *Proc Natl Acad Sci U S A* 102, 5685-5690.

Li, F., and Higgs, H. N. (2003). The mouse Formin mDia1 is a potent actin nucleation factor regulated by autoinhibition. *Curr Biol* 13, 1335-1340.

Li, F., and Higgs, H. N. (2005). Dissecting requirements for auto-inhibition of actin nucleation by the formin, mDia1. *J Biol Chem* 280, 6986-6992.

Linder, S., Nelson, D., Weiss, M., and Aepfelbacher, M. (1999). Wiskott-Aldrich syndrome protein regulates podosomes in primary human macrophages. *Proc Natl Acad Sci U S A* 96, 9648-9653.

Lynch, E. D., Lee, M. K., Morrow, J. E., Welsh, P. L., Leon, P. E., and King, M. C. (1997). Nonsyndromic deafness DFNA1 associated with mutation of a human homolog of the *Drosophila* gene diaphanous. *Science* 278, 1315-1318.

Machesky, L. M., and Gould, K. L. (1999). The Arp2/3 complex: a multifunctional actin organizer. *Curr Opin Cell Biol* 11, 117-121.

Marchand, J. B., Kaiser, D. A., Pollard, T. D., and Higgs, H. N. (2001). Interaction of WASP/Scar proteins with actin and vertebrate Arp2/3 complex. *Nat Cell Biol* 3, 76-82.

Marshall, J. G., Booth, J. W., Stambolic, V., Mak, T., Balla, T., Schreiber, A. D., Meyer, T., and Grinstein, S. (2001). Restricted accumulation of phosphatidylinositol 3-kinase products in a plasmalemmal subdomain during Fc gamma receptor-mediated phagocytosis. *J Cell Biol* 153, 1369-1380.

Massol, P., Montcourrier, P., Guillemot, J. C., and Chavrier, P. (1998). Fc receptor-mediated phagocytosis requires CDC42 and Rac1. *Embo J* 17, 6219-6229.

May, R. C., Caron, E., Hall, A., and Machesky, L. M. (2000). Involvement of the Arp2/3 complex in phagocytosis mediated by Fc gamma R or CR3. *Nat Cell Biol* 2, 246-248.

May, R. C., and Machesky, L. M. (2001). Phagocytosis and the actin cytoskeleton. *J Cell Sci* 114, 1061-1077.

Michaelson, D., Silletti, J., Murphy, G., D'Eustachio, P., Rush, M., and Philips, M. R. (2001). Differential localization of Rho GTPases in live cells: regulation by hypervariable regions and RhoGDI binding. *J Cell Biol* 152, 111-126.

Miki, H., Sasaki, T., Takai, Y., and Takenawa, T. (1998). Induction of filopodium formation by a WASP-related actin-depolymerizing protein N-WASP. *Nature* 391, 93-96.

Miki, H., and Takenawa, T. (2003). Regulation of actin dynamics by WASP family proteins. *J Biochem (Tokyo)* 134, 309-313.

Mitchison, T. J. (1992). Compare and contrast actin filaments and microtubules. *Mol Biol Cell* 3, 1309-1315.

Miyawaki, A., Griesbeck, O., Heim, R., and Tsien, R. Y. (1999). Dynamic and quantitative Ca²⁺ measurements using improved cameleons. *Proc Natl Acad Sci U S A* 96, 2135-2140.

Miyawaki, A., and Tsien, R. Y. (2000). Monitoring protein conformations and interactions by fluorescence resonance energy transfer between mutants of green fluorescent protein. *Methods Enzymol* 327, 472-500.

Mochizuki, N., Yamashita, S., Kurokawa, K., Ohba, Y., Nagai, T., Miyawaki, A., and Matsuda, M. (2001). Spatio-temporal images of growth-factor-induced activation of Ras and Rap1. *Nature* 411, 1065-1068.

Mott, H. R., Owen, D., Nietlispach, D., Lowe, P. N., Manser, E., Lim, L., and Laue, E. D. (1999). Structure of the small G protein Cdc42 bound to the GTPase-binding domain of ACK. *Nature* 399, 384-388.

Nakano, A. (2002). Spinning-disk confocal microscopy -- a cutting-edge tool for imaging of membrane traffic. *Cell Struct Funct* 27, 349-355.

Nalbant, P., Hodgson, L., Kraynov, V., Touthkine, A., and Hahn, K. M. (2004). Activation of endogenous Cdc42 visualized in living cells. *Science* 305, 1615-1619.

Nguyen, A. W., and Daugherty, P. S. (2005). Evolutionary optimization of fluorescent proteins for intracellular FRET. *Nat Biotechnol* 23, 355-360.

Nicholson-Dykstra, S., Higgs, H. N., and Harris, E. S. (2005). Actin dynamics: growth from dendritic branches. *Curr Biol* 15, R346-357.

Nobes, C. D., and Hall, A. (1995). Rho, rac, and cdc42 GTPases regulate the assembly of multimolecular focal complexes associated with actin stress fibers, lamellipodia, and filopodia. *Cell* *81*, 53-62.

Nobes, C. D., and Hall, A. (1999). Rho GTPases control polarity, protrusion, and adhesion during cell movement. *J Cell Biol* *144*, 1235-1244.

Otomo, T., Otomo, C., Tomchick, D. R., Machius, M., and Rosen, M. K. (2005a). Structural basis of Rho GTPase-mediated activation of the formin mDia1. *Mol Cell* *18*, 273-281.

Otomo, T., Tomchick, D. R., Otomo, C., Panchal, S. C., Machius, M., and Rosen, M. K. (2005b). Structural basis of actin filament nucleation and processive capping by a formin homology 2 domain. *Nature* *433*, 488-494.

Ozaki-Kuroda, K., Yamamoto, Y., Nohara, H., Kinoshita, M., Fujiwara, T., Irie, K., and Takai, Y. (2001). Dynamic localization and function of Bni1p at the sites of directed growth in *Saccharomyces cerevisiae*. *Mol Cell Biol* *21*, 827-839.

Pawson, T., and Scott, J. D. (1997). Signaling through scaffold, anchoring, and adaptor proteins. *Science* *278*, 2075-2080.

Pear, W. S., Nolan, G. P., Scott, M. L., and Baltimore, D. (1993). Production of high-titer helper-free retroviruses by transient transfection. *Proc Natl Acad Sci U S A* *90*, 8392-8396.

Pelham, R. J., and Chang, F. (2002). Actin dynamics in the contractile ring during cytokinesis in fission yeast. *Nature* *419*, 82-86.

Pellegrin, S., and Mellor, H. (2005). The Rho family GTPase Rif induces filopodia through mDia2. *Curr Biol* *15*, 129-133.

Pertz, O., and Hahn, K. M. (2004). Designing biosensors for Rho family proteins-deciphering the dynamics of Rho family GTPase activation in living cells. *J Cell Sci* *117*, 1313-1318.

Petersen, J., Nielsen, O., Egel, R., and Hagan, I. M. (1998). FH3, a domain found in formins, targets the fission yeast formin Fus1 to the projection tip during conjugation. *J Cell Biol* *141*, 1217-1228.

Plafker, K. S., and Macara, I. G. (2002). Fluorescence resonance energy transfer biosensors that detect Ran conformational changes and a Ran.GDP:importin- β :RanBP1 complex in vitro and in intact cells. *J Biol Chem*.

- Pollard, T. D., and Borisy, G. G. (2003). Cellular motility driven by assembly and disassembly of actin filaments. *Cell* 112, 453-465.
- Pollard, T. D., and Cooper, J. A. (1984). Quantitative analysis of the effect of Acanthamoeba profilin on actin filament nucleation and elongation. *Biochemistry* 23, 6631-6641.
- Pollard, T. D., and Cooper, J. A. (1986). Actin and actin-binding proteins. A critical evaluation of mechanisms and functions. *Annu Rev Biochem* 55, 987-1035.
- Price, L. S., Leng, J., Schwartz, M. A., and Bokoch, G. M. (1998). Activation of Rac and Cdc42 by integrins mediates cell spreading. *Mol Biol Cell* 9, 1863-1871.
- Pring, M., Evangelista, M., Boone, C., Yang, C., and Zigmond, S. H. (2003). Mechanism of formin-induced nucleation of actin filaments. *Biochemistry* 42, 486-496.
- Pufall, M. A., and Graves, B. J. (2002). Autoinhibitory domains: modular effectors of cellular regulation. *Annu Rev Cell Dev Biol* 18, 421-462.
- Ridley, A. J. (2001). Rho proteins: linking signaling with membrane trafficking. *Traffic* 2, 303-310.
- Ridley, A. J., and Hall, A. (1992). The small GTP-binding protein rho regulates the assembly of focal adhesions and actin stress fibers in response to growth factors. *Cell* 70, 389-399.
- Ridley, A. J., Paterson, H. F., Johnston, C. L., Diekmann, D., and Hall, A. (1992). The small GTP-binding protein rac regulates growth factor-induced membrane ruffling. *Cell* 70, 401-410.
- Rizzo, M. A., Springer, G. H., Granada, B., and Piston, D. W. (2004). An improved cyan fluorescent protein variant useful for FRET. *Nat Biotechnol* 22, 445-449.
- Romero, S., Le Clainche, C., Didry, D., Egile, C., Pantaloni, D., and Carlier, M. F. (2004). Formin is a processive motor that requires profilin to accelerate actin assembly and associated ATP hydrolysis. *Cell* 119, 419-429.
- Rose, R., Weyand, M., Lammers, M., Ishizaki, T., Ahmadian, M. R., and Wittinghofer, A. (2005). Structural and mechanistic insights into the interaction between Rho and mammalian Dia. *Nature* 435, 513-518.

Rudolph, M. G., Bayer, P., Abo, A., Kuhlmann, J., Vetter, I. R., and Wittinghofer, A. (1998). The Cdc42/Rac interactive binding region motif of the Wiskott Aldrich syndrome protein (WASP) is necessary but not sufficient for tight binding to Cdc42 and structure formation. *J Biol Chem* 273, 18067-18076.

Rudolph, M. G., Linnemann, T., Grunewald, P., Wittinghofer, A., Vetter, I. R., and Herrmann, C. (2001). Thermodynamics of Ras/effector and Cdc42/effector interactions probed by isothermal titration calorimetry. *J Biol Chem* 276, 23914-23921.

Sagot, I., Klee, S. K., and Pellman, D. (2002). Yeast formins regulate cell polarity by controlling the assembly of actin cables. *Nat Cell Biol* 4, 42-50.

Scheffzek, K., Ahmadian, M. R., and Wittinghofer, A. (1998). GTPase-activating proteins: helping hands to complement an active site. *Trends Biochem Sci* 23, 257-262.

Scott, C. C., Dobson, W., Botelho, R. J., Coady-Osberg, N., Chavrier, P., Knecht, D. A., Heath, C., Stahl, P., and Grinstein, S. (2005). Phosphatidylinositol-4,5-bisphosphate hydrolysis directs actin remodeling during phagocytosis. *J Cell Biol* 169, 139-149.

Seder, R. A., Paul, W. E., Davis, M. M., and Fazekas de St Groth, B. (1992). The presence of interleukin 4 during in vitro priming determines the lymphokine-producing potential of CD4+ T cells from T cell receptor transgenic mice. *J Exp Med* 176, 1091-1098.

Seth, A., Otomo, T., Yin, H. L., and Rosen, M. K. (2003). Rational design of genetically encoded fluorescence resonance energy transfer-based sensors of cellular Cdc42 signaling. *Biochemistry* 42, 3997-4008.

Shaner, N. C., Campbell, R. E., Steinbach, P. A., Giepmans, B. N., Palmer, A. E., and Tsien, R. Y. (2004). Improved monomeric red, orange and yellow fluorescent proteins derived from *Discosoma* sp. red fluorescent protein. *Nat Biotechnol* 22, 1567-1572.

Shaner, N. C., Steinbach, P. A., and Tsien, R. Y. (2005). A guide to choosing fluorescent proteins. *Nat Methods* 2, 905-909.

Sharpless, K. E., and Harris, S. D. (2002). Functional characterization and localization of the *Aspergillus nidulans* formin SEPA. *Mol Biol Cell* 13, 469-479.

Sorokina, E. M., and Chernoff, J. (2005). Rho-GTPases: new members, new pathways. *J Cell Biochem* 94, 225-231.

Spudich, J. A., and Watt, S. (1971). The regulation of rabbit skeletal muscle contraction. I. Biochemical studies of the interaction of the tropomyosin-troponin complex with actin and the proteolytic fragments of myosin. *J Biol Chem* 246, 4866-4871.

Stowers, L., Yelon, D., Berg, L. J., and Chant, J. (1995). Regulation of the polarization of T cells toward antigen-presenting cells by Ras-related GTPase CDC42. *Proc Natl Acad Sci U S A* 92, 5027-5031.

Swanson, J. A., and Hoppe, A. D. (2004). The coordination of signaling during Fc receptor-mediated phagocytosis. *J Leukoc Biol* 76, 1093-1103.

Symons, M., and Settleman, J. (2000). Rho family GTPases: more than simple switches. *Trends Cell Biol* 10, 415-419.

Teruel, M. N., and Meyer, T. (2000). Translocation and reversible localization of signaling proteins: a dynamic future for signal transduction. *Cell* 103, 181-184.

Thompson, G., Owen, D., Chalk, P. A., and Lowe, P. N. (1998). Delineation of the Cdc42/Rac-binding domain of p21-activated kinase. *Biochemistry* 37, 7885-7891.

Tooley, A. J., Jacobelli, J., Moldovan, M. C., Douglas, A., and Krummel, M. F. (2005). T cell synapse assembly: proteins, motors and the underlying cell biology. *Semin Immunol* 17, 65-75.

Toutchkine, A., Kraynov, V., and Hahn, K. (2003). Solvent-sensitive dyes to report protein conformational changes in living cells. *J Am Chem Soc* 125, 4132-4145.

Tskvitaria-Fuller, I., Rozelle, A. L., Yin, H. L., and Wulfing, C. (2003). Regulation of sustained actin dynamics by the TCR and costimulation as a mechanism of receptor localization. *J Immunol* 171, 2287-2295.

Tzima, E., Kiosses, W. B., del Pozo, M. A., and Schwartz, M. A. (2003). Localized cdc42 activation, detected using a novel assay, mediates microtubule organizing center positioning in endothelial cells in response to fluid shear stress. *J Biol Chem* 278, 31020-31023.

- Van Aelst, L., and D'Souza-Schorey, C. (1997). Rho GTPases and signaling networks. *Genes Dev* *11*, 2295-2322.
- Wallar, B. J., and Alberts, A. S. (2003). The formins: active scaffolds that remodel the cytoskeleton. *Trends Cell Biol* *13*, 435-446.
- Watanabe, N., and Higashida, C. (2004). Formins: processive cappers of growing actin filaments. *Exp Cell Res* *301*, 16-22.
- Watanabe, N., Kato, T., Fujita, A., Ishizaki, T., and Narumiya, S. (1999). Cooperation between mDia1 and ROCK in Rho-induced actin reorganization. *Nat Cell Biol* *1*, 136-143.
- Watanabe, N., Madaule, P., Reid, T., Ishizaki, T., Watanabe, G., Kakizuka, A., Saito, Y., Nakao, K., Jockusch, B. M., and Narumiya, S. (1997). p140mDia, a mammalian homolog of *Drosophila* diaphanous, is a target protein for Rho small GTPase and is a ligand for profilin. *Embo J* *16*, 3044-3056.
- Wulfig, C., Sumen, C., Sjaastad, M. D., Wu, L. C., Dustin, M. L., and Davis, M. M. (2002). Costimulation and endogenous MHC ligands contribute to T cell recognition. *Nat Immunol* *3*, 42-47.
- Xu, Y., Moseley, J. B., Sagot, I., Poy, F., Pellman, D., Goode, B. L., and Eck, M. J. (2004). Crystal structures of a Formin Homology-2 domain reveal a tethered dimer architecture. *Cell* *116*, 711-723.
- Yayoshi-Yamamoto, S., Taniuchi, I., and Watanabe, T. (2000). FRL, a novel formin-related protein, binds to Rac and regulates cell motility and survival of macrophages. *Mol Cell Biol* *20*, 6872-6881.
- Yoshizaki, H., Ohba, Y., Kurokawa, K., Itoh, R. E., Nakamura, T., Mochizuki, N., Nagashima, K., and Matsuda, M. (2003). Activity of Rho-family GTPases during cell division as visualized with FRET-based probes. *J Cell Biol* *162*, 223-232.
- Zeng, R., Cannon, J. L., Abraham, R. T., Way, M., Billadeau, D. D., Bubeck-Wardenberg, J., and Burkhardt, J. K. (2003). SLP-76 coordinates Nck-dependent Wiskott-Aldrich syndrome protein recruitment with Vav-1/Cdc42-dependent Wiskott-Aldrich syndrome protein activation at the T cell-APC contact site. *J Immunol* *171*, 1360-1368.
- Zhang, J., Campbell, R. E., Ting, A. Y., and Tsien, R. Y. (2002). Creating new fluorescent probes for cell biology. *Nat Rev Mol Cell Biol* *3*, 906-918.

Zheng, Y. (2001). Dbl family guanine nucleotide exchange factors. *Trends Biochem Sci* 26, 724-732.

Zheng, Y., Fischer, D. J., Santos, M. F., Tigyi, G., Pasteris, N. G., Gorski, J. L., and Xu, Y. (1996). The faciogenital dysplasia gene product FGD1 functions as a Cdc42Hs-specific guanine-nucleotide exchange factor. *J Biol Chem* 271, 33169-33172.

Zigmond, S. H. (2000). How WASP regulates actin polymerization. *J Cell Biol* 150, 117-120.

Zigmond, S. H. (2004). Formin-induced nucleation of actin filaments. *Curr Opin Cell Biol* 16, 99-105.

Ziman, M., Preuss, D., Mulholland, J., O'Brien, J. M., Botstein, D., and Johnson, D. I. (1993). Subcellular localization of Cdc42p, a *Saccharomyces cerevisiae* GTP-binding protein involved in the control of cell polarity. *Mol Biol Cell* 4, 1307-1316.

VITAE

Abhinav Seth was born in Teaneck, NJ on July 30, 1976, the son of Mrs. Usha Seth and Mr. Suresh C. Seth. After graduating from Tenafly High School (Tenafly, NJ) in 1994, he entered Harvard University (Cambridge, MA). During the summer of 1996, he worked at Vertex Pharmaceuticals (Cambridge, MA) under the guidance of Dr. Keith P. Wilson. From January 1997 – June 1998, he worked in the lab of Dr. Stuart L. Schreiber in the Harvard Chemistry Department. He graduated *summa cum laude* with a BA in Biochemical Sciences and an MA in Biological Sciences in 1998. He also received a 1998 Thomas Temple Hoopes Thesis Prize for his work in the Schreiber Lab. In July of 1998, he entered the Tri-Institutional Medical Scientist Training Program at Cornell University Medical College. After two years of medical school, he joined the lab of Dr. Michael K. Rosen at Memorial Sloan-Kettering Cancer Center. In 2001, he moved with the Rosen Lab to UT Southwestern Medical Center and transferred to its Medical Scientist Training Program. In December of 2001, he married best friend and fellow graduate student, Rashu Bhargava, who joined him happily on the move from New York to Dallas. He looks forward to completing his clinical training and pursuing a career in academic medicine and scientific research.

Permanent Address: 286 East Saddle River Road
Upper Saddle River, NJ 07458

aseth@post.harvard.edu